Phosphorylation of the E3 ubiquitin ligase PUB22 controls its ubiquitination activity to dampen the immune response

Dissertation

zur Erlangung des
Doktorgrades der Naturwissenschaften (Dr. rer. nat.)

der

Naturwissenschaftlichen Fakultät I – Biowissenschaften –

der Martin-Luther-Universität
Halle-Wittenberg,

vorgelegt

von Frau Giulia Furlan

geb. am 24/10/1986 in Padova (Italien)

Gutachter:

Prof. Dr. Dierk Scheel – Leibniz-Institut für Pflanzenbiochemie

Prof. Dr. Marcel Quint – Martin-Luther-Universität Halle-Wittenberg

Prof. Dr. Claus Schwechheimer – Technische Universität München

Verteidigung: 29.06.2017

Index

List of abbreviations

μM	micromolar		ETI	effector-triggered immunity
A. tumefaciens	*Agrobacterium tumefaciens*		ETS	effector-triggered susceptibility
ABA	abscisic acid		FDR	false discovery rate
AEBSF	4-(2-Aminoethyl) benzenesulfonyl fluoride hydrochloride		FLARE	flagellin rapidly elicited
			flg22	22 amino acid peptide derived from flagellin
Ala (A)	alanine			
Arabidopsis (*At*)	*Arabidopsis thaliana*		g	9,81 m/s^2 (gravitation force)
ARM	armadillo-like repeat		g	grams
ATP	adenosine triphosphate		GFP	green fluorescent protein
Avr	avirulence		Glu (E)	glutamic acid
BiFC	bimolecular fluorescence complementation		Gly (G)	glycine
			Gm	*Glycine max*
Ca^{2+}	calcium		GST	glutathione-S-transferase
CBB	coomassie brilliant blue		h	hour
CDS	coding sequence		HCl	hydrochloric acid
CDS	Coding sequence		HECT	homologoues to the E6Ap carboxyl terminus
cfu	colony forming units			
CHX	cycloheximide		HEPES	4-(2-hydroxyethyl)-1-piperazineethanesulfonic acid
cLUC	C-terminal part of luciferase			
cm	centimeter		His	histidine
co-IP	co-immunoprecipitation		*Hpa*	*Hyaloperonospora arabidopsidis*
Col-0	wild-type Arabidopsis ecotype Columbia-0			
			HR	hypersensitive response
CRL	cullin-RING-ligase		HR/AM	high resolution accurate mass
cYFP	C-terminal part of YFP		HR/AM LC-MS	high resolution accurate mass mass spectrometry
Cys (C)	cysteine			
DAMP	damage-associated molecular pattern		HRP	horsereadish peroxidase
			Hs	*Homo sapiens*
DDA	data dependent acquisition		ICD	INF1-triggered cell death
DMSO	dimethyl sulfoxide		ID	inner diameter
DNA	deoxyribonucleic acid		Ile (I)	isoleucin
DTT	dithiothreitol		IP	immunoprecipitation
DUB	deubiquitinating enzyme		IPTG	isopropyl β-D-1-thiogalactopyranoside
E. coli	*Escherichia coli*			
E1	ubiquitin-activating enzyme		JA	jasmonic acid
E2	ubiquitin-conjugating enzyme		KB	kings broth
E3	ubiquitin ligase		kDa	kilodalton
EDTA	ethylenediaminetetraacetic acid		LB	lysogeny broth
			LC	liquid chromatography
EF-Tu	translation elongation factor Tu		Leu (L)	leucine
			LPS	lipopolysaccharide
elf18	18 amino acid peptide derived from EF-Tu		LRR	leucine rich repeat
			Lys (K)	lysine
ER	endoplasmic reticulum		M	molar
ERAD	endoplasmic reticulum-associated degradation		MAPK	mitogen-activated protein kinase

MAPKK	MAPK kinase
MAPKKK	MAPKK kinase
Max IP	maximum injection time
MBP	maltose-binding protein
MBP	myelin basic protein
MEK	MAPK and ERK kinase
MEKK	MEK kinase
MES	2-(N-morpholino)ethanesulfonic acid
MG132	26S-proteasome inhibitor
min	minute
Mm	*Mus musculus*
MS	mass spectrometry
MS	Murashige and Skoog
MSA	multi stage activation
MVB	multivesicular bodies
NADPH	nicotinamide adenine dinucleotide phosphate
NB	nucleotide binding
NEB	New England Biolabs
nLUC	N-terminal part of luciferase
nm	nanometer
nM	nanomolar
nYFP	N-terminal part of YFP
OA	okadaic acid
OD600	optical density at 600 nm
Os	*Oryza sativa*
P. infestans	*Phytophthora infestans*
PAGE	polyacrylamide gel electrophoresis
PAMP or MAMP	pathogen- or microbe-associated molecular pattern
Pc	*Petroselinum crispum*
PCD	programmed cell death
PCR	polymerase chain reaction
PGN	peptidoglycan
Phe (F)	phenylalanine
PI	proteasome inhibitor
PM	plasma membrane
PR	pathogenesis related
PRRs	pattern recognition receptors
Pst	*Pseudomonas syringae* patovar *tomato*
PTI	PAMP-triggered immunity
PUB	plant U-box protein
pub22 pub23 pub24	*pub22 pub23 pub24* triple knock-out genotype
PVDF	polyvinylidene fluoride
RBR	RING-in-between-RING

Rho-GAP	Rho GTPase-activating protein
RING	really interesting new gene
RLCK	receptor-like cytoplasmic kinase
RLK	receptor-like kinase
ROS	reactive oxygen species
R-protein	resistance protein
RT	room temperature
RTK	receptor tyrosine kinase
RT-qPCR	quantitative reverse-transcription PCR
S.E.M	standard error of the mean
SA	salicylic acid
SAR	systemic acquired resistance
Sc	*Saccharomyces cerevisiae*
SDM	site directed mutagenesis
SDS	sodium dodecyl sulfate
Ser (S)	serine
SERK	somatic embryogenesis receptor kinase
Sl	*Solanum lycopersicum*
SOC	super optimal broth with catabolite repression
Sp	*Solanum pennellii*
St	*Solanum tuberosum*
Taq	*Thermus aquaticus*
TF	transcription factor
TGN	trans-golgi network
Thr (T)	threonine
TIR	Toll/interleukin (IL)-1 receptor
TRP	tetratricopeptide repeat
Trp (W)	tryptophan
TTSS	type three secretion system
Tyr (Y)	tyrosine
Ub	ubiquitin
UBQ10	*Ubiquitin10*
UEV	Ubiquitin conjugating enzyme variant
UND	U-box N-terminal domain
UPS	ubiquitin-proteasome system
VQP	VQ-motif-containing protein
WT	wild-type
YFP	yellow fluorescent protein
Zm	*Zea mays*
ΔC_t	delta of threshold cycle

1. Introduction

1.1 Plant immunity

For a world with an ever-growing population, it is vital to secure food resources and develop strategies to increase food production. Crop losses due to plant diseases constitute an important matter in this regard. Comprehensive studies summarized by Oerke (2006) and Strange & Scott (2005), showed that in the last 40 years the usage of pesticides did not result in a significant decrease in crop loss, but on the contrary, crop losses have often increased. Nowadays, there is a general awareness among plant scientists that a wider and deeper understanding of plant pathogens' virulence strategies and the immune system of the host, will permit the generation of biotechnologically improved crop plants.

In the last 35 years, *Arabidopsis thaliana* (from here on referred to as Arabidopsis) has been an excellent model for plant studies, including plant-microbe interactions. Outstanding discoveries in regards to disease resistance have been achieved by the employment of Arabidopsis, and this knowledge is applicable to many other plant pathosystems, including crops (Nishimura & Dangl 2010).

1.1.1 PAMP-triggered immunity (PTI)

In difference to animals, plants lack a circulatory system, a prerequisite for the vertebrates' acquired immunity, which relies on specialized white blood cells (lymphocytes). Instead, plants only possess an innate immune system, which functions in a cell-autonomous manner. The very first layer of defence in plants is enacted by physical barriers, such as the plant cell wall or the cuticle. Should they prove ineffective, inducible resistance is triggered by the direct perception of pathogens. Inducible plant and animal innate immunities, display striking similarities (Boller & Felix 2009). Conserved non-self microbial signatures, called pathogen- or microbe-associated molecular patterns

1. Introduction

(PAMPs or MAMPs), can be perceived by pattern recognition receptors (PRRs) (Zipfel 2009). PAMPs consist of molecular motifs, often vital for the pathogen survival and therefore, inherent to a whole class of pathogens. The lipopolysaccharide (LPS) molecule from the outer membrane of Gram-negative bacteria, and flagellin, the main component of bacterial flagella, are two well-characterized examples of PAMPs for plants (Ranf et al. 2015, Zipfel et al. 2004). Interestingly, LPS and flagellin are PAMPs also for other higher eukaryotes, however, the recognized molecular epitopes within the molecule vary among the different species. Additional identified plant PAMPs are for instance the intracellular bacterial elongation factor Tu (EF-Tu) (Kunze et al. 2004), peptidoglycans (PGNs) (Gust et al. 2007), which are cell wall component of Gram-positive bacteria, the fungal cell wall component chitin (Walker-Simmons et al. 1983) or Pep13, a short peptide identified as first PAMP molecule from an oomycete cell wall transglutaminase (Nürnberger et al. 1994). Although thought to be mostly invariant, PAMPs are occasionally modified by pathogens to disguise their presence from the plant and avert detection (Sun et al. 2006). Likewise, endogenous plant elicitor peptides, such as the PROPEP1-derived Pep1, can also activate immune responses (Huffaker et al. 2006). They belong to the damage-associated molecular patterns (DAMPs) group.

The immune system in plants can be conceptually divided into two main branches. Perception of PAMPs by the corresponding PRRs occurs at the plasma membrane (PM) and results in the activation of PAMP-triggered immunity (PTI), representing the first branch of induced plant immunity. PTI provides a non-specific response to limit pathogen growth and, it was demonstrated to contribute to plant protection.

Flagellin-sensing 2 (FLS2), is a PRR receptor-like kinase (RLK), which is located at the PM. *fls2* mutant plants, which are insensitive to flg22, display enhanced disease susceptibility (Zipfel et al. 2004). RLKs such as FLS2, possess an intracellular serine/threonine (Ser/Thr) protein kinase domain, followed by a transmembrane domain and an extracellular leucine-rich repeat (LRR) domain, which binds to the ligand. In the case of flagellin, the molecular epitope sufficient for the recognition by FLS2 in Arabidopsis, is the N-terminal 22 amino acid peptide flg22 (Zipfel et al. 2004, Chinchilla et al. 2006). The mammalian flagellin receptor toll-like receptor 5 (TLR5) instead, recognizes different epitopes of flagellin (Donnelly & Steiner 2002, Zipfel & Felix 2005). Plants contain a battery of RLKs and recent work has identified numerous immune receptors (Zipfel et al. 2006, Yamaguchi et al. 2006, Yamaguchi et al. 2010, Petutschnig et al. 2010, Cao et al. 2014, Ranf et al. 2015). A fundamental component of immune signalling following perception, is the brassinosteroid

insensitive 1 (BRI1)-associated kinase 1 (BAK1), an LRR-RLK. BAK1 forms ligand-dependent heteromeric complexes with several PRRs, namely FLS2, the Brassicaceae EF-Tu receptor (EFR1) (Roux et al. 2011) or the Pep1 receptors 1 and 2 (PEPR1 and PEPR2) (Chinchilla et al. 2007), and is required for the full signal transduction (Tang et al. 2015). Notably, PRRs can also function independently of BAK1 (Gimenez-Ibanez et al. 2009, Ranf et al. 2015). Receptor-like cytoplasmic kinases (RLCKs), are found downstream of the receptor complexes and include the *Botrytis*-induced kinase 1 (BIK1) (Lu et al. 2010). Specifically, BIK1 constitutively interacts with FLS2, EFR1, PEPR1/2 and the chitin elicitor receptor kinase 1 (CERK1) (Zhang et al. 2010). BIK1 is central for the transduction of the immune signalling triggered by flg22, as shown by the *bik1* mutants compromised signalling (Lu et al. 2010).

Beyond the mentioned events at the PM, PAMP perception triggers several subsequent processes. In both plants and animals, central hallmarks of PTI are the production of reactive oxygen species (ROS), the intracellular calcium increase and the activation of mitogen-activated protein kinase (MAPK) cascades (Bigeard et al. 2015). A detailed account of the MAPK signalling network in plant defence is presented in 1.1.3. In plants, ROS production induces stomatal closure (Miller et al. 2009, Dubiella et al. 2013) and distal defence responses (Kwak et al. 2003). The Arabidopsis NADPH oxidases, respiratory burst oxidase homolog D (RBOHD) and RBOHF, play important roles in ROS production during immunity. *rbohD rbohF* double mutant plants are impaired in salicylic acid (SA)-dependent cell death (Torres et al. 2002) and in abscisic acid (ABA)-induced stomatal closure (Kwak et al. 2003). In parallel, calcium (Ca^{2+}) is a universal messenger and changes in calcium function in the regulation of the activity of calcium-dependent proteins, including kinases, during immunity.

The activation of signalling elements results in the transcriptional reprogramming of the cell. A transcriptome analysis carried out by Navarro and colleagues (Navarro et al. 2004), surveyed the early transcriptional response upon flg22 treatment in Arabidopsis, and identified flagellin rapidly elicited (FLARE) genes, which included transcription factors (TFs), kinases, phosphatases, as well as, proteins belonging to the ubiquitin-proteasome system (UPS). A central role was attributed to WRKY TFs (Bakshi & Oelmüller 2014), because the WRKY TFs binding sites (W-boxes) are found in the promoter of numerous pathogenesis-related (*PR*) genes (Eulgem & Somssich 2007). Worth noting is that several WRKYs are phosphorylated by MAPKs (Popescu et al. 2009).

A later defence response activated by PTI is the production and deposition of the β-(1,3)-glucan polymer callose, which is thought to function as both a physical barrier and a matrix for deposition of antimicrobial compounds (Luna et al. 2011). Additionally, hormones play an important role at later time points. Among the plant hormones, SA is one of the most important for orchestrating the reprogramming of various *PR* genes, mostly by the action of the transcription coactivator, nonexpresser of *PR* genes 1 (NPR1) (Moore et al. 2011). SA triggers a physiological response called systemic acquired resistance (SAR) through SA, which confers long-term protection to the tissues distal to the infection site from subsequent infections (D. Wang et al. 2006, Fu & Dong 2013).

1.1.2 Effector-triggered immunity (ETI)

Pathogens have evolved strategies to escape or suppress PTI to successfully colonize the plant tissues. Virulence factors, termed effectors, which manipulate the plant host physiology, have been intensively studied. The mechanisms by which effectors are delivered into the host vary. Bacterial pathogens use a type three secretion system (TTSS), while some filamentous fungi penetrate the cell wall via appressoria and deliver effectors through their feeding organs. Indeed, effectors are integral to all pathogens including fungi, bacteria, oomycetes (Asai and Shirasu 2015) and viruses (Mandadi & Scholthof 2013).

A well-established plant-pathogen system to study plant disease is the Arabidopsis-*Pseudomonas syringae* pv *tomato* (*Pst*) interaction. *Pst* is a hemibiotrophic bacterium that enters leaves through stomata or wounds, and delivers effectors to the apoplast and to the plant cell cytosol through its TTSS (Katagiri et al. 2002). Disease symptoms include necrotic lesions occasionally surrounded by diffuse chlorosis. Examples of cytosolic effectors from *Pst* are the HopX1 and HopZ1a, which support jasmonic acid (JA) responses to counteract the activation of the SA pathway and lead to stomata aperture (Gimenez-Ibanez et al. 2014).

As a result of manipulation by effectors, a second branch of induced immunity evolved (Jones & Dangl 2006). This branch operates mainly via intracellular receptors called the disease resistance (R) proteins. Most of the R proteins contain nucleotide binding (NB)-LRR, which can sense pathogen effectors, both directly and indirectly, and activate the effector triggered immunity (ETI). ETI can be

described as an accelerated and amplified PTI response, characterized by the hypersensitive response (HR), which includes localized programmed cell death (PCD). In the absence of appropriate receptors, plants undergo effector triggered susceptibility (ETS), in which effectors successfully suppress PTI and the pathogen successfully infects the plant tissue.

Historically, an effector is termed avirulence (Avr) factor, because it is required to trigger ETI and induce resistance against a specific pathogen carrying it, thus resulting in an incompatible interaction and avirulence. However, it has become evident that throughout evolution, sequential layers of effectors and paired R proteins have originated, with pathogens gaining more effectors to escape recognition or to suppress PTI, and with the plant host selecting for suitable R proteins to recognize and fend them off. A well-studied example is AvrRpm1 from *P. syringae* pv *maculicola*, which induces the phosphorylation of RPM1 interacting protein 4 (RIN4) and activates the R protein RPM1 NB-LRR (Mackey et al. 2002). Additionally, AvrRpt2 is a cysteine protease, which cleaves RIN4 to overcome the action of RPM1 (Kim et al. 2005). The RIN4 cleavage however, is detected by RPS2 NB-LRR (Mackey et al. 2003).

1.1.3 The early immune response: insights in the MAPK signal transduction

Activation of MAPKs is one of the earliest events and a central hallmark of the initiation of plant immunity. MAPKs are involved in various defence responses, including immunity-related phytohormones regulation and defence gene induction (Meng & Zhang 2013). The typical MAPK pathway is structured in a three-tiered kinase cascade, with MAPKs, which are related to the mammalian extracellular signal-regulated kinase (ERK) subfamily, at the bottom of the cascade. In mammals, ERKs are activated by phosphorylation of a threonine and a tyrosine (Tyr) residue in the Thr-X-Tyr activation motif, by an upstream MAPK kinase (MAPKK) or MAPK and ERK kinase (MEK) (Chang & Karin 2001). This is in turn activated by a MAPKK kinase (MAPKKK) or MEK kinase (MEKK) through the phosphorylation of two Ser/Thr residues in the Ser/Thr-X_{3-5}-Ser/Thr motif. There are 20 MAPKs, 10 MAPKKs and approximately 60 MAPKKKs encoded in the Arabidopsis genome, more than in animals and yeast (Meng & Zhang 2013). Treatment with diverse immune elicitors such as flg22, EF-Tu, chitin, and DAMPs such as Pep1, which are perceived by different receptors, leads to the transient activation of MAPK and their nuclear translocation (Meng & Zhang 2013).

1. Introduction

The function of MAPKs in the immune response has been best studied in MPK3, MPK6, and MPK4, which are all transiently activated by PAMPs. Besides their role in immunity, MAPKs are involved in the transduction of other environmental and developmental signals, such as abiotic stress and development (Suarez-Rodriguez et al. 2010). Interestingly, their regulation is proposed to branch already at the receptor complex formation. This is suggested by the *bak1-5* mutant allele, which carries a C408Y substitution that impairs its flg22-regulated kinase activity, blocking MPK4 phosphorylation, but not influencing MPK3 and MPK6 phosphorylation (Schwessinger et al. 2011). MPK4 was originally classified as a negative regulator of immunity, because the *mpk4* mutant displays a dwarf phenotype and constitutive *PR* genes expression (Petersen et al. 2000). However, the autoimmune phenotype of *mpk4* is entirely dependent on SUMM2, an NB-LRR R protein guarding MPK4 (Zhang et al. 2012). On the other hand, MPK3 and MPK6, which are close homologs, were considered to be partially redundant in the positive regulation of immunity. The *mpk3* and *mpk6* single mutant plants do not display any developmental phenotype, whereas the double *mpk3 mpk6* mutation is lethal (Wang et al. 2007). However, recent transcriptomic analysis of flg22-regulated genes in these *mpk* mutants, revealed a more complex network, in which more than one MAPK may be required for gene regulation, and that the regulation of MAPKs is highly interconnected (Frei dit Frey et al. 2014). Moreover, a proteomic microarray approach showed that MPK3 shares 40 % of its targets with MPK6, but also 50 % with MPK4, indicating intensive synergy (Popescu et al. 2009).

WRKY33 is among the best-characterized targets of MAPKs. It is a critical TF, which binds the *phytoalexin deficient 3* (*PAD3*) promoter to activate the expression of camalexin biosynthetic genes (Qiu et al. 2008, Mao et al. 2011). MPK3 and MPK6 regulate WRKY33's function by activating it through phosphorylation, as well as by inducing its expression (Mao et al. 2011). WRKY33 is required for resistance against the necrotrophic fungal pathogen *Botrytis cinerea* (Zheng et al. 2006). It forms a nuclear complex with MPK4 and MPK substrate 1 (MKS1), which upon phosphorylation by MPK4, may determine the release of the WRKY33-MKS1 complex from MPK4 and promote *PAD3* expression (Qiu et al. 2008). Other important WRKYs are WRKY22 and WRKY29, which are positive regulators of immunity induced by the MAPK pathway (Asai et al. 2002).

Besides PAMP perception, MPK3 and MPK6 activation can also be triggered by H_2O_2 (Nakagami et al. 2006). An important component of the signal transduction pathway, linking ROS burst to downstream responses, is the oxidative signal-inducible 1 (OXI1), a Ser/Thr kinase, induced by ROS

and required for full MAPKs activation (Rentel et al. 2004). In guard cells, where MAPKs are highly expressed, MPK3 plays a key role in stomatal movements. Specific *mpk3* silencing in guard cells, showed that MPK3 is required for stomatal closure after exogenous H_2O_2 treatment, whereas it was dispensable for the ABA-induced closure (Gudesblat et al. 2007). Interestingly, MPK8 can be activated in a Ca^{2+}-dependent manner by interacting with the Ca^{2+}-binding protein calmodulin and bypassing the canonical MAPK cascade activation (Takahashi et al. 2011).

In Arabidopsis, a complete MAPK cascade was identified downstream of FLS2, which consists of MEKK1 (the MAPKKK), MKK4 and MKK5 (the MAPKKs), and MPK3 and MPK6 (the MAPKs) (Asai et al. 2002). Later, however, it was shown that *mekk1* mutant plants are impaired in flg22-triggered MPK4 activation, but show normal MPK3 and MPK6 activation (Suarez-Rodriguez et al. 2007, Ichimura et al. 2006), questioning whether MEKK1 functions upstream of MKK4 and MKK5. Expression of active MKK4 or MKK5 results in the activation of MPK3 and MPK6 and enhanced resistance to *Pst* and *Botrytis cinerea* (Asai et al. 2002). Biochemical studies further identified MKK1 and MKK2 as interactors of both MPK4 and MEKK1 (Gao et al. 2008). In this cascade, MEKK1 is required for the flg22-activation of MPK4, although it was proposed to act as scaffold given that its activity is not necessary (Suarez-Rodriguez et al. 2007).

1.1.4 Dampening of PTI signalling

The activation of defence responses upon pathogen infection requires the exact gaging of timing and intensity to avoid excessive metabolic penalties. Despite the increasing amounts of data available on PTI signalling, little is known about how homeostasis is maintained during immune responses. However, downregulation of the immune response is critical for all organisms. Negative regulatory loops are inherent to all signalling circuits and allow the fine-tune signalling events, and more importantly, are essential to bestow stability and robustness (Ferrell 2013).

Considering the myriad of phosphorylation events involved in the activation of immunity, it is not surprising that various phosphatases, as well as kinases, have been identified as negative regulators. Downregulation of immune signalling starts already at the PRR level, and one of the first players is the kinase-associated protein phosphatase (KAPP). KAPP is a protein phosphatase type 2C (PP2C)

that associates with the kinase domain of FLS2, and although its effect on FLS2 activity has not been clarified, its overexpression reduces flg22 binding and signalling (Gómez-Gómez et al. 2001). By contrast, the role of the protein phosphatase type 2A (PP2A) is well characterized. PP2A constitutively interacts with BAK1 (Segonzac et al. 2014). PP2A chemical inhibition by treatment with the PP2A phosphatase inhibitor cantharidin was sufficient to activate PTI and results in enhanced pathogen resistance. Cantharidin treatment leads to a steady-state hyper phosphorylation of BAK1, which suggests that PRR complexes are under constant negative regulation.

In addition to PP2A's regulation of BAK1, which is an important immunity amplifier influencing multiple signalling cascades, an additional novel mechanism was identified. The LRR-RLK BAK1-interacting receptor-like kinase 2 (BIR2) is in a complex with BAK1 and serves as substrate (Halter et al. 2014). By interacting with BIR2 under uninduced conditions, BAK1 is sequestered and unavailable for inactive PRRs, preventing premature PTI signalling. Interestingly, *bir2* mutants displayed increased immune responses, consistently with an hyper-activation of BAK1. However, *bir2* plants do not show any brassinosteroid-related phenotype.

Similarly, the positive regulator RLCK BIK1 is constitutively negatively regulated by the Ca^{2+}-dependent protein kinase 28 (CPK28) (Monaghan et al. 2014). CPK28 interacts with and phosphorylates BIK1, which facilitates BIK1 turnover, resulting in the attenuation of the BIK1-mediated responses. Loss of *CPK28* results in enhanced PTI. In addition, genetic analysis identified the RLCK AvrPphB susceptible 1 (PBS1)-like kinase 13 (PBL13) as a negative regulator of immunity. PBL13 was reported to be an active kinase, required to suppress defence (Z.-J. D. Lin et al. 2015). Interaction studies showed that it dissociates from RBOHD in a flg22-dependent manner. Nevertheless, PBL13 dependent phosphorylation of RBOHD remains to be shown.

Another mechanism to downregulate PRRs' signalling is the depletion of ligand-activated receptors from the PM via internalization and degradation. Indeed, relocalization of the immune signalling components by vesicular trafficking is proposed to be a major process in signal attenuation. The best example is provided by the study of a functional GFP fusion of FLS2, which was shown to be endocytosed upon flg22 treatment (Robatzek et al. 2006). Additional inhibitor studies indicated that flg22-activated FLS2 receptors are transported via the late endosomes and finally degraded in the vacuole (Beck et al. 2012). This process has been proposed to function in the dampening of immune

responses and also resulting in the desensitization of the flg22-treated leaf tissue to additional flg22 stimuli within one hour after the initial elicitation (Smith et al. 2014).

Besides PM components, immune signalling downregulation at the MAPK cascades level plays an important function. An unusual role was recently reported for the MAPKKK enhanced disease resistance 1 (EDR1). As the name suggests, *edr1* mutants display enhanced resistance to the fungus *Erysiphe cichoracearum*, the causal agent of powdery mildew (Frye & Innes 1998). Recently, EDR1 was proposed to function via MKK4 and MKK5, as it is able to interact with them and contribute to their degradation (C. Zhao et al. 2014). This is consistent with the *edr1* mutant having more abundant MPK3 and MPK6 with increased basal activity levels, resulting in an enhanced resistance phenotype. Similar to *mkk4* and *mkk5*, *mpk3* was also epistatic to *edr1*.

MAPK-phosphorylated threonine and tyrosine residues can be dephosphorylated by AP2C1 or PP2C5 (PP2C-type) (Brock et al. 2010). *ap2c1* and *pp2c5* mutants display increased levels of MPK3 and MPK6 activation by ABA treatment, suggesting a function in the attenuation of their activation. Pathogens exploit this possibility by injecting effectors such as the *Pst* HopAI1, which is a phosphothreonine lyase targeting MPK3, MPK4, and MPK6 and directly dephosphorylating them (Zhang et al. 2007).

Another post-translation modification involved in both the positive and negative modulation of the immune response is ubiquitination. The major findings implicating ubiquitination in plant immunity and the integration of phosphorylation in the UPS and signalling are described in 1.2.1.

1.2 The Ubiquitin-Proteasome System (UPS)

Ubiquitin is a central element in eukaryotic physiology. Its name refers to its ubiquitous nature in light of the fact that ubiquitin is consistently found throughout almost all tissues. Composed of 76 amino acids, its genetic sequence is remarkably conserved, with the plant ubiquitin differing from its human counterpart in only three residues. It has a compact and stable structure with a hydrophobic core β-grasp fold or ubiquitin-fold, and a vast number of hydrogen bonds that render the protein highly soluble and heat resistant.

1. Introduction

Ubiquitination (or ubiquitylation) is the process of attachment of one or more ubiquitin molecules to a substrate protein. The phosphorylation modification provides binary information, namely the presence or absence of a phosphate group on the specific substrate amino acid. By contrast, ubiquitination can transmit a variety of instructions stored in the definite length, linkage type and site of ubiquitin chains formation (Pickart & Eddins 2004). These different configurations are advantageous for delineating variegated outcomes, as protein ubiquitination can act not only on protein stability as a degradation signal, but also on localization or on activity. Altogether, ubiquitination is involved in the modulation of the most, if not the entirety, of cellular processes (Trujillo & Shirasu 2010, Furlan et al. 2012).

The ubiquitination process has been dissected in the sequential action of principally three enzymes (de Bie & Ciechanover 2011). The typical journey of ubiquitin (Ub) (Figure 1-1) starts with the activation of ubiquitin, mediated by the ubiquitin-activating enzyme (E1) in an ATP-dependent manner. At first, an ubiquitin-adenylate intermediate is formed at the C-terminal glycine (Gly) of ubiquitin, which then can bind to the active site cysteine on the E1, forming an E1~ubiquitin thioester bond (~). The second enzyme of the cascade is the ubiquitin-conjugating enzyme (E2), which transfers ubiquitin onto its active site cysteine via trans(thio)esterification, creating a E2~ubiquitin conjugate. As last, the ubiquitin ligase (E3) acts as a scaffold between a specific target protein and the E2~ubiquitin conjugate, both of which are bound to the E3. The E3 increases the transfer rate of ubiquitin, which results in an isopeptide bond between the C-terminal glycine of ubiquitin and the ε-amino group of a specific lysine (Lys) residue on the target protein. Chains are produced by attaching additional ubiquitin molecules to a lysine of one of the preceding ubiquitins with multiple rounds of repetition. Furthermore, ubiquitin-like modifiers possessing an ubiquitin-fold, such as Nedd8 and SUMO, were identified upon genome sequencing, and appear to share the same biochemical mechanism for substrate attachment as ubiquitin (Downes & Vierstra 2005). Ubiquitination is a reversible process. Deubiquitinating enzymes (DUBs) can recognize the C-terminal ubiquitin footprint very specifically and cleave off ubiquitin after amino acid 76 (Komander et al. 2009).
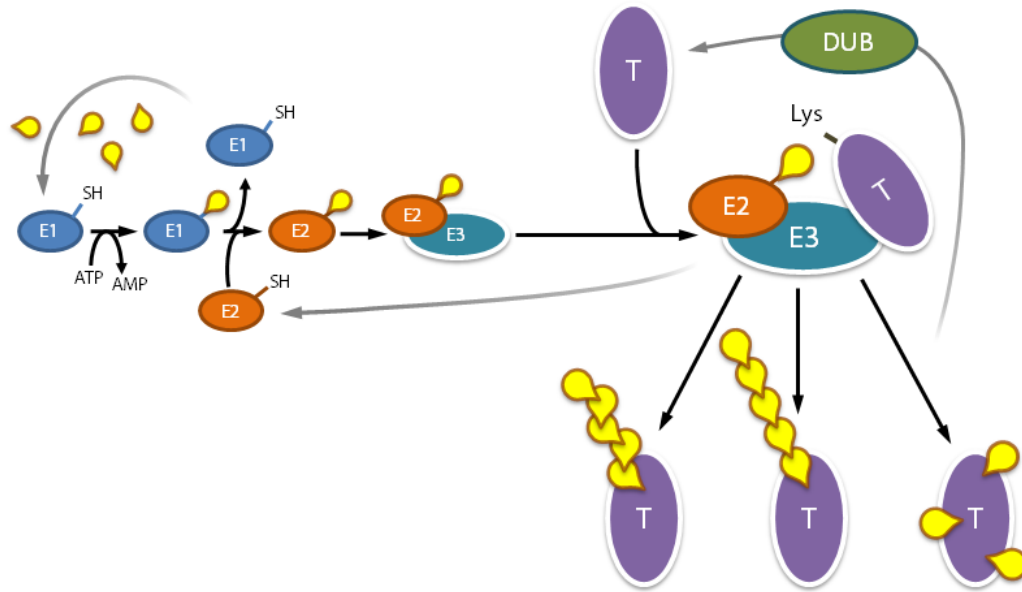
Figure 1-1 Schematic representation of the ubiquitination cascade. The ubiquitin-activating enzyme (E1) activates ubiquitin and binds it. Ubiquitin is transferred to the ubiquitin-conjugating enzyme (E2). The ubiquitin ligase enzyme (E3) recruits both the E2 enzyme and target protein (T). Targets can undergo different types of ubiquitination. DUBs can remove ubiquitin moieties from ubiquitinated proteins.

The Nobel winner prize Avram Hershko showed for the first time in 1982 that the E1, E2 and E3 purified enzymes, in presence of ATP and ubiquitin, are necessary and sufficient for the reconstitution of the ubiquitination cascade *in vitro* (Hershko et al. 1983). This makes use of the puzzling feature, inherent to most E3s, to autoubiquitinate (self-catalysed ubiquitination) *in vitro*, namely to attach ubiquitin moieties on itself. Consequently, the establishment of *in vitro* ubiquitination assays has since then improved and facilitated the study of E3 ligase activity, substrate ubiquitination and ubiquitin chain composition.

Although ubiquitin itself is extraordinarily conserved, the components of the UPS have greatly expanded and differentiated during evolution. The latter is especially true for plants, as approximately 6 % of the Arabidopsis proteome is predicted to consist of UPS components; these include 16 ubiquitin genes, two E1s, 38 E2s and approximately 1500 E3s (Downes & Vierstra 2005).

E3s confer specificity to the ubiquitination reaction by recognizing the appropriate substrates to be modified. They have been broadly divided into four classes according to the their domain composition and mode of action (Vierstra 2009): the U-box-, the really interesting new gene (RING)- and the homologous to the E6AP carboxyl terminus (HECT)-type, belonging to the single-unit E3s,

and the cullin-RING-ligase (CRL)-type, which are multisubunit E3s. HECT E3 ligases are large proteins of roughly 3700 amino acids possessing a HECT domain. Ubiquitin is transferred by trans(thio)esterification to a catalytic cysteine onto the E3 HECT domain prior to the linking onto the substrate. The mechanism of ubiquitin transfer of RING, U-box and CRL E3 ligases, comprises instead the non-covalent binding of E2s via the RING or U-box domain or the RING-box 1 (RBX1) subunit (which itself contains a RING finger), and the formation of an E2~ubiquitin/E3/substrate complex. During the formation of this complex, ubiquitin is directly transferred from the E2 onto the substrate. U-box and RING E3s will be introduced in details in 1.2.1.1. While HECT, RING and U-box E3s are composed by a single polypeptide, CRLs are multisubunit E3s containing a cullin, the catalytic module RBX1 in complex with E2~Ub and the second module called adaptor for target recognition.

There are four types of cullins in Arabidopsis, each one interacting with specific types of substrate adaptor modules (Choi et al. 2014). Cullin1 (CUL1) and CUL1b associate to the substrate recognition modules F-box proteins (FBXs) through the S-phase kinase-associated protein 1 (SKP1), forming SKP1-CUL1-F-box (SCF) E3 ligases. Similarly, CUL4 requires the DNA damage-binding (DDB) DDB1 protein to connect to the WD40 domain-containing DWD proteins, which bind the targets. CUL3a and CUL3b instead, simply employ the bric-a-brac–tramtrack protein (BTB) as a substrate recognition module. Finally the anaphase-promoting complex (APC) is an intricate 11 subunits complex including relatives of cullins (APC2) and RBX1 (APC11).

While E3 enzymes determine substrate specificity, the type and length of the ubiquitin chain is considerably dependent on the function of distinct E2 enzymes, which appropriately orientate its conjugated ubiquitin to form ubiquitin chains. Ubiquitin contains seven lysines: K6, K11, K27, K29, K33, K48 and K63. Polyubiquitin chains can be formed through each of these seven lysine residues or through the N-terminal methionine (M1), which creates linear chains (Kirisako et al. 2006). The countless possible combinations attest for the high versatility of the system. While a considerable number of details regarding the topology of protein ubiquitination, and its function, have been elucidated in yeast and mammals, little is understood in plants. The first view of the ubiquitinated proteome in plants was given by Maor and colleagues, by employing large-scale proteomic approaches on Arabidopsis cell suspension culture (Maor et al. 2007). Additionally, with this approach, the relative abundance of the different types of ubiquitin linkage in Arabidopsis was

determined (Maor et al. 2007, Kim et al. 2013). K48, K63 and K11 being the most frequent, while K33, K29 and K6 linkages are only present in low concentrations.

The canonical and most abundant chain linkage between ubiquitin moieties is through K48, which has been implicated in many organisms in protein recruitment to the proteasome and subsequent degradation (Fu et al. 1998). Indeed, a chain of four K48-linked ubiquitins was found to be sufficient to target proteins to the 26S proteasome (Pickart & Fushman 2004). The 26S proteasome is the major cellular protease present in the cytoplasm and in the nucleus. It is composed of one catalytic core particle (20S) and two regulatory particle (19S) (Bedford et al. 2010). Protein proteolysis has been implicated in many physiological and cellular processes. In plants, several ubiquitinated proteins undergo proteasomal degradation, suggesting that they have been modified with K48-linked ubiquitin chains (Maraschin et al. 2009).

K63-linked ubiquitin chains are the second most abundant type of chain and were found to regulate many processes in a non-proteolytic fashion. The formation of K63-linked chains is mediated by a specialized E2 enzyme, namely Ubc13 in yeast (Hofmann & Pickart 1999). Arabidopsis possesses two homologs of Ubc13, called UBC35 (UBC13A) and UBC36 (UBC13B). UBC35 and UBC36, in combination with one of the four ubiquitin conjugating enzyme variants (UEVs), can form K63-linked chains (Wen et al. 2006). In yeast as well as in plants, genetic analysis confirmed an important role for K63-linked chains in DNA repair (Hofmann & Pickart 1999, Wen et al. 2006). Moreover, in plants, apical dominance and root development mediated by auxin were also regulated through K63-linked ubiquitination (Yin et al. 2007, Wen et al. 2014).

K63-linked ubiquitination is known not to play a role in proteasomal degradation (Xu et al. 2009, Jacobson et al. 2009). However, only recently, experiments by Nathan and colleagues clarified the reason. In mammalian cells, the endosomal sorting complex required for transport 0 (ESCRT0) and its STAM and Hrs components, enact a protective mechanism by selectively binding to K63-linked chains and shielding them from proteasome binding and degradation (Nathan et al. 2013). In agreement with this, K63-linked ubiquitination is an important regulatory signal for the intracellular trafficking of several membrane proteins (Erpapazoglou et al. 2014). Especially, K63-linked ubiquitination is crucial for efficient sorting of cargo into multivesicular bodies (MVBs) through the recognition by the ESCRT complexes, and subsequent lysosomal/vacuolar degradation. As an example, the Gap1 permease in yeast was shown to require K63-linked ubiquitination for sorting to

MVBs and degradation (Lauwers et al. 2009). However, monoubiquitination was sufficient to induce Gap1 endocytosis. The requirement of K63-linked chain modification for MVBs sorting and vacuolar degradation is valid also in plants. Both the PM-located PIN2 (an auxin efflux carrier protein) and BRI1 were shown to be ubiquitinated by K63-linked chains and that loss of ubiquitination results in their impaired vacuolar targeting (Leitner et al. 2012, Martins et al. 2015). Instead, the role of ubiquitination during endocytosis remains controversial in plants.

Moreover, current interesting studies are shedding more light on additional functions of unconventional chains in mammals and yeast. For instance, K11 linkage was assigned a role in the specialized endoplasmic reticulum-associated degradation (ERAD) during ER stress (Xu et al. 2009), K33 linkage in the regulation post-Golgi protein trafficking (Yuan et al. 2014), as well as linear ubiquitin chains in signalling pathway activation and apoptosis (Ikeda et al. 2011).

1.2.1 E3 ubiquitin ligases in plant immunity

The process of ubiquitination is highly engaged in the orchestration of multiple processes. Among the many known functions of ubiquitination, the 26S proteasome-mediated degradation, enables plants to rapidly respond to sudden environmental changes or pathogen attack. Among the UPS components, numerous single-unit E3 ligases play important roles as positive and negative regulators of immune responses, while CRLs are mostly involved in hormone and light signalling (Trujillo & Shirasu 2010).

1.2.1.1 Single-unit E3 ligases in immunity

In Arabidopsis, seven HECT-, 64 U-box- and 477 RING-type E3 ligases are predicted (Vierstra 2009). Up to date, none of the HECT E3s were implicated in the regulation of immune responses. Also, despite their considerable number, only few RING E3s have been associated with immunity. One family in particular, the *Arabidopsis toxicos para levadura* (*ATL*), has received attention as its members were induced upon various PAMP treatments (Navarro et al. 2004). One member, *ATL9*, was additionally confirmed as a regulator of immunity, since *atl9* mutant plants were more susceptible to the fungus *Erysiphe cichoracearum* (Ramonell et al. 2005).

U-box-type E3 ligases in PTI

On the other hand, the subgroup of the U-box E3s has frequently been associated with diverse stress responses, including immunity. This is highlighted by the induction of the *AtPUB* genes expression under different biotic and abiotic stresses (Yee and Goring 2009). The *PUB* genes take their name from the acronym of plant U-box proteins, which includes all U-box containing proteins with the exception of the Carboxyl-terminus of Hsp70 Interacting Protein (CHIP). Several of the PUB proteins possess E3 ligase activity, as demonstrated by *in vitro* ubiquitination assays (Mudgil et al. 2004, Wiborg et al. 2008). The analysis of their domain composition uncovered a large class of PUBs that possess a C-terminal armadillo-like repeat (ARM) domain in addition to the N-terminal U-box domain (Mudgil et al. 2004). An extensive description of the U-box and ARM domains is provided in 1.3.1. Moreover, a U-box N-terminal domain (UND) with yet unknown function is also often predicted in PUB-ARM proteins.

The closely related E3 ligases PUB22, PUB23 and PUB24 are PUB-ARM proteins involved in the negative regulation of PTI (Trujillo et al. 2008). All knockout mutants displayed enhanced responsiveness towards flg22 treatment, including enhanced defence genes induction and enhanced ROS production. Importantly, quantitative ROS assays showed that the *pub* mutations have an additive effect, with the *pub22 pub23 pub24* triple mutants having the strongest phenotype, suggesting a partial redundancy in their function. Of note, a specific prolongation of MPK3 activation was observed in the flg22 elicited triple mutants. Consequently, triple mutants were significantly more resistant against *Pst* and *Hpa* infections. Strikingly, *pub22*, *pub23* and *pub24* mutations do not cause any developmental abnormalities, indicating that they are dedicated to dampening of activated stress signalling. Triple mutants were also more responsive to other elicitors such as elf18 or chitin. This suggests that PUB22, PUB23 and PUB24 act in concert in a shared process downstream of various PRRs. Especially, PUB22 and PUB24 have dominant phenotypes over PUB23, as demonstrated by the resemblance of the *pub22 pub24* double mutant phenotype to the triple. In-depth description of PUB22 is given in 1.3.

The homologous PUB12 and PUB13 are extensively studied PUB-ARM proteins, which possess a UND domain at the N-terminus. Biochemical studies indicate that they are required for the endogenous ubiquitination and degradation of FLS2 during immunity (Lu et al. 2011). Notably, PUB12 and PUB13 interact with, but do not ubiquitinate BAK1. Upon flg22 treatment BAK1 complexes with FLS2 and

phosphorylates PUB12 and PUB13, which subsequently ubiquitinate FLS2 (Figure 1-4 A). In fact, *pub12 pub13* double mutants display reduced degradation of FLS2 upon flg22 treatment in comparison to wild-type plants, suggesting a role in the attenuation of the FLS2-mediated signalling (Lu et al. 2011).

A recent study reported that PUB13 is recruited to the trans-golgi network (TGN), by the small GTPase RabA4B and the phosphatidylinositol-4 lipid kinases PI4Kβ1/β2 (Antignani et al. 2015). Similarly to PUB13, PI4Kβ1/β2 are also negative regulators of immunity, as *pi4kβ1/β2* double mutant plants display enhanced resistance to *Pst* DC3000. Because PUB13 localizes at the TGN, this suggests that PUB13-mediated FLS2 ubiquitination may occur after endocytosis, as a signal for vacuolar sorting at the TGN, rather than for internalization at the PM. Indeed, FLS2 continuously cycles between PM and TGN (Beck et al. 2012). Further *in vitro* pull-down experiments confirmed the direct interaction between PUB13 and BAK1, but not between PUB13 and FLS2 (Zhou et al. 2015). Kinase inhibitor experiments suggested that BAK1-mediated phosphorylation of PUB13 is necessary for PUB13-FLS2 interaction (Lu et al. 2011). The interaction with BAK1 is mediated by the ARM domain of PUB13, as it was sufficient to pull down its cytoplasmic domain *in vitro*. The ARM domain overexpression results in a dominant negative phenotype, putatively due to its protective effect on FLS2 degradation from the action of the endogenous PUB12 and PUB13. Some bacterial pathogens have evolved the ability to manipulate the plant UBS by effectors mimicking E3 ligases. The AvrPtoB effector of *P.syringae*, presents a domain structurally resembling and acting as a U-box/RING E3 ligase. AvrPtoB ubiquitinates both FLS2 and CERK1 receptors and hence, mediates their degradation attenuating PTI (Figure 1-4 B) (Göhre et al. 2008, Gimenez-Ibanez et al. 2009).

Consistently with the reduced FLS2 degradation, *pub12 pub13* mutants displayed enhanced early immune responses resulting in enhanced pathogen resistance (Lu et al. 2011), resembling the *pub22 pub23 pub24* mutant phenotype. Interestingly, the *pub13* knockout was reported to display spontaneous cell death, accumulation of H_2O_2 and SA (Li et al. 2012), suggesting that PUB13 may be required to constitutively suppress immune signalling or that PUB13 plays an alternative function, the absence of which results in pleiotropic effects. PUB13 putative ortholog in rice, spotted leaf 11 (SPL11), probably has a conserved function, since *spl11* mutants also display spontaneous cell death lesions and enhanced resistance to rice fungal and bacterial pathogens (Zeng et al. 2004). A target of SPL11 was recently identified as SPL11-interacting protein 6 (SPIN6) a Rho GTPase-activating protein (Rho-GAP) acting on *Os*Rac1, a key component of rice immunity (Liu et al. 2015). Interestingly, loss

of both *pub13* and *spl11* results in the alteration of flowering time, although with opposite effects (Vega-Sánchez et al. 2008, Li et al. 2012).

The mutation of another PUB protein, PUB44 or SAUL1, causes spontaneous cell death (Salt et al. 2011, Disch et al. 2016). *saul1* mutants displayed increased expression of SA-dependent and *PR* genes, which leads to enhanced pathogen resistance. Potentially, SAUL1 is guarded by an R protein. Conversely, Avr9/Cf9 rapidly induced (ACRE) genes *ACRE74* (or *CMPG1*) and *ACRE276* of *Nicotiana tabacum* are PUB E3 ligases induced by elicitation with Avr9 and required for the consequent HR response (González-Lamothe et al. 2006, Yang et al. 2006). Silencing of the tomato *CMPG1* results in decreased resistance to *Cladosporium fulvum* (González-Lamothe et al. 2006). The *ACRE276* homolog in Arabidopsis, *AtPUB17*, is a positive regulator of HR and its expression can complement the phenotype of *ACRE276* silenced tobacco plants (Yang et al. 2006). Interestingly, *AtPUB20* and *AtPUB21*, homologs of *CMPG1*, and *AtPUB17* together with other *PUB* genes were identified in the FLARE data set of flg22-induced genes (Navarro et al. 2004).

U-box-type E3 ligases in hormone signalling

PUB proteins were also often implicated in the regulation of ABA-signalling (Hoth et al. 2002, Cho et al. 2008). Besides regulation of seed germination and plant development, ABA is an important hormone involved in abiotic and biotic stresses (Cao et al. 2011). One of the ABA-mediated responses is the stomatal closure, which upon drought stress minimizes water loss and upon pathogen attack restricts the entry of pathogens (Melotto et al. 2006). Recently, the PP2C protein ABA insensitive 1 (ABI1) was identified as an additional target of PUB12 and PUB13 (Kong et al. 2015). ABI1 is an important ABA co-receptor, constitutively suppressing ABA responses (Gosti et al. 1999). The *pub12 pub13* mutant plants display elevated levels of ABI1 in comparison to Col-0 plants and in consequence are less sensitive to ABA. Indeed, upon ABA treatment they show reduced inhibition of root elongation and reduced seed germination, similarly to the dominant *abi1-1* mutation, as well as reduced stomatal closure and increased drought sensitivity.

Differently, PUB22 and PUB23, together with PUB18 and PUB19 (Seo et al. 2012), were reported to play a role in the negative regulation of drought responses (Cho et al. 2008). Both *pub22 pub23* and *pub18 pub19* double mutants exhibit enhanced drought tolerance. However, while *pub18 pub19*

double mutants display an ABA-mediated increase in stomatal closure, *pub22 pub23* stomatal movements mediated by ABA were invariant in comparison to wild-type plants (Seo et al. 2012). This indicates that PUB22 and PUB23 function through an alternative mechanism independent of ABA in the downregulation of drought responses. Interestingly, PUB22 and PUB23 ubiquitinate the RPN12a subunit of the regulatory particle of the 26S proteasome *in vitro* (Cho et al. 2008). Whether RPN12a function is related to drought responses or whether ubiquitination regulates its stability or other aspects, still need to be investigated.

In addition, PUB10 interacts with a regulator of JA signalling, namely MYC2 (Jung et al. 2016). In root growth assays, *pub10* mutant seedlings phenocopied MYC2 overexpression lines and were both hypersensitive to methyl jasmonate. The stability of MYC2 is enhanced in *pub10* mutant plants, whereas is decreased by expression of PUB10. This suggests that PUB10 destabilizes MYC2. Indeed, PUB10 was able to ubiquitinate MYC2 *in vitro*.

1.3 PUB22

PUB22 was first implicated in plant immunity in the transcriptome analysis performed by Navarro and colleagues (Navarro et al. 2004). Together with its close homologs PUB23 and PUB24, it was identified as a FLARE gene. Subsequent real-time PCR analysis and promoter-GUS fusions confirmed their induction by flg22, *Pst* or *Hyaloperonospora arabidopsidis* (Trujillo et al. 2008). PUB23 and PUB24 have the same domain composition as PUB22 and display 85 % and 51 % of sequence similarity to PUB22 respectively.

Because genetic analyses revealed its prominent role among the *PUB22 PUB23 PUB24* triplet in controlling the intensity of the immune responses upon pathogen attack (Trujillo et al. 2008), further attention has been directed toward PUB22, which led to the identification of Exo70B2 as one of its substrates (Stegmann et al. 2012). This uncovered vesicular trafficking as one of the cellular pathways targeted by PUB22 during immunity.

1.3.1 Domain composition

PUB22 is a U-box-type E3 ubiquitin ligase that belongs to the PUB-ARM subgroup. An Interpro protein sequence analysis (EMBL-EBI) identifies a U-box domain at the N-terminus (aa 6-81) and an ARM-like domain composed of four ARM repeats at the C-terminus (aa 106-413) (Figure 1-2). Furthermore, three disordered regions are predicted by the Russel/Linding definition. They are located between the two domains (aa 83-93), after the first ARM repeat (aa 150-167) and in the final C-terminal end (aa 427-433).
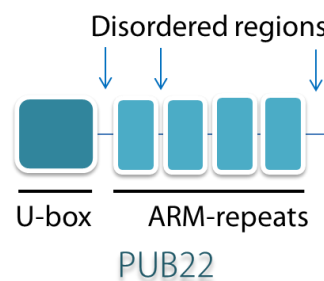
Figure 1-2 Schematic representation of PUB22 domains. PUB22 is composed of a U-box domain at the N-terminus to mediate E2 binding and four ARM-repeats at the C-terminus for target recognition. Disordered regions are indicated by arrows.

1.3.1.1 The U-box domain

The U-box motif is a modified RING domain with similar structure and function. The RING domain is a type of zinc finger domain, with a fold based on the chelation of two zinc ions by a conserved octet of cysteine and histidine residues forming a so-called cross-braced secondary structure (Freemont et al. 1991, Barlow et al. 1994). By contrast, the U-box domain is stabilized by a more dynamic network of hydrogen bonds, which substitute the conserved zinc binding motif located in the RING domains. However, RING and U-box domains share a similar pattern of hydrophobic and polar amino acids (Ohi et al. 2003).

Although clearly essential for substrate ubiquitination, the molecular mechanisms exerted by RING and U-box domains in the transfer of ubiquitin are not fully understood. The crystal structure and superimposition analysis of several animal RING and U-box domains in complex with various

E2~ubiquitin, has suggested that they allosterically promote the transfer of ubiquitin via the modulation of the E2~Ub conjugate stability (Budhidarmo et al. 2012).

Currently, 64 genes in the *Arabidopsis* genome are predicted to encode U-box containing proteins, plainly more than in comparison to the two found in yeast (Ufd2 and Prp19) or the six in mammals (CHIP, CYC4, PRP19, KIAA0860, UFD2a and UFD2b also called ubiquitination factor E4A and E4B) (Hatakeyama et al. 2001). This suggests a diversification of functions in the regulation of plant processes. The U-box domain was first identified in *Saccharomyces cerevisiae* ubiquitin fusion degradation 2 (Ufd2), which was initially thought to function as an E4 ubiquitin elongating factor, and later shown also to function as an E3 playing a role in cell survival during stress conditions (Koegl et al. 1999). All the mammalian U-box containing proteins display E3 ligase activity *in vitro* and have been involved in different biological processes. For example, the precursor RNA processing 19 (PRP19) is an essential pre-mRNA splicing factor (Chanarat & Sträßer 2013) and CHIP is a regulator of cellular proteostasis (Paul & Ghosh 2014).

PUB22 E3 ligase activity was confirmed *in vitro* by autoubiquitination assays, first in combination with yeast E1 and UbcH5b (Trujillo et al. 2008) and subsequently with *At*UBA1 and *At*UBC8 (Stegmann et al. 2012). C13A and W40A U-box mutations abolished its activity (Trujillo et al. 2008), showing that the integrity of the U-box domain is required for E2 binding and activity.

1.3.1.2   The ARM domain

ARM repeats are named after the drosophila armadillo protein, homolog of the human β-catenin (Coates 2003). Each ARM motif, or unit, is composed by three alpha-helices, which are encoded in tandem and create a cylindrical structure called superhelical domain. ARM repeat domains, as well as, ARM-like domains, so named for sharing a similar fold, function in protein-protein interaction. The ARM-like domain of PUB22 was assigned a role in substrate binding, since it was necessary and sufficient to mediate the substrate interaction in Stegmann et al. (2012).

1.3.2 Stabilization

PUB22 is an unstable protein *in vivo*. Proteasome inhibitor treatment led to its accumulation, suggesting a continuous turnover (Figure 1-3 A). Because the inactive mutant PUB22[C13A] displayed enhanced stability *in vivo* (Figure 1-3 A), it is possible that PUB22 constitutively degrades itself via autoubiquitination. However, upon activation of the immune responses by flg22, PUB22 was stabilized. The kinetic of PUB22 stabilization was therefore investigated. As shown in Figure 1-3 B, PUB22 stabilizes already 5 minutes after flg22 treatment, peaks after one hour and becomes unstable again after three hours, suggesting a rapid a transient mechanism for regulation of PUB22 stability and therefore activity.
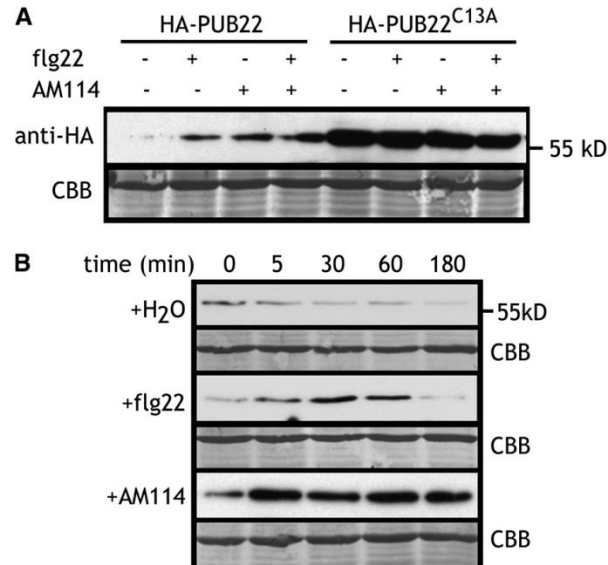
Figure 1-3 PUB22 is stabilized upon flg22 treatment. (A) PUB22 is stabilized 1 h after treatment with 1 µM flg22 or 20 µM AM114 (proteasome inhibitor) in protoplasts. PUB22[C13A] displays intrinsic increased stability. (B) PUB22 stabilization analysis after treatment with 1 µM flg22 or 20 µM AM114 at the indicated time points in transiently transformed protoplasts (Stegmann et al. 2012).

1.3.3 The substrate Exo70B2

In the attempt to elucidate the function of PUB22, a yeast two-hybrid screen carried out with the ARM domain, identified several potential interactors involved in vesicular traffic (Stegmann et al.

2012). This suggests a potential role of PUB22 in the regulation of vesicular trafficking during immunity. Among the identified candidates, Exo70B2 was confirmed as a *bona fide* substrate of PUB22. Exo70B2 is a subunit of the exocyst complex, which is a hetero-octameric protein complex involved in the tethering of vesicles to the PM during exocytosis (Terbush et al. 1996). It functions at the early stage of exocytosis, before SNARE-mediated fusion. The Exo70 subunit works as a spatiotemporal regulator by binding to numerous lipids and proteins. Exo70B2's importance in immunity is supported by the enhanced susceptibility phenotype of the *exo70b2* knockout mutant plants against *Pst* and *Hpa* (Stegmann et al. 2012).

Biochemical *in vitro* analysis confirmed the physical interaction between PUB22 and Exo70B2 as well as Exo70B2 ubiquitination, which most likely has a degradative effect *in vivo*. In fact, Exo70B2 is degraded upon flg22 treatment only when expressed in Columbia 0 (Col-0), but not in *pub22 pub23 pub24* triple mutant protoplasts. Despite the interaction between PUB22 and Exo70B2 is constitutive, flg22 enhanced Exo70B2 degradation as soon as 30 minutes after treatment, which is consistent with PUB22 stabilization. Finally, the interaction with PUB22 was confirmed *in vivo* via bimolecular fluorescence complementation (BiFC) and interestingly, Exo70B2 could also interact with PUB23 and PUB24, highlighting the importance of Exo70B2 regulation. Although the intracellular pathway in which Exo70B2 functions has not yet been identified, unpublished data from our group suggest its involvement in the sorting of PRRs.

In plants, an Exo70 subunit was previously found to potentially be targeted by a PUB E3 ligase. Exo70A1, a putative component of the exocyst complex, was identified as an interactor and an *in vitro* substrate of ARM-repeat containing 1 (ARC1) in *Brassica napus* (Samuel et al. 2009). ARC1 belongs to the subgroup of UND-PUB-ARM proteins and it was the first PUB for which a biological role was identified. ARC1 is required for the rejection of self-pollen in the self-incompatibility (SI) reaction, given that ARC1 knockdown lines display compromised SI (Stone 1999). A similar phenotype was reported for lines overexpressing Exo70A1 in the stigmas, which partially overcome SI (Samuel et al. 2009). In agreement with this, ARC1 was proposed to ubiquitinate Exo70A1 in order to mediate its degradation during the SI response. From its side, Exo70A1 probably mediates the polarized secretion of compatibility factors.

1.4 Regulation of E3 ubiquitin ligases activity

Conceptually, ubiquitination is a linear process. However, substrate ubiquitination is highly regulated, indicating that multiple levels of regulation are present within the ubiquitination cascade. E3 ligases represent the tremendous majority of the UPS components, with a ratio of approximately 1:40 between E2s and E3s. Furthermore, they function as substrate recruiters and therefore their regulation is of critical importance for achieving flawless ubiquitination.

For instance, the accomplishment of a specific ubiquitination event can be modulated through the transcriptional induction of the required E3 ligase, the expression of which would complete the required ubiquitination cascade. As mentioned above, microarray analysis demonstrated that many E3 ligases are indeed induced by different cues such as flg22 (Navarro et al. 2004). Nevertheless, ubiquitination also mediates rapid responses. Thus, posttranscriptional regulation mechanisms are potentially in place to enact the activity of E3 ligases.

Among the CRLs, SCF complexes play a prominent role in phytohormones signalling pathways. The F-box proteins transport inhibitor response 1 (TIR1) and coronatine insensitive 1 (COI1) are regulated by direct binding of the hormone molecule, auxin (Dharmasiri et al. 2005) and JA-Ile (Thines et al. 2007) respectively. This promotes efficient binding to their corresponding substrate proteins, the transcriptional repressors auxin/indole-3-acetic acid (Aux/IAA) and jasmonate ZIM-domain (JAZ). Their subsequent degradation allows auxin/Ja-Ile responsive gene expression. Another layer of regulation relies on the cullin subunit. In all CRLs except for APC/C, the ubiquitin-like modifier NEDD8 is conjugated to cullin. This modification promotes CRL ubiquitination activity by causing structural changes (Duda et al. 2008). Neddylation precludes binding of the Cullin-associated neddylation dissociated CAND1 protein and thereby activates the complex. Indeed, the binding of CAND1 prevents CRL assembly by blocking the substrate adaptor binding site and the neddylation site (Goldenberg et al. 2004). Extensively studied is also the SA signalling activation pathway through the BTB containing proteins NPR3, NPR4, functioning via NPR1. NPR1 is responsible for the transcriptional induction of almost the entirety of SA-responsive genes (Kinkema et al. 2000). In presence of SA, NPR1 binds and transactivates TGA TFs, which mediate SA-responsive genes expression (Zhou et al. 2000, Després et al. 2000). NPR1 possesses several mechanisms of

regulation: redox-regulated oligomerization status (Mou et al. 2003), relocalization from cytosol to the nucleus and phosphorylation and ubiquitination modifications (Spoel et al. 2009).

While the mechanisms controlling CRLs activity are well-characterized, the regulation of the activity of single unit E3 ligases is still a relatively unexplored field in plants.

1.4.1 Regulation of single unit E3 ligases activity

1.4.1.1 Spatial confinement

In the modulation of protein ubiquitination, surely one layer of regulation relies on the physical interaction between the E3 ligase and its substrates or its regulatory proteins. Should the E3 ligase be confined in a separate cellular compartment from them, it would restrict its activity. Keep on going (KEG) RING ligase is a central regulator of ABA signalling that physically interacts with the protein kinase EDR1 (Gu and Innes 2011). EDR1 receives its name from the phenotype of the loss of function *edr1* mutant, which displays enhanced resistance to powdery mildew (Frye & Innes 1998). While KEG resides at the TGN/EE, EDR1 normally localizes at the ER. However, when co-expressed, EDR1 is recruited by KEG to the TGN/EE. EDR1 was proposed to function as a regulator of KEG, by potentially mediating its phosphorylation. Similarly, the PM located *Lotus japonicus* symbiosis receptor-like kinase (SYMRK) relocalizes to punctate structures in the presence of its interactor, the E3 ligase Seven in absentia 4 (SINA4) (Figure 1-4 C) (Den Herder et al. 2012). In this case, SINA4 is proposed to mediate the degradation of SYMRK by ubiquitination. Moreover, also the previously mentioned ARC1, undergoes relocalization in dependency to its putative substrate Exo70A1. When co-expressed with Exo70A1, ARC1 relocalizes to punctate structures (Samuel et al. 2009).

1.4.1.2 Protein-protein interaction

The modulation of ligase activity may also be influenced by an interactor protein. Inhibition of ABI1 phosphatase activity through the binding with the ABA receptor proteins PYLs complexed with ABA is required to activate ABA responses. Despite PUB12 and PUB13 co-immunoprecipitated with ABI1 *in vivo*, ABI1 could not be readily ubiquitinated *in vitro* (Kong et al. 2015). Interestingly, the addition of purified PYLs proteins, as well as ABA, activated ABI1 ubiquitination. Given that the direct

interaction between PUB12/13 and ABI1 remains to be tested, PYLs proteins may enable ABI1 ubiquitination by functioning as a scaffold. Alternatively, their binding to ABI1 may provoke an allosteric conformational change in it, which exposes the target amino acids to be ubiquitinated.

1.4.1.3   Phosphorylation

Interaction studies reported the recurrent association of RING/U-box E3 ligases to the intracellular kinase domain of RLKs, which in several instances leads to their phosphorylation (Furlan et al. 2012). Since the function of RLKs is to relay external cues into the cell, it seems reasonable to hypothesize that ligase phosphorylation modulates their activity, and hence contributes to signal transduction.
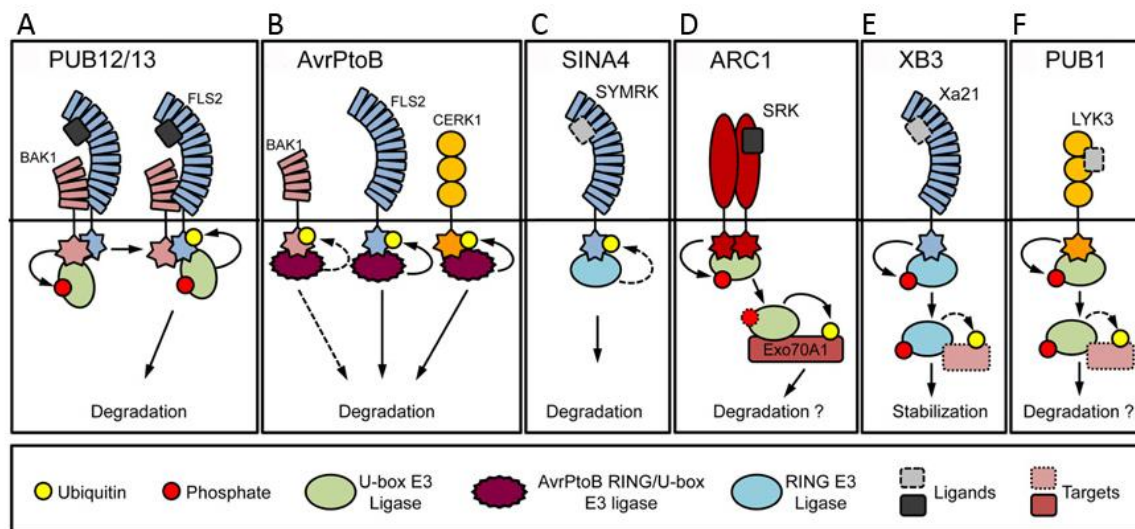
Figure 1-4 Ubiquitin ligases that interact with receptor kinases. (A) The U-box ligases PUB12 and PUB13 constitutively interact with and are phosphorylated by BAK1. Upon flg22-mediated association of BAK1 with FLS2, PUB12 and PUB13 ubiquitinate FLS2 to mediate its degradation. (B) The effector protein AvrPtoB from *Pst* binds and ubiquitinates BAK1, FLS2, and CERK1. Ubiquitination leads to the degradation of FLS2 and CERK1. The function of BAK1 ubiquitination is also proposed to be degradatory. (C) *Lj*SINA4 interacts with and mediates the degradation of SYMRK. Shapes with dotted lines denote potential involvement (e.g., ligand) or a hypothetical target. (D) *Bn*ARC1 interacts with and is phosphorylated by SRK during SI reaction. ARC1 was proposed to regulate SI through Exo70A1 ubiquitination. (E) *Os*XB3 interacts with and is phosphorylated by XA21. XB3 contributes to XA21 accumulation, probably via targeting a XA21-regulating protein. (F) *Mt*PUB1 interacts with and is phosphorylated by LYK3, however LYK3 is not ubiquitinated by PUB1. (adapted from Furlan et al. 2012).

The first described example in plants was reported for ARC1 in Brassica, which interacts and is phosphorylated by the *S*-locus receptor kinase (SRK) (Figure 1-4 D) (Gu et al. 1998). SRK encodes a

functional Ser/Thr kinase, which functions in the SI response. ARC1 co-expression with an active SRK results in its relocalization from the cytosol to the ER (Stone et al. 2003), suggesting that phosphorylation mediates the regulation of ARC1 localization and therefore activity. Other examples of RLK-E3 ligase association include the rice RLK *Xanthomonas oryzae* pv *oryzae* resistance 21 (XA21) which phosphorylates the RING E3 ligase XA21-binding protein 3 (XB3) (Figure 1-4 E) (Y.-S. Wang et al. 2006) and the *Medicago truncatula* Lys motif RLK 3 (LYK3) which phosphorylates PUB1 during symbiosis (Figure 1-4 F) (Mbengue et al. 2010). In spite of E3s phosphorylation being a frequent theme, the impact of their modification is still unknown.

In animals, the function of phosphorylation in the modulation of E3 ligase activity has been more thoroughly studied. Various examples report a phosphorylation-dependent recognition (Stacey et al. 2012) or relocalization of the substrate protein. On the other hand, E3 ligases phosphorylation often results in the modulation of their activity not only by promoting or inhibiting the substrate or the E2 binding, but also by promoting or inhibiting their autoubiquitination (see 1.4.1.5).

1.4.1.4   Autoubiquitination

In addition, another layer of regulation exists, which is inherent to most E3 ligases *in vitro*, the self-catalysed ubiquitination or autoubiquitination. Even though widely employed and accepted for assessing E3 ligase activity *in vitro*, the detailed molecular mechanisms and the functional effects of autoubiquitination *in vivo* have not been elucidated in plants yet. Nevertheless, several plant E3 ligases were reported to require activity to undergo proteasomal degradation, suggesting a role of autoubiquitination in the protein self-destruction. In animals, the regulation of E3 ligases by autoubiquitination and degradation has been documented in a few instances (de Bie & Ciechanover 2011).

In plants, only a few E3 ligases have been shown to be ubiquitinated *in vivo*. KEG ubiquitination and degradation is one of the best characterized examples. ABA treatment was shown to induce KEG ubiquitination and destabilization by degradation through the 26S proteasome (Liu and Stone 2010). Because the ABA-dependent destabilization phenotype was lost in a KEG inactive RING mutant with impaired autoubiquitination activity, it is likely that KEG mediates its own ubiquitination via autoubiquitination. Importantly, autophosphorylation by the kinase domain of KEG is required for its ubiquitination and degradation, providing an additional layer of complexity.

Few PUBs were reported to undergo degradation via the 26S proteasome. The potato E3 ligase CMPG1 is required for the cell death response triggered by a range of pathogen elicitors, including Infestin 1 (Bos et al. 2010). CMPG1 mediates its constant degradation and its activity is necessary for that. The *Phytophthora infestans* (*P. infestans*) effector Avr3a can stabilize CMPG1 by binding to it. Notably, silencing of CMPG1 enhanced the resistance against *P. infestans*. Whether CMPG1 stabilization is the result of its inactivation by masking of the E2 interaction surface or by other means which would permit substrate ubiquitination, requires further investigation.

1.4.1.5 Phosphorylation in the regulation of autoubiquitination of animal E3 ligases

In the animal field, more information are available on the regulation of autoubiquitination. Autoubiquitination was shown to occur via different mechanisms (de Bie & Ciechanover 2011). The nature of the autoubiquitination reaction can be intramolecular (autoubiquitination *in cis*) or intermolecular (autoubiquitination *in trans*). In the latter case, a prerequisite for autoubiquitination is the formation of homooligomers or heterooligomers, in which one protomer mediates the ubiquitination of another protomer in a unidirectional or reciprocal manner.

The HECT ligase Itch is an important regulator of T helper 2 (Th2) cells differentiation. Itch degradation is mediated by autoubiquitination, which occurs intramolecularly (Gallagher et al. 2006). Indeed, gel filtration results from Gallagher and colleagues indicate that Itch is a monomeric protein. Interestingly, phosphorylation enhances its autoubiquitination rate by causing a conformational change that releases the intramolecular inhibition of the HECT domain. Itch phosphorylation results in its enhanced susceptibility to proteolysis.

On the other hand, RING ligases often form oligomers via their RING domain (Deshaies & Joazeiro 2009). The tumor necrosis factor (TNF) receptor-associated factor 6 (TRAF6)-mediated signalling in the NF-κB pathway requires the activation of TRAF6, a RING finger domain containing protein (Chen 2012). TRAF6 is activated by the attachment of non-degradative K63-linked chains, which is mediated by autoubiquitination (Deng et al. 2000). TRAF6 RING homodimerization is required for this, because TRAF6 homodimerization mutants fail to undergo autoubiquitination (Yin et al. 2009). Yet, they preserve the ability to bind the E2. Therefore, should TRAF6 autoubiquitination occur *in trans*, the loss of autoubiquitination activity in those mutants may be attributed to the loss of physical proximity of the two protomers. Indeed, the crystal structure of TRAF6 suggests that

autoubiquitination occurs *in trans*, namely from one E2-TRAF6 complex onto another TRAF6. TRAF6 can also trimerize through its C-terminal coiled-coil and TRAF-C domain (Ye et al. 2002). Phosphorylation in its TRAF6-C region by the STE20-like kinase (MST4) kinase results in the disruption of trimer formation and reduction of autoubiquitination, which ultimately inhibits TRAF6-mediated signalling (Jiao et al. 2015).

Also in the case of the X-linked inhibitor of apoptosis (XIAP), a potent inhibitor of caspases, dimerization via the RING domain is essential for its activity. However, differently from TRAF6, XIAP dimerization is required for E2 binding and subsequent ubiquitin transfer (Nakatani et al. 2013). XIAP was reported to undergo phosphorylation at specific residues, which results in the modulation of its activity. Following virus infection, XIAP is phosphorylated at S430, located in the proximity of the RING domain. This leads to K48-linked autoubiquitination at K322/328, its consequent proteasomal degradation and apoptosis (Nakhaei et al. 2012). On the other hand, phosphorylation in the BIR1 domain at S87 stabilizes XIAP and suppresses cell death during stress conditions, preventing apoptotic neuronal loss (Kato et al. 2011). Despite the molecular mechanisms through which phosphorylation modulates XIAP autoubiquitination activity are not identified yet, one can speculate that it is unlikely that phosphorylation influences dimerization, because neither of the phosphorylated residues is located in the RING domain. Instead, phosphorylation may determine conformational changes, as in the case of Itch, or the recruitment of interacting proteins modifying XIAP activity.

1.5 Aim of the present work

The PUB22, PUB23 and PUB24 triplet was shown to play an important role in the dampening of the immune response. The E3 triplet is involved in the coordination of the intracellular vesicular trafficking through the targeting of its regulatory components for ubiquitination during PTI. Recent work has highlighted the central role of PUB E3s in the regulation of stress responses. However, in spite of the increasing studies regarding the manifold roles of PUB E3 ligases, the mechanisms that regulate ubiquitination, remain unknown. The same holds true for the circa 490 predicted RING/U-box E3 ligases in Arabidopsis.

Therefore, this work aimed at the elucidation of the processes controlling PUB22 activity, which is the best characterized among the PUB22, PUB23 and PUB24 triplet. While PUB22 was highly unstable *in vivo*, the PUB22^{C13A} mutant inactive in autoubiquitination, accumulated to higher levels. Hence, I hypothesized that PUB22 may continuously mediate its degradation *in vivo* via autoubiquitination. However, upon activation of the immune responses, PUB22 is rapidly stabilized, suggesting the existence of a mechanism rescuing PUB22 from degradation. Here, I aimed at identifying the molecular switch regulating PUB22 stability, which potentially acts on its autoubiquitination activity. In particular, I focused my attention on phosphorylation as a putative regulatory modification of PUB22, because of the rapidity of PUB22 stabilization and because of the multitude of phosphorylation events during immunity. Furthermore, I aimed at the molecular understanding of the events through which phosphorylation may modulate both PUB22 auto- and substrate ubiquitination activity. In doing so, I intended to elucidate the cryptic function of E3s autoubiquitination together with its regulation.

2. Materials and methods

2.1 Materials

2.1.1 Chemicals

All chemicals were used in analytical quality. If not specified differently, chemicals and antibiotics were acquired from Carl Roth (Karlsruhe, Germany), SIGMA Aldrich (St. Louis, USA), Merck KGaA (Darmstadt, Germany), Applichem GmbH (Darmstadt, Germany). Plant medium was ordered from Duchefa (Haarlem, Netherlands). Enzymes were acquired from Thermo Fisher Scientific (Waltham, USA), Serva (Heidelberg, Germany). Primers were obtained from MWG (Ebersberg, Germany). Flg22 and elf18 were synthesized in house by Petra Majovsky in the laboratory of Dr. Wolfgang Hoehenwarter at the Leibniz Institute for Plant Biochemistry (Germany).

2.1.2 Media

Lysogeny broth (LB) medium (Luria/Miller): 10 g/l tryptone; 5 g/l yeast extract; 10 g/l sodium chloride. 15 g/l agar-agar were added for solid LB medium.

Rich medium: 10 g/l tryptone; 5 g/l yeast extract; 5 g/l sodium chloride. After autoclaving at 121°C, 2 g/l glucose were added.

Super Optimal broth with Catabolite repression (SOC) medium: 20 g/l tryptone; 5 g/l yeast extract; 0,5 g/l NaCl; 0,18 g/l KCl; pH was adjusted to 7 with NaOH. After autoclaving at 121°C, 0,95 g/l $MgCl_2$ and 3,6 g/l glucose were added. The medium was subsequently sterile filtrated.

Kings broth (KB) medium: 20 g/l peptone; 1,5 g/l K_2HPO_4; 1,5 g/l $MgSO_4$ $5H_2O$; 10 ml/l glycerol. 15 g/l agar-agar were added for solid KB medium.

Half strength Murashige and Skoog (½ MS) medium: 2,2 g/l MS salts including vitamins; 2,5 g/l sucrose; 0,5 g/l MES; pH was adjusted to 5,6 with KOH. 8 g/l phyto agar were added for solid ½ MS medium. 8 g/l Gelrite^{TM} (Duchefa) phyto agar was used for root growth assays.

2.1.3 Plants and plant growth conditions

Arabidopsis thaliana ecotype Col-0 plants and mutants for experiments were grown in phytochambers under short day conditions (8 h light, 16 h dark at 21°C and 60 % humidity). Plants for setting seeds were grown in greenhouse long day conditions (16 h light, 8 h dark at 21°C). Seeds for _pub22 pub23 pub24_ triple mutant plants (SALK_07261, SALK_133841, and SALK_041046 respectively) were generated and provided by Dr. Marco Trujillo (Trujillo et al. 2008). Seeds for _mpk3_ mutant plants (SALK_151594) were described previously (Wang et al. 2007) and were provided by Dr. Justin Lee. Seeds for _PUB22$_{prom}$::GFP-PUB22_ were provided by the host laboratory and generated by cloning 2 Kb of the PUB22 upstream region.

For growth in sterile conditions, seeds were vapor-phase sterilized. The seeds were prepared in ~50 seeds aliquots in 2 ml tubes and placed into a vessel for seed sterilization. 10 ml of 12 % NaClO solution were placed in a beaker into the vessel and 4 ml of 37 % HCl were added. The vessel was sealed and sterilization by chlorine fumes was performed for at least 1 h. Seeds were sowed in liquid ½ MS medium in sterile 6- or 24-well plates according to the amount of plant tissue needed. Alternatively, seeds were also sowed on solid ½ MS medium in round or squared petri dishes. All the seeds were first stratified for two days at 4°C in the dark.

2.1.4 Bacteria

For the purpose of cloning and plasmid preparation, the Top10 strain of _Escherichia coli_ (_E.coli_) bacteria was used with the exception of spectinomycin resistant plasmids which were transformed into the Mach1 strain of _E.coli_. DB3.1 _E.coli_ cells were used for propagation of plasmids containing the _ccd_B gene, such as destination vectors of the Gateway system (Invitrogen). Top10, Mach1, and

DB3.1 cells were grown in LB medium supplemented with the appropriate antibiotics (50 µg/ml kanamycin; 100 µg/ml ampicillin; 100 µg/ml spectinomycin; and/or 34 µg/ml chloroamphenicol) overnight at 37°C. For expression of recombinant fusion proteins, the Rosetta 2(DE3)pLysS strain was used. Recombinant fusion proteins were expressed in LB medium containing the appropriate antibiotics with the exception of recombinant maltose binding protein (MBP) fusion proteins which were expressed in Rich medium. For stable Arabidopsis transformation *Agrobacterium tumefaciens* (*A.tumefaciens*), GV3101::pMP90 strain was employed and grown in LB medium supplemented with 50 µg/ml rifampicin, 25 µg/ml gentamycin (strain) and 100 µg/ml spectinomycin (binary plasmid) for 2 days at 28°C. For pathogen infection *Pseudomonas syringae* pv *tomato* (*Pst*) DC3000 *ΔavrPto/ΔavrPtoB* (Lin & Martin 2005) was used. Bacteria were grown in KB solid medium supplemented with 50 µg/ml rifampicin, 25 µg/ml kanamycin and 50 µg/ml spectinomycin for 2 days at 28°C.

2.1.5 Plasmids

pENTR™/D-TOPO® plasmids carrying the coding sequences (CDS) for *PUB22*, and *PUB24* were generated by Dr. Martin Stegmann (Stegmann et al. 2012) and provided by the host laboratory. For stability assays, the *PUB22* N-terminally HA-tagged construct *pGWB415-PUB22*, the *Exo70B2* N-terminally GFP-tagged construct *pGWB506-Exo70B2* and the *Exo70B2* N-terminally cMyc-tagged construct *pGWB418-Exo70B2* were also provided (Stegmann et al. 2012). For BiFC assay, *pESPYNE-MPK3*, *pESPYNE-MPK4*, *pESPYNE-MPK6*, *pESPYNE-MPK*8 and *pESPYNE-MPK11* plasmids for expression of N-terminal cMyc-nYFP fusions (Pecher et al. 2014) were provided by Dr. Justin Lee. *pCL112-Avr3a^{KI}* plasmid for expression of nYFP-Avr3a^{KI}, effector protein from *P. infestans*, (Engelhardt et al. 2012) was provided by Prof. Paul Birch. Plasmids for expression of the N-terminally cMyc-tagged *Petroselinum crispum* (*Pc*) *MKK5^{KR}* and *MKK5^{DD}* fusion constructs under the control of the 35S promoter (Lee et al. 2004) were provided by Dr. Justin Lee.

For GST-PUB22 recombinant protein expression, the *pGEX-4T-1-PUB22* plasmid (Trujillo et al. 2008) was provided by the host laboratory. *pGEX-4T-1-MPK3* and *pGEX-4T-1-MPK*6 plasmids for expression of N-terminal GST fusions (Feilner et al. 2005) were provided by Dr. Justin Lee. For

expression of recombinant N-terminally His-tagged UBA1 and UBC8, *pDEST17-UBA1* and *pDEST17-UBC8* constructs were provided by the host laboratory.

2.2 Methods

2.2.1 Cloning

2.2.1.1 Site-directed mutagenesis (SDM)

SDM was performed on *pENTR-PUB2*2 or on *pJet1.2-PUB22* entry vectors. PUB22^{T62A}, PUB22^{T62E}, PUB22^{T88A}, PUB22^{T88E}, PUB22^{S422A} and PUB22^{S422E} mutations were generated using the "Type II's restriction digest"-based mutagenesis method for MAPK phosphosites mutation described in Palm-Forster et al. (2012) and a HaeII or a BanII restriction site were introduced at the site of mutagenesis as described in appendix Table I. PUB22^{F10E}, PUB22^{I25R}, PUB22^{W40A}, and PUB22^{T62I} mutations were generated by adapting the "Type II's restriction digest"-based mutagenesis method. Reactions were performed as followed.

SDM polymerase chain reaction (PCR) mix:

Component	Volume [µl]
5X HF buffer	5
dNTPs (10 mM)	0,5
Each Primer (10 µM)	1,25
Template (50 ng/µl)	0,5
DNA polymerase[1]	0,25
Water	16,25

PCR conditions:

Temperature [°C]	Duration	Cycles
98	10''	5
46[2]	30''	5
72	2' 30''	5
98	10''	30
72[3]	2' 30''	30
72	10'	

---

[1] Use exclusively a commercial high-fidelity DNA polymerase (e.g. Phusion Hot Start II High Fidelity DNA Polymerase, Thermo Scientific).
[2] Calculate and use the annealing temperature of the complementary sequence of the primer.
[3] Calculate and use the annealing temperature of the complete primer sequence (maximum 72°C).

After gel electrophoresis, the band corresponding to the size of the plasmid template was eluted in 30 µl of water.

Restriction-ligation reaction mix:

Component	Volume [µl]
Eluate	17
10X Type II restriction buffer	2,5
Type II restriction enzyme	0,4
DpnI fast digest	0,5
T4 DNA ligase	1,5
ATP (10 mM)	1
Water	2,1

Conditions:

Temperature [°C]	Duration	Cycles
37	5'	10
16	5'	10

2-5 µl were used for *E. coli* transformation. The mutation event was confirmed by sequencing. All the primers used for SDM are listed in appendix Table I.

2.2.1.2 Entry clones

PUB22$^{U\text{-}box}$ (1-108 aa; U-box domain and linker region) was cloned into *pDONR201* entry vector via BP reaction (Invitrogen) using the *pESPYNE-PUB22$^{U\text{-}box}$* construct generated by Dr. Martin Stegmann and following the manufacturer instructions. For C-terminal fusions, *PUB22$^{U\text{-}box}$* and *PUB22$^{U\text{-}box}$* mutants without stop codon were cloned via User cloning (New England Biolabs, NEB) from *pENTR-PUB22* and *pENTR-PUB22* mutants into *pENTR3C* entry vector using the primers listed in appendix Table II. Constructs were verified by sequencing.

2.2.1.3 Gateway cloning

Afore-mentioned *pENTR™/D-TOPO®*, *pENTR3C*, and *pDONR201* entry clones for *PUB22* and *PUB22*$^{U-box}$ were used for LR recombination using the Gateway® LR clonase® II enzyme mix (Invitrogen) into different gateway compatible destination plasmids following the manufacturer instructions.

Constructs for plant transformation: To generate N-terminal GFP tag constructs, *PUB22* or *PUB22* mutants were cloned into *pUBN-GFP-Dest* destination plasmid (Grefen et al. 2010). For bimolecular fluorescence complementation assay, *PUB22*^{W40A} was cloned into *pESPYCE-gw* to generate N-terminal HA-cYFP fusion (Ehlert et al. 2006). For split luciferase complementation assay, *PUB22*$^{U-box}$ and *PUB22*$^{U-box}$ carrying F10E, I25R, W40A, T62A, T62E, and T62I point mutations without stop codon were cloned into *pCAMBIA/des/cLuc* and *pCAMBIA/des/nLuc* (Chen et al. 2008) for C-terminal fusions.

Constructs for recombinant protein expression in bacteria: To generate N-terminal GST and His tag, *PUB22*$^{U-box}$ was cloned into *pDEST15* and *pDEST17* respectively (Thermo Fisher Scientific).

2.2.1.4 Classical cloning for recombinant protein expression in bacteria

For cloning into *pMAL-c2X* (NEB), *PUB22* CDS was amplified from *pENTR-PUB22* using primers introducing a 5'-SalI and a 3'-PstI restriction sites. *PUB24* CDS was amplified from *pENTR-PUB24* using primers introducing a 5'-EcoRI and a 3'-PstI restriction sites. Blunt products from PCR were first cloned into *pJET1.2*/blunt (Fermentas), digested with the appropriate combination of restriction enzymes and introduced into the open *pMAL-c2X* by ligation with T4 ligase (Fermentas). All the primers used for cloning are listed in appendix Table II.

The fusion constructs used in this study were tested by restriction digest. The resulting fusion proteins and their size are listed in appendix Table V.

2.2.2 DNA preparation

According to the amount of DNA required, 5 ml or 500 ml of LB medium cultures were used for DNA isolation. DNA purification was performed using Nucleobond® PC 20 Miniprep kit (Macherey Nagel) and Nucleobond® PC 500 Maxiprep kit (Macherey Nagel) respectively by following the manufacturer instructions.

2.2.3 Bacteria Transformations

2.2.3.1 *E.coli* heat shock transformation

A 50 µl aliquot of chemically competent *E.coli* bacteria was thawed for 5 min on ice. 50 ng of plasmid DNA were added to the cells and incubated for 30 min on ice. The cells were then heat shocked for 50 sec at 42°C and subsequently cooled down for 1 min on ice. 150 µl of SOC medium were added and the bacteria were regenerated for at least 1 h at 37°C shaking at 900 rpm. 100 µl of cells were plated on LB plates containing the appropriate antibiotics and incubated overnight in a 37°C incubator.

2.2.3.2 *A. tumefaciens* cold shock transformation

A 50 µl aliquot of chemically competent *A. tumefaciens* bacteria was thawed for 30 min on ice. 200 ng of plasmid DNA were added to the cells and incubated for 30 min on ice. The cells were then cold shocked for 2 min in liquid nitrogen and subsequently thawed at 37°C. 300 µl of SOC medium were added and the bacteria were regenerated for 3 h at 28°C shaking at 500 rpm. 300 µl of cells were plated on LB plates containing the appropriate antibiotics and incubated for 2-3 days in a 28°C incubator.

2.2.4 Generation of transgenic lines

2.2.4.1 Arabidopsis floral-dip transformation

For stable transformation of Arabidopsis, the floral dip method was used. *pub22 pub23 pub24* triple mutant plants were grown for six weeks under short day conditions and then shifted to long day

conditions until flowers were formed. The binary vector *pUBN-GFP* recombined with *PUB22*, *PUB22^{W40A}*, *PUB22^{T62/88A}*, or *PUB22^{T62/88E}* was transformed into GV3101::pMP90 cells of *A. tumefaciens* as described in 2.2.3.2. One resistant colony was picked, inoculated in 50 ml of LB medium and grown at low shaking speed as described in 2.1.4. After 2 days, the bacterial culture was centrifuged for 15 min at 4000 g and the pellet was resuspended to 0,8 of OD_{600} in 5 % sucrose solution and silwet L-77 was added to a final concentration of 0,05 %. The bacterial solution was pipetted onto all inflorescences and plants were sealed for 24 h in autoclavable polyethylene bags. The inflorescences transformation was repeated for 3 times at 7-day intervals. T1 generation dry seeds were collected in paper bags and screened for positive lines.

2.2.4.2   Selection of positive plant lines

T1 generation seeds were sowed on soil and selected by BASTA. 5 days after germination BASTA was sprayed on the seedlings at 200 mg/l concentration. The selection was repeated for 3 times at 7-day intervals. BASTA resistant seedlings were grown under long day conditions and T2 generation seeds were harvested from at least 100 individual T1 plant lines. Approx. 20 T2 generation seeds per line were sowed in liquid ½ MS medium and seedlings were grown for 2 weeks under short day conditions. The lines were screened for the fusion protein expression by immunoblots as in 2.2.9.

2.2.4.3   Segregation analysis and generation of homozygous plants

Lines expressing detectable levels of GFP-PUB22 were selected for segregation analysis. T2 generation seeds were sowed on solid ½ MS medium containing 10 µg/ml glufosinate and single insertion lines were selected based on the survival rate (75 %). Glufosinate-resistant seedlings were grown under long day conditions and T3 generation seeds were harvested from at least 10 individual T2 plants. T3 generation seeds were sowed on solid ½ MS medium containing 10 µg/ml glufosinate and homozygous T3 generation seeds were selected based on the survival rate (100 %). To compare the fusion protein transcripts expression in different lines, 3 individual homozygous plants per line were grown for six weeks under short day conditions and RT-qPCR analyses were performed as described in 2.2.18. Biochemical analyses were performed on homozygous seedlings or on samples consisting of at least 50 pooled seedlings of T2 generation.

2.2.5 Genotyping of T-DNA insertion mutants

2.2.5.1 Genomic DNA isolation

For genotyping analysis, a small portion (approx. 20 mm^2) of adult leaves was harvested in 150 µl of DNA extraction buffer (220 mM Tris-HCl pH 8; 0,8 M NaCl; 22 mM EDTA; 140 mM mannitol; 1 % N-Lauroylsarcosine; 0,8 % CTAB; 1,4 µl/ml β-mercaptoethanol). Leaves were processed in a tissue lyser for 3 min at 24 Hz. 600 µl of DNA extraction buffer were added to the samples. 750 µl of chloroform was added and the solution was mixed by vortexing. Samples were incubated for 1 h at 65°C and subsequently centrifuged for 10 min at 7500 g at 4°C. The supernatant was transferred to a fresh tube and 700 µl of isopropanol were added. The solution was incubated for 15 min at room temperature (RT) after vortexing. DNA was pelleted by centrifuging for 10 min at 23200 g at 4°C. The supernatant was removed and the pellet was washed with 70 % ethanol. DNA pellet was dried at 37°C and dissolved in 20 µl of water.

2.2.5.2 Genotyping PCR

PCR was used to verify T-DNA insertion mutants. Primers used for genotyping are listed in appendix Table III. Per each reaction, 1 µl of genomic DNA isolated as described in 2.2.5.1 was used in the PCR mix:

Component	Volume [µl]
10X Taq Buffer	2
dNTPs (10 mM)	0,4
Each Primer (10 µM)	1
DNA	1
Taq polymerase	0,2
Water	14,4

PCR conditions:

Temperature [°C]	Duration	Cycles
98	30''	35
48	1'	35
72	2'	35
72	10'	

2.2.6 Microsomal fractionation from seedlings

For microsomal fractionation analysis, seeds were sowed on solid ½ MS medium. Seedlings were grown for two weeks under short day conditions. At least 20 seedlings per sample were transferred in 1 ml of ½ MS liquid medium in a clean 24-well plate, where the specified treatments were performed applying vacuum. Seedling samples were then dried on paper, weighed, flash-frozen in liquid nitrogen and ground in a mortar. The frozen powder was resuspended at 0,5 mg/µl in homogenization buffer (250 mM sucrose; 50 mM HEPES-KOH pH 7,5; 5 % glycerol; 10 mM EDTA; 3 mM DTT; 40 µM MG132; 25 mM NaF; 0,5 mM Na_3VO_4; 15 mM β-glycerophosphate; 1 % Protease Inhibitor Cocktail [final concentrations 0,2 mM AEBSF, 0,7 µM Bestatin, 0,7 µM Pepstatin A, 10 µM Leupeptin, 1,4 µM E-64, 1,4 µM Phenanthroline]) and the solution was centrifuged for 5 min at 14000 g at 4°C. The supernatant was transferred into an ultracentrifuge tube and ultracentrifuged for 50 min at 100000 g at 4°C. All the supernatant was removed and the pellet was resuspended without any additional solution by using a plastic pistil. 50 µl of homogenization buffer were used to rinse the stick and added to the solution containing the membrane fraction. 50 µl of supernatant were used for the soluble fraction. 50 µl of SDS-PAGE sample buffer (240 mM Tris-HCl pH 6,8; 0,5 M DTT; 10 % SDS; 50 % glycerol) were added and samples were incubated for 10 min at 65°C. 30 µl were used for immunoblot analysis.

2.2.7 Protoplasts preparation and transformation

Mesophyll protoplasts were isolated from *pub22 pub23 pub24* triple mutant plants, unless otherwise stated, using the "Tape-*Arabidopsis* Sandwich" method as previously described (Wu et al. 2009). The abaxial epidermal layer of well-expanded leaves from six-week-old plants was peeled off by using labelling tape and scotch tape. The peeled surface of the leaves was incubated for 3 h in 10 ml enzyme solution (0,4 M mannitol; 20 mM KCl; 20 mM MES pH 5,7; 1 % cellulose[4]; 0,25 % macerozyme[5]; 0,1 % BSA; 10 mM $CaCl_2$) in a Petri dish. The solution containing the protoplasts was

---

[4] Use exclusively from Serva Cat. N°16419
[5] Use exclusively from Serva Cat. N°28302

then carefully pipetted into a 12 ml-cell culture tube[6] and centrifuged for 3 min at 100 g. The supernatant was removed by inversion of the tube and the protoplast pellet was resuspended in 5 ml W5 solution (154 mM NaCl; 125 mM $CaCl_2$; 5 mM KCl; 2 mM MES pH 5,7). The solution was incubated for 20 min on ice and the protoplasts were pelleted by gravity. The protoplast concentration was determined at this step by using a Fuchs-Rosenthal counting chamber. The supernatant was removed by pipetting and the protoplast concentration was adjusted to $3,5x10^5$ cells per ml of MMG solution (0,4 M mannitol; 15 mM $MgCl_2$; 4 mM MES pH 5,7).

Plasmid DNA for protoplast transformation was prepared by maxiprep as described in 3.1.2. DNA concentration was adjusted to 1 µg/µl and only preparations yielding DNA with high purity (ratio of the absorbance at 260 and 280 nm ($A_{260/280}$) at 1,8-1,9) were used. 10 to 100 µg of the plasmid of interest per each ml of protoplast solution were prepared in a new cell culture tube. Volume of one protoplast transformation varies from 200 µl to 1 ml. The appropriate volume of protoplast solution (1 V) was added to the tube containing DNA. Before the protoplasts settled at the bottom, 1,1 V of PEG solution was added (0,2 M mannitol; 0,1 M $CaCl_2$; 0,8 g/ml PEG 4000[7]). The solution was slowly mixed by inversion of the tube for at least 2 min and incubated at RT for a total of 10 min. The protoplasts were then pelleted by centrifuging for 1 min at 200 g. The supernatant was removed by pipetting and the protoplasts were resuspended in 1 V of W1 solution (0,5 M mannitol; 20 mM KCl; 4 mM MES pH 5,7). Tubes containing transformed protoplasts were incubated overnight horizontally in an air-conditioned room at approx. 20°C.

2.2.8 Protoplast assays and protein extraction

To test the stability of PUB22 in different genetic backgrounds, 30 µg/ml of the *HA-PUB22* construct were transformed in equal protoplast concentrations derived from the indicated plant genotypes. Alternatively, 30 µg/ml of the *HA-PUB22* construct were cotransformed with 40 µg/ml of the *cMyc-PcMKK5* construct. To assess the stability of different PUB22 mutants, 50 µg/ml of the *GFP-PUB22* constructs were used for protoplast transformation. *GFP-Exo70B2* and *cMyc-Exo70B2* were used at 20 µg/ml. 1 h after transformation, 150 µl of protoplasts were aliquoted into 2 ml tubes. The

---

[6] Use exclusively 12 ml-cell culture tubes from Greiner Cat. N° 163 160
[7] Use exclusively PEG MW4000 from Fluka Cat. N° 81242

specified treatments were performed one day after transformation. For protein expression analysis, the protoplasts cells were pelleted for 1 min at 200 g and flash-frozen in liquid nitrogen after removal of the supernatant. 150 µl of protein extraction buffer "Lyse & Load" (50 mM Tris–HCl pH 6,8; 4 % sodium dodecylsulfate [SDS]; 8 M urea; 30 % glycerol; 0,1 M dithiothreitol [DTT]; 0,005 % bromophenol blue) were added to the protoplast pellet and incubated for 10 min at 68°C. 20 µl were used for immunoblot analysis.

2.2.9 Seedling assays and protein extraction

Seeds for PUB22 stability assay were sowed in ½ MS liquid medium. For the analysis of MAPKs activation, seeds were sowed on solid ½ MS medium. Two independent transgenic lines (A and B) were used for analysis. Seedlings were grown for two weeks under short day conditions. Pools of at least 20 seedlings were transferred in 1 ml of ½ MS liquid medium in a clean 24-well plate, where the specified treatments were performed. Seedling samples were then dried on paper, weighed, flash-frozen in liquid nitrogen and ground in a mortar. The frozen powder was resuspended at 1 mg/µl in protein extraction buffer "Lyse & Load", incubated for 10 min at 68°C and centrifuged for 5 min at 6000 g. 30 µl were used for immunoblot analysis. For comparison of proteins from different transgenic lines, PAGE was carried out in parallel, gel sections containing the protein of interest were blotted onto a single membrane and developed by exposing films to chemiluminescence.

2.2.10 BiFC assay

For BiFC assay, 50 µg/ml of the *HA-cYFP-PUB22*^{W40A} construct and 50 µg/ml of the *cMyc-nYFP* fusion construct for one of the indicated *MPKs* were used to transform 500 µl protoplasts together with 30 µg/ml of a plasmid encoding the mCherry fluorescent protein. One day after transformation the protoplasts were treated with the indicated compounds and analysed. The YFP reconstitution signal was assessed by LSM710 (Zeiss) with the following settings: YFP excitation 488 nm; emission detection 510-560 nm; mCherry excitation 594 nm; emission detection 600-640 nm. For protein expression analysis, protoplast samples were prepared as in 2.2.8.

2.2.11 Split-luciferase assay

For split luciferase assay, 50 µg/ml of plasmids expressing *PUB22$^{U\text{-}box}$-cLuc* and *PUB22$^{U\text{-}box}$-nLuc* (and the indicated mutant combinations) were used to transform 500 µl protoplasts. Luciferase assays were performed one day after transformation in white 96-well titer plates. 1 µl of the 100 mM stock solution of the substrate D-luciferin was aliquoted in each well to have a final concentration of 1 mM. 99 µl of the transformed protoplasts were then added to each well. After 3 min of incubation in the dark, the luminescence signal was measured by an Infinite® 200 PRO (Tecan) plate reader with a signal integration time of 20 s. For protein expression analysis, protoplast samples were prepared as in 2.2.8.

2.2.12 Immunoprecipitation assay (IP)

For IP, seeds of the indicated genotype were sowed in ½ MS liquid medium and seedlings were grown for two weeks under short day conditions. Approx. 50-75 seedlings were transferred in 5 ml of ½ MS liquid medium in clean 6-well plates, where the specified treatments were performed. Seedling samples were then dried on paper, weighed, flash-frozen in liquid nitrogen and ground in a mortar. The powder (approx. 1 g) was then resuspended in 1 ml of lysis buffer (50 mM Tris-HCl pH 7,5; 150 mM NaCl; 5 % glycerol; 1 mM EDTA, 5 mM DTT; 50 µM MG132; 50 µM PR-619; 50 µM NSC-632839; 1 mM 4- benzenesulfonyl fluoride hydrochloride; 1 % Protease Inhibitor Cocktail; 1 mM NaF; 0,5 mM Na$_3$VO$_4$; 15 mM β-glycerophosphate; 1 % Nonidet P-40) and cleared by centrifugation for 10 min at 14000 g. The supernatant was diluted with 1 ml of dilution buffer (lysis buffer lacking Nonidet P-40) and incubated under rotation for 3 h at 4°C with 10 µl of GFP-Trap-A beads (Chromotek) for co-IP experiments or 30 µl of GFP-Trap-A beads for *in vivo* ubiquitination experiments and for mass spectrometry analysis. Beads were washed four times with 500 µl of dilution buffer and the bound fraction was eluted by adding 40 µl of SDS-PAGE sample buffer and cooking the beads for 10 min at 95°C. 15 µl were used for immunoblot analysis with the specified antibodies. For mass spectrometry analysis the complete eluate was separated on SDS-PAGE and after staining with Pierce® Silver Stain for mass spectrometry, the GFP-PUB22 corresponding band was excised.

2.2.13 *In vitro* assays

2.2.13.1 Recombinant protein expression and purification
<u>MBP-tagged recombinant proteins expression and purification</u>

pMAL-c2X vectors carrying *PUB22*, *PUB22^{F10E}*, *PUB22^{I25R}*, *PUB22^{W40A}*, *PUB22^{T62A}*, *PUB22^{T62E}*, *PUB22^{T62I}*, *PUB22^{T88A}*, *PUB22^{T88E}*, *PUB22$^{T62/88A}$*, *PUB22$^{T62/88E}$*, or *PUB24* were transformed into Rosetta 2(DE3)pLysS strain as described in 2.2.3.1. One resistant colony was picked to inoculate 5 ml of Rich medium supplemented with 34 µg/ml chloramphenicol and 100 µg/ml ampicillin and bacteria were grown overnight at 37°C with shaking. 1 ml of overnight culture was used to inoculate 100 ml of fresh Rich medium (34 µg/ml chloramphenicol; 100 µg/ml ampicillin) and bacteria were grown for approx. 3 h at 37°C with shaking. At OD_{600} = 0,5, protein expression was induced with 0,2 mM Isopropylthiogalactosid (IPTG) and the culture was incubated for more 3 h at 28°C with shaking. Bacteria were harvested in 50 ml aliquots by centrifuging for 15 min at 6000 g and the pellet was frozen at -20°C. 10 ml of chilled Column buffer (20 mM Tris-HCl pH 7,5; 200 mM NaCl; 1 mM EDTA; 1 mM DTT; 1 mM AEBSF) were added to the bacterial pellet and the cells were resuspended by vortexing. 1 mg/ml lysozyme was added and enzymatic digestion was carried out for 30 min on ice. Bacteria were lysed using a Bandelin SONOPULS homogenizer with a VS70T probe by sonicating for three cycles consisting of 15 s pulse and 15 s pause at 50 % output each. Triton X-100 was added at 0,5 % final concentration and the solution was incubated for 30 min at 4°C under slow rotation. Debris was pelleted by centrifuging for 30 min at 4°C at 23200 g. The supernatant was incubated with 100 µl of amylose beads (NEB) for 1 h at RT under slow rotation in 15 ml tubes. Beads were pelleted by centrifuging for 5 min at 500 g and were washed with 3 ml of chilled Column buffer for three times. After the last washing step, residual Column buffer on the beads was completely removed by using pipet tips for gel loading. Elution was performed by adding 100 µl of elution buffer (Column buffer supplemented with 10 mM maltose) to the beads and incubating for 30 min at RT. The eluted protein[8] was recovered using pipet tips for gel loading and the protein concentration was measured using a Direct Detect® Spectrometer.

---

[8] MBP-PUB22, MBP-PUB22 mutants and MBP-PUB24 purified proteins were used for experiments only within the same day of protein preparation due to activity loss during the storage conditions tested.

GST-tagged recombinant proteins expression and purification

pDEST15-PUB22[U-box], *pGEX-4T-1-PUB22*, *pGEX-4T-1-MPK3*, *pGEX-4T-1-MPK6*, and empty *pGEX-4T-1* plasmids for N-terminal GST fusions expression or free GST expression were transformed into Rosetta 2(DE3)pLysS strain as described in 2.2.3.1. One resistant colony was picked to inoculate 5 ml of LB medium supplemented with 34 µg/ml chloramphenicol and 100 µg/ml ampicillin and bacteria were grown overnight at 37°C with shaking. 1 ml of overnight culture was used to inoculate 100 ml of fresh LB medium (34 µg/ml chloramphenicol; 100 µg/ml ampicillin) and bacteria were grown for approx. 3 h at 37°C with shaking. At OD_{600} = 0,3, protein expression was induced with 0,2 mM IPTG for GST-PUB22[U-box], 0,25 mM IPTG for GST-PUB22 and 0,4 mM IPTG for GST-MPKs and the cultures were incubated for more 3 h at 28°C with shaking. Bacteria were harvested in 50 ml aliquots by centrifuging for 15 min at 6000 g and the pellet was frozen at -20°C. 10 ml of chilled PBS (140 mM NaCl; 2,7 mM KCl; 10 mM Na_2HPO_4; 1,8 mM KH_2PO_4; 2,5 mM DTT; 1 mM AEBSF) were added to the bacterial pellet and the cells were resuspended by vortexing (for GST-PUB22, 0,75 % N-Lauroylsarcosine was used in addition). 1 mg/ml lysozyme was added and enzymatic digestion was carried out for 30 min on ice. Bacteria were lysed using a Bandelin SONOPULS homogenizer with a VS70T probe by sonicating for three cycles consisting of 15 s pulse and 15 s pause at 50 % output each. Triton X-100 was added at 0,5 % final concentration (for GST-PUB22, 1,5 % TritonX-100 final concentration was used) and the solution was incubated for 30 min at 4°C under slow rotation. Debris was pelleted by centrifuging for 30 min at 4°C at 23200 g. The supernatant was incubated with 100 µl of Protino® Glutathione Agarose 4B beads (Macherey-Nagel) for 1 h at RT under slow rotation in 15 ml tubes (for GST-PUB22, 1 ml aliquots in 1,5 ml tubes were incubated with 15 µl beads). Beads were pelleted by centrifuging for 5 min at 500 g and were washed with 3 ml of chilled PBS for three times (for GST-PUB22, 1 ml was used). After the last washing step, residual PBS on the beads was completely removed by using pipet tips for gel loading. In case of GST-PUB22[U-box], GST-MPK3, GST-MPK6 and free GST, elution was performed by adding 100 µl of elution buffer (50 mM Tris-HCl and 15 mM reduced glutathione at pH 8) to the beads and incubating for 30 min at RT. The eluted protein was recovered using pipet tips for gel loading and the protein concentration was assessed by SDS-PAGE and coomassie brilliant blue (CBB). In case of GST-PUB22 elution was not performed, but protease cleavage to generate the untagged protein was carried out as described in 2.2.13.3.

2. Materials and methods

His-tagged recombinant proteins expression and purification

pDest17 vectors carrying *UBA1* or *UBC8* were transformed into Rosetta 2(DE3)pLysS strain as described in 2.2.3.1. One resistant colony was picked to inoculate 5 ml of LB medium supplemented with 34 µg/ml chloramphenicol and 100 µg/ml ampicillin and bacteria were grown overnight at 37°C with shaking. 5 ml of overnight culture was used to inoculate 500 ml of fresh LB medium (34 µg/ml chloramphenicol; 100 µg/ml ampicillin) and bacteria were grown for approx. 3 h at 37°C with shaking. At OD_{600} = 0,5, protein expression was induced with 0,5 mM IPTG and the culture was incubated for more 2 h at 28°C for UBA1 or 4 h at 22°C for UBC8 with shaking. Bacteria were harvested by centrifuging for 15 min at 6000 g and the pellet was frozen at -20°C. 25 ml of chilled Lysis-Elution-Washing (LEW) buffer (50 mM NaH_2PO_4; 300 mM NaCl; 1 mM DTT; 1 mM AEBSF at pH 8) were added to the bacterial pellet and the cells were resuspended by vortexing. 1 mg/ml lysozyme was added and enzymatic digestion was carried out for 30 min on ice. Bacteria were lysed using a Bandelin SONOPULS homogenizer with a VS70T probe by sonicating for six cycles consisting of 15 s pulse and 20 s pause at 60 % output each. Debris was pelleted by centrifuging for 30 min at 4°C at 23200 g. The supernatant was filtrated through 0,45 µm cellulose acetate filters. The supernatant was incubated with 500 mg of Protino Ni-Ted resin (Macherey Nagel) for 1 h at RT under slow rotation (batch purification) or in columns (gravity flow purification) pre-equilibrated with LEW buffer. Beads were washed with 15 ml of LEW buffer. Elution was performed by adding 3 ml of elution buffer (LEW buffer supplemented with 200 mM imidazole) to the resin. The His-UBA1 eluted protein was concentrated using Amicon 100K and His-UBC8 using Amicon 10K centrifugal filter units (Merck Millipore) following manufacturer instructions. Protein concentration was measured using a Direct Detect® Spectrometer. Concentrated His-UBA1 and His-UBC8 were stored at 1-10 µg/µl concentration in LEW buffer supplemented with 25 % glycerol in 5 µl aliquots at -80°C.

2.2.13.2 *In vitro* pull-down assays

PUB22 interaction with MPKs

For pull-down assays, GST-MPK3, GST-MPK6 or free GST were used as baits and MBP-PUB22 as prey. Proteins were expressed as described in 2.2.13.1 and free GST and GST fusion proteins were immobilized on 15 µl of Protino® Glutathione Agarose 4B beads (Macherey Nagel) per sample and washed three times with PBS. 1 ml of syringe filtrated bacterial lysates containing MBP-PUB22 was

added to the beads and co-incubated for 1 h at RT under slow rotation. Beads were pelleted by centrifuging for 5 min at 500 g and were washed with PBS for three times. After the last washing step, residual PBS on the beads was completely removed by using pipet tips for gel loading. Elution was performed by adding 60 µl of elution buffer (50 mM Tris-HCl and 15 mM reduced glutathione at pH 8) and incubating it for 10 min at RT. Eluates were analysed by immunoblot.

PUB22 homo- and heterooligomerization

For pull-down assays to test PUB22 homooligomerization or heterooligomerization with PUB24, GST-PUB22^{U-box} or free GST were used as baits and His-PUB22^{U-box}, MBP-PUB22, MBP-PUB22^{W40A} or MBP-PUB24 as preys. Proteins were expressed as described in 2.2.13.1 and free GST and GST fusion proteins were immobilized on 15 µl of Protino® Glutathione Agarose 4B beads (Macherey Nagel) per sample and washed three times with PBS. 1 ml of syringe filtrated bacterial lysates containing preys was added to the beads and co-incubated for 1 h at RT under slow rotation. Beads were pelleted by centrifuging for 5 min at 500 g and were washed with PBS for three times. After the last washing step, residual PBS on the beads was completely removed by using pipet tips for gel loading. Elution was performed by adding 30 µl of SDS-PAGE sample buffer and incubating the samples for 10 min at 68°C. Eluates were analysed by immunoblot.

2.2.13.3   *In vitro* ubiquitination assays
Untagged PUB22 preparation and autoubiquitination assay

To obtain untagged PUB22 to be used in a ubiquitination assay, the GST-PUB22 fusion protein was expressed and purified as described in 2.2.13.1. GST-PUB22 was immobilized on Protino® Glutathione Agarose 4B (Macherey Nagel) and, after washing, the beads were incubated in 25 µl PBS buffer in the presence of 1 unit of Thrombin for 4 h at 22°C. The supernatant containing the untagged PUB22 was then transferred into a new tube and incubated in a total of 30 µl with ubiquitination buffer (25 mM Tris-HCl pH 7,5, 5 mM MgCl$_2$, 50 mM KCl, 0,6 mM dithiothreitol, 2 mM ATP, 2 µg ubiquitin from bovine erythrocytes), 0,2 µg of His-UBA1 and 1,2 µg of His-UBC8 overnight at 22°C. The ubiquitination reaction was stopped by addition of 30 µl of SDS-PAGE sample buffer and incubation for 10 min at 68°C. 30 µl were used for immunoblot analysis.

2. Materials and methods

PUB22 autoubiquitination assay

Enzymes required for ubiquitination assay were expressed and purified as described in 2.2.13.1. In a total of 30 µl, 0,2 µg of His-UBA1 and 1,2 µg of His-UBC8 were mixed together with 2 µg of recombinant PUB22 or recombinant PUB22 mutants in ubiquitination buffer (25 mM Tris-HCl pH 7,5, 5 mM $MgCl_2$, 50 mM KCl, 0,6 mM dithiothreitol, 2 mM ATP, 2 µg ubiquitin from bovine erythrocytes) and incubated at 30°C for the indicated time. The reaction was stopped by the addition of 10 µl of SDS-PAGE sample buffer and incubated for 10 min at 68°C. 10 µl were used for immunoblot analysis.

Substrate ubiquitination assay

Enzymes required for ubiquitination assay and target proteins were expressed and purified as described in 2.2.13.1. For substrate ubiquitination assay His-Exo70B2, purified by Dr. Marco Trujillo, was used as a substrate of MBP-PUB22 (Stegmann et al. 2012) and MBP-PUB22 mutants. For transubiquitination assay MBP-PUB22^{W40A} was used as a substrate of GST-PUB22^{U-box}. 2 µg of the indicated E3 ligases and 3 µg of the respective substrates were incubated together with 0,2 µg of His-UBA1 and 1,2 µg of His-UBC8 in a total of 30 µl of ubiquitination buffer lacking ubiquitin for 1 h at 30°C to allow interaction. After addition of ubiquitin, the ubiquitination reaction was carried out at 30°C for the indicated time. The reaction was stopped by the addition of 10 µl of SDS-PAGE sample buffer and incubated at 68°C for 10 min. 10 µl were used for immunoblot analysis.

2.2.13.4 *In vitro* phosphorylation assay

In vitro phosphorylation assays were performed by Dr. Lennart Eschen-Lippold in the laboratory of Dr. Justin Lee at the Leibniz Institute for Plant Biochemistry (Germany). *In vitro* phosphorylation assays were performed in kinase buffer (20 mM HEPES pH 7,5; 15 mM $MgCl_2$; 5 mM EGTA; 1 mM DTT; 0,1 mM ATP; 2 µCi [gamma-^{32}P]ATP) using recombinant MBP-PUB22 and MBP-PUB24 and active GST-MPK3, GST-MPK4 or non-tagged MPK6 (preactivation was performed using constitutively active *Pc*MKK5^{DD} [Lee et al., 2004]). Samples were incubated for 30 min at 37 °C; reactions were stopped by the addition of SDS-PAGE sample buffer and separated by 10 % bis-acrylamide SDS-PAGE. Gels were stained with CBB and analysed by autoradiography.

2.2.14 Pathogen infection assay

Arabidopsis plants were grown for six weeks in a short day condition phytochamber. The day before infiltration, plants were brought in the laboratory where the infiltration takes place in order to acclimatize and watered copiously. *Pst ΔavrPto/ΔavrPtoB* were grown for two days at 28°C on KB media as described above. Using a plating spatula, the bacteria were resuspended in sterile water and the bacterial solution was adjusted to 10^8 cfu/ml (OD_{600} = 0,2). The solution was then diluted to 10^5 cfu/ml and used for infiltration. Three plants per genotype were used for one experiment and two leaves per plant were infiltrated with a needleless 1 ml syringe. Two days after infiltration, four leaf discs per plant were harvested using a 5 mm diameter biopsy punch (Ratiomed®) in a 2 ml tube. After adding 100 µl of sterile water and a metallic grinding bead per tube, samples were ground for 3 min at 27 rpm in a tissue lyser. 20 µl lysate was added to 180 µl sterile water to give the first 10^{-1} dilution in 96 well plates. Subsequent 1 to 10 dilution series were done in the same manner. A 15 µl drop of the 10^{-2} to 10^{-7} dilutions was pipetted and dried on LB plated containing rifampicin (50 mg/ml). Cfu were scored two days after incubation at 28°C. Logarithmic functions of the bacteria scores in the three plants were used to calculate the average growth per genotype.

2.2.15 Root growth inhibition assay

For root growth inhibition assays, T3 generation homozygous seedlings selected as described in 2.2.4.3 were used. Seeds were sowed on solid ½ MS medium plates, stratified and germinated vertically for 5 days under long day conditions. Seedlings with the same size were then transferred onto solid ½ MS medium square plates supplemented with 1 µM flg22 or DMSO as a vehicle control. Twelve seedlings per plate were placed on a row at 2 cm from the top edge and 0,9 cm between one another. They were grown vertically for 14 days under long day conditions. Root length was measured using ImageJ software.

2.2.16 Proteomics

Identification of phosphopeptides by LC-MS/MS

Mass spectrometry analyses were performed by Petra Majovsky in the laboratory of Dr. Wolfgang Hoehenwarter at the Leibniz Institute for Plant Biochemistry (Germany). Site-specific phosphorylation of PUB22 by MPK3 and MPK4 was studied *in vitro* by kinase assay followed by liquid chromatography on-line with high-resolution accurate mass mass spectrometry (HR/AM LC-MS). Proteins were separated with SDS-PAGE. Following in-solution protein digestion with trypsin, phosphorylated peptides were enriched using TiO_2 affinity chromatography. Peptides were separated using C18 reverse-phase chemistry employing a pre-column (EASY column SC001, length 2 cm, ID 100 µm, particle size 5 µm) in line with an EASY column SC200 with a length of 10 cm, an inner diameter (ID) of 75 µm and a particle size of 3 µm (both from Thermo Fisher Scientific). Peptides were eluted into a Nanospray Flex ion source (Thermo Fisher Scientific) with a 30 min gradient increasing from 5 % to 40 % acetonitrile in ddH_2O and electrosprayed into an Orbitrap Velos Pro mass spectrometer (Thermo Fisher Scientific). The source voltage was set to 1.9 kV, the S-Lens RF level to 50 %. The delta multipole offset was -7.00. The phospho-peptide fraction was measured with a data-dependent acquisition (DDA) scan strategy with inclusion list to specifically target PUB22 peptides bearing an MAPK phosphorylation site motif potentially phosphorylated by MPK3, MPK4 and MPK6 for MS/MS peptide sequencing. The AGC target value was set to 1e06 and the maximum injection time (max IT) to 500 ms in the Orbitrap. The parameters were set to 1e04 and 100 ms in the LTQ with an isolation width of 2 Da for precursor isolation and MS/MS scanning. Multi stage activation (MSA) was applied to further fragment ion peaks resulting from neutral loss of the phosphate moiety by dissociation of the high energy phosphate bond to generate b- and y-fragment ion series rich in peptide sequence information. MS/MS spectra were used to search the TAIR10 database with the Mascot software v.2.5 integrated in Proteome Discoverer v.1.4. The enzyme specificity was set to trypsin and two missed cleavages were tolerated. Carbamidomethylation of Cys was set as a fixed modification and oxidation of methionine and phosphorylation of Ser and Thr as variable modifications. The precursor tolerance was set to 7 ppm and the product ion mass tolerance was set to 0.8 Da. A decoy database search was performed to determine the peptide false discovery rate (FDR). The phosphoRS module was used to localize the phosphorylation site in the peptide's primary structure.

To identify the phosphorylation sites *in vivo*, *UBQ10::GFP-PUB22^W40A^/pub22 pub23 pub24* seedlings were grown for 14 days in ½ MS liquid medium and treated +/- flg22 (1 µM) for 30 min. GFP-PUB22 was immunoprecipitated using GFP-trap beads as described in 2.2.12 and separated with SDS-PAGE and in-gel digested using a combination of Glu-C and trypsin. Phosphorylated peptides were enriched as above and separated as above on an EASY-nLC 1000 LC system with a column length of 50 cm, ID of 75 µm and a particle size of 2 µm using a 90 min gradient and a flow rate of 250 nl/min. Peptides were electrosprayed on-line into a QExactive Plus mass spectrometer from Thermo Fisher Scientific. The spray voltage was 1.9 kV, the capillary temperature 275°C and the Z-Lens voltage 240 V. A full MS survey scan was carried out with chromatographic peak width set to 15 s, resolution 70,000, automatic gain control (AGC) 3E+06 and a max IT of 200 ms. MS/MS peptide sequencing was performed using a Top10 DDA inclusion list scan strategy as above with HCD fragmentation. MS/MS scans were acquired with resolution 17,500, AGC 5E+04, IT 150 ms, isolation width 1.6 m/z, normalized collision energy 28, under fill ratio 3 % and an intensity threshold of 1E+04. MS/MS spectra were searched as above with enzyme specificity set to trypsin + Glu-C tolerating three missed cleavages, a precursor tolerance of 5 ppm and a product ion mass tolerance of 0.02 Da.

Identification of ubiquitinated peptides by LC-MS/MS

Mass spectrometry analysis was performed by Dr. Hirofumi Nakagami at the RIKEN Center for Sustainable Resource Science in Yokohama (Japan). GST-PUB22 was incubated overnight for autoubiquitination assay with His-UBA1 and His-UBC8 as described in 2.2.13.3. Proteins were separated with SDS-PAGE. In-gel digestions were performed as described previously (Shevchenko et al. 2006). Digested peptides in gel pieces were recovered by adding 5 % formic acid/acetonitrile, desalted using StageTips (Rappsilber et al. 2003), dried in a vacuum evaporator, and were dissolved in 5 % acetonitrile containing 0.1 % trifluoroacetic acid. An LTQ-OrbitrapXL coupled with an EASY-nLC1000 (Thermo Fisher Scientific) was used for LC-MS/MS analyses. Self-pulled needle packed with C18 resin was used as an analytical column (Ishihama et al. 2002). Spray voltage of 2,400 V was applied. Mobile phase consisted of 0.5 % acetic acid (A) and 0.5 % acetic acid and 80 % acetonitrile (B). Two-step linear gradient of 0 % to 40 % B in 30 min, 40 % to 100 % B in 5 min, and 100 % B for 10 min was employed at a flow rate of 500 nL/min. MS scan range was m/z 300 to 1,400. Top-10 precursor ions were selected in MS scan by Orbitrap with 100,000 resolution and for subsequent

MS/MS scans by ion trap in automated gain control mode, where automated gain control values of 5.00e+05 and 1.00e+04 were set for full MS and MS/MS, respectively. Normalized collision-induced dissociation was set to 35.0. Lock mass function was used to obtain constant mass accuracy during gradient analysis (Olsen et al. 2005). Database searching was performed as described previously (Nakagami et al. 2010). Peptides were identified by means of automated database searching using Mascot version 2.5 (Matrix Science) in the TAIR database containing protein sequence information of GST-fused PUB22 with a precursor mass tolerance of 3 ppm, a fragment ion mass tolerance of 0.8 Da, and strict trypsin specificity (Olsen et al. 2004) allowing for up to two missed cleavages. Carbamidomethylation of Cys was set as a fixed modification, and oxidation of Met and diGly modification of Lys were allowed as variable modifications.

2.2.17 Immunoblot and antibodies

Protein samples were analysed on 10 % bis-acrylamide SDS-PAGE. Following the separation on SDS-PAGE, the proteins were transferred in wet conditions onto PVDF membranes (GE Healthcare) for 70 min at 100 V. Membranes were then blocked with blocking solution (3 % milk solution in TBS-T 0,1 % Tween 20) for 1 h at RT. Membranes were immunoblotted overnight at 4°C using blocking solution supplemented with the following primary antibodies:

2. Materials and methods

Antibody	Producer	Catalogue number	Dilution	Secondary antibody
anti-*At*MPK3	Sigma-Aldrich	M8318	1:5000	anti-rabbit
anti-cMyc	Sigma Aldrich	C3956	1:5000	anti-rabbit
anti-GFP	Santa Cruz Biotechnology	Sc-8334	1:3000	
anti-GST	GE Healthcare	27-4577	1:5000	anti-goat
anti-HA	Eurogentec	MMS-101P	1:1000	anti-mouse
anti-His	MACS	130-092-785	1:10000	
anti-HSP90	Provided by Prof. Ken Shirasu		1:5000	anti-rabbit
anti-Luciferase	Sigma-Aldrich	L0159	1:5000	anti-rabbit
anti-MBP	Sigma-Aldrich	M1321	1:5000	anti-mouse
anti-phospho-p44/42 MAPK	Cell Signaling Technology	9101	1:1000[9]	anti-rabbit
anti-PIP2:2	Agrisera	AS09 490	1:5000	anti-rabbit
anti-PUB22	Thermo Fisher Scientific	generated against the C-terminal peptide RVWRESPCVPRNLYD SYPA	1:5000[10] 1:1000[11]	anti-rabbit
anti-ubiquitin	Santa Cruz Biotechnology	sc-8017	1:5000	anti-mouse

And the following secondary antibodies coupled to HRP:

Antibody	Producer	Catalogue number	Dilution
anti-goat	Santa Cruz Biotechnology	sc-2020	1:30000
anti-mouse	Sigma Aldrich	A8924	1:5000
anti-rabbit	Sigma Aldrich	A6154	1:5000

---

[9] Use 3 % BSA in TBS-T 0,1 % Tween 20 as blocking solution. After blocking, antibodies were added to the BSA blocking solution.
[10] Use this dilution for the detection of recombinant proteins expressed in *E. coli*.
[11] Use this dilution for the detection of fusion proteins expressed *in vivo*. Use 3 % BSA in TBS-T 0,1 % Tween 20 as blocking solution. After blocking, antibodies were added to the BSA blocking solution.

2.2.18 cDNA synthesis and quantitative PCR

Analysis was performed by Kathrin Kowarschik in the laboratory of Dr. Marco Trujillo at the Leibniz Institute for Plant Biochemistry (Germany).

Total RNA was prepared from adult Arabidopsis leaves using a Plant RNA Mini Kit (E.Z.N.A.® Omega bio-tek) followed by a DNaseI digestion (Thermo Fisher Scientific). For first-strand synthesis, 1 µg of total RNA was converted into cDNA with the Maxima First Strand cDNA Synthesis Kit for RT-qPCR (Thermo Fisher Scientific) according to the manufacturer's protocol. The cDNA was diluted to fixed quantities (9,5 ng per reaction of reverse transcribed total RNA).

Quantitative PCR was performed in 20 µl reaction volume, including 9,5 ng of reverse transcribed total RNA, 0,3 µM of each gene-specific primer (appendix Table IV) and Maxima SYBR Green qPCR Master Mix 2X (Thermo Fisher Scientific). Corresponding minus reverse transcriptase and no template controls were performed with each primer pair. The qPCR reaction was performed using a Bio-Rad CFX device with the following protocol:

Temperature [°C]	Duration	Cycles
95	10'	1
95	15''	40
60	30''	40
72	30''	40

Subsequent standard dissociation protocol to validate the presence of a unique PCR product was performed.

In order to calculate relative transcription levels, the delta of threshold cycle (ΔCt) values were calculated by subtracting the arithmetic mean Ct values of the target *PUB22* from the arithmetic mean Ct value of the normalizing *AtPP2A* (*At*1G13320), which was obtained from the three technical replicates. The relative transcription level ($2^{-\Delta Ct}$) of each biological replicate is represented by the arithmetic mean of the three technical replicates.

3. Results

3.1 The role of the transcriptional regulation of PUB22 in protein accumulation

The aim of this work was to elucidate the mechanisms regulating PUB22 activity. The transcriptional induction of *PUB22* was shown to be strongly and rapidly enhanced within one hour upon pathogen perception (Trujillo et al. 2008). However, when expression was driven by a strong constitutive promoter such as the *Ubiquitin10* (*UBQ10*) promoter, PUB22 protein levels were found to be low and PUB22 was constitutively degraded by the 26S proteasome in naive plants (Stegmann et al. 2012). As mentioned, PUB22 degradation was dependent on an active U-box to mediate the interaction with an E2 enzyme. Also, PUB22 was stabilized upon activation of immune responses with flg22. To detect the native protein, an antibody was raised against a PUB22 synthetic peptide (RVWRESPCVPRNLYDSYPA). This antibody however, failed to detect the endogenous protein in Col-0 seedlings treated with flg22 and/or proteasome inhibitor (data not shown). Therefore, in order to analyse the transcriptional regulation of PUB22, together with the protein accumulation, a line expressing *GFP-PUB22* under control of the native *PUB22* promoter was used.
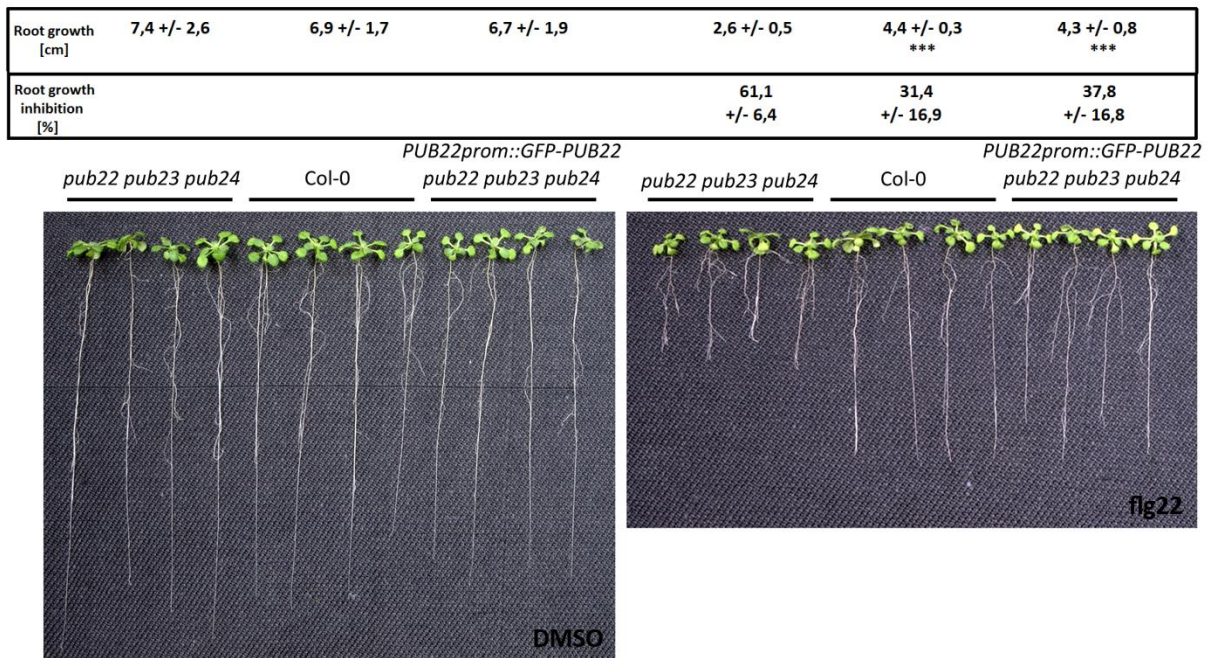
3.1.1 The GFP-PUB22 fusion driven by its native promoter is functional

For the transcriptional regulation analysis of PUB22, a transgenic line carrying *PUB22* with an N-terminal GFP fusion under the control of the native promoter (kindly generated and provided by Dr. Jörn Klinkenberg) was employed. Because the line was generated in a *pub22 pub23 pub24* genetic background, I assessed the functionality of the GFP-PUB22 fusion protein by testing complementation of the enhanced responsiveness to flg22 in a root growth inhibition assay (Figure 3-1). In presence of flg22, the growth of Arabidopsis seedlings is inhibited due to the constant activation of PTI responses. By measuring the inhibition of elongation of the main root in

comparison to a control, growth reduction was employed as a read-out to quantify the intensity of the immune response.

Col-0, *pub22 pub23 pub24* triple mutant, and *PUB22prom::GFP-PUB22* transgenic seedlings were grown vertically in long day conditions for five days on ½ MS plates and subsequently grown for additional 14 days on ½ MS plates supplemented with 1 µM flg22 or the vehicle DMSO. Col-0 seedlings displayed a 31,4 % of growth reduction (Figure 3-1, right panel), in agreement with published results (Stegmann et al. 2012). *pub22 pub23 pub24* mutant seedlings showed an increased growth inhibition (61,1 %), consistent with their enhanced resistance phenotype. On the other hand, the inhibition of *pub22 pub23 pub24* triple mutant plants carrying the *PUB22prom::GFP-PUB22* transgene was very similar to that of Col-0 seedlings (37,8 %), indicating a full complementation of the *pub* triple mutation by the native promoter fusion construct. Importantly, none of the analysed genotypes presented any developmental phenotype under normal growth conditions (Figure 3-1, left panel).

| Root growth [cm] | 7,4 +/- 2,6 | 6,9 +/- 1,7 | 6,7 +/- 1,9 | 2,6 +/- 0,5 | 4,4 +/- 0,3 *** | 4,3 +/- 0,8 *** |
| Root growth inhibition [%] | | | | 61,1 +/- 6,4 | 31,4 +/- 16,9 | 37,8 +/- 16,8 |

Figure 3-1 Root growth inhibition assay to test complementation of a line carrying *PUB22prom::GFP-PUB22* in the *pub22 pub23 pub24* genetic background. Measurements of root growth inhibition were performed on 20 days old seedlings grown for 14 days in 1 µM flg22 or DMSO containing ½ MS solid medium. Data is shown as mean of three independent experiments +/- S.E.M. (n=12). Statistical significance compared to *pub22 pub23 pub24* triple mutant plants is indicated by asterisks (Student's t-Test, ***p < 0,001).

3.1.2 PUB22 accumulation is induced by flg22

Real-time PCR data published in the work of Trujillo and colleagues (2008) showed a strong induction of *PUB22* transcripts within one hour after activation of the immune response by application of flg22 to seedlings, or one to seven days after *Pst* or *Hyaloperonospora arabidopsidis* (*Hpa*) infection in plants. Native promoter-GUS lines displayed strong GUS accumulation after stimulus with flg22, supporting the responsiveness of *PUB22* promoter during immunity. In order to link the promoter activity to the accumulation of PUB22 protein, I performed a time-course analysis on two-week-old *PUB22prom::GFP-PUB22* seedlings treated with flg22 for the indicated time and analysed total protein samples via immunoblot.

No accumulation of PUB22 was detected 0 or 30 minutes after flg22 treatment (Figure 3-2). After 60 minutes, the expected 77,3 kDa band, corresponding to the GFP-PUB22 fusion protein, appeared and its intensity increased until 120 minutes. At the last time point, 180 minutes after flg22 treatment, the protein level was slightly reduced, suggesting an attenuation of the induction and the expression of *PUB22*. These data confirmed the flg22 responsiveness of the promoter of *PUB22*, which results in the accumulation of PUB22 protein as soon as 60 minutes after treatment and peaks after 120 minutes. In the absence of an immunity trigger, PUB22 does not accumulate to detectable levels.
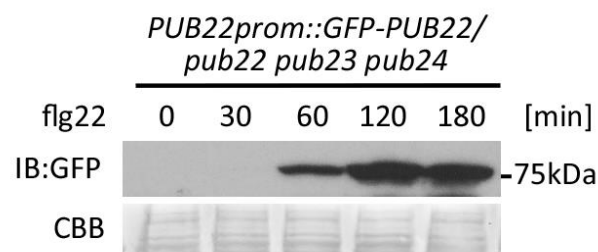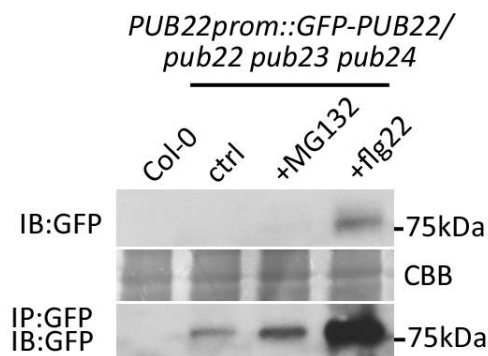

Figure 3-2 Time-course analysis of PUB22 protein accumulation upon flg22 treatment in a native promoter line. Two-week-old seedlings expressing *PUB22prom::GFP-PUB22* grown in ½ MS liquid medium, were treated for the indicated time with 1 µM flg22. Total protein samples were analysed by SDS-PAGE and immunoblot using anti-GFP antibodies. CBB was used as control for equal loading. Similar results were obtained in three independent experiments.

3.1.3 PUB22 has constitutive basal expression and is degraded by the 26S proteasome

Figure 3-2 shows that no PUB22 accumulation was detected at 0 or 30 minutes after flg22 treatment, and that promoter induction and *de novo* protein translation result in detectable protein accumulation after 60 minutes. Nevertheless, I reasoned that the threshold of PUB22 detection in a total protein extract may be too high to detect PUB22 in naive plants. To test this hypothesis, I performed immunoprecipitation experiments on *PUB22prom::GFP-PUB22* seedlings after different treatments.

Upon protein purification by immunoprecipitation, low amounts of PUB22 were detected in untreated seedlings, otherwise invisible in total protein samples (Figure 3-3). Treatment with the proteasome inhibitor MG132 resulted in a modest increase of protein accumulation, whereas flg22 treatment led to a drastic enhancement of PUB22 levels after two hours. This indicates that indeed, in the absence of a stimulus, *PUB22* promoter possesses a low basal activity that leads to low levels of PUB22 accumulation, and that PUB22 is continuously degraded by the 26S proteasome.

Figure 3-3 Immunoprecipitation of GFP-PUB22 using the native promoter line. Two-week-old seedlings expressing *PUB22prom::GFP-PUB22* grown in ½ MS liquid medium, were treated for two hours with DMSO, 50 µM MG132 or 1 µM flg22. Col-0 seedlings were used as control. After IP with GFP-trap beads, protein samples were analysed by SDS-PAGE and immunoblot using anti-GFP antibodies. CBB was used as control for equal loading of the input samples. Similar results were obtained in three independent experiments.

Consequently, I wanted to test whether the 26S proteasome plays a role in the turnover of PUB22 after the activation of immune responses. To do so, I treated *PUB22prom::GFP-PUB22* seedlings

with flg22 for two hours to induce protein expression and, after washing flg22 away, cycloheximide (CHX) was applied at time point 0. PUB22 protein levels were monitored 30 and 60 minutes after CHX application, in samples with or without MG132 proteasome inhibitor (PI). Despite the large initial amount of protein, inhibition of the *de novo* protein synthesis by CHX, led to a fast reduction of PUB22 levels, and it was almost depleted at 60 minutes (Figure 3-4). By contrast, samples which were additionally supplemented with MG132 displayed a higher stability over time. In summary, these data confirmed that *PUB22* promoter possesses a low basal activity and that PUB22 undergoes a constant turnover via the 26S proteasome.
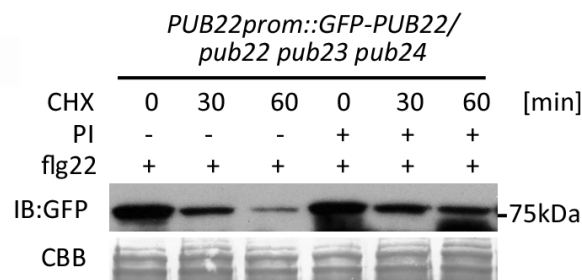
Figure 3-4 Stability analysis of PUB22 upon cycloheximide (CHX) treatment. Two-week-old seedlings expressing *PUB22prom::GFP-PUB22* grown in ½ MS liquid medium, were treated for two hours with 1 µM flg22 to induce protein expression. Flg22 was removed and 50 µM CHX was added to the samples (time point 0). 50 µM of MG132 proteasome inhibitor (PI) was used. Total protein samples were analysed by SDS-PAGE and immunoblot using anti-GFP antibodies. CBB was used as control for equal loading. Similar results were obtained in three independent experiments.

3.1.4 PUB22 is localized in the cytosol and associates to membranes

Previous work published in 2012 by Stegmann and colleagues revealed the identity of the first substrate of PUB22, namely Exo70B2, a component of the exocyst complex responsible for membrane tethering during vesicle trafficking. Biochemical studies showed that PUB22 binds and ubiquitinates Exo70B2, causing its degradation. However, the identity of the cellular compartments where PUB22 and Exo70B2 function is still unknown. This interaction data unveiled a connection between PUB22 and vesicle trafficking during immunity. Taking advantage of the GFP fusion line, I analysed PUB22 localization. Due to the low fluorescence signal in *PUB22prom::GFP-PUB22* lines, which precluded a cell biological approach, I opted for biochemical analyses.

In order to test membrane association, membrane fractionations were isolated and analysed from *PUB22prom::GFP-PUB22* seedlings after different treatments. Untreated samples displayed no accumulation of PUB22 in either the soluble or the microsomal fraction (Figure 3-5), confirmed respectively by the presence of the soluble HSP90 or the membrane marker PIP2. After treatment with flg22 or flg22 together with MG132, PUB22 was detected in a weak band in the soluble fraction and in a more intense band in the microsome-enriched fraction. These results indicate the existence of at least, cytoplasmic and membrane-associated pools of PUB22 protein.
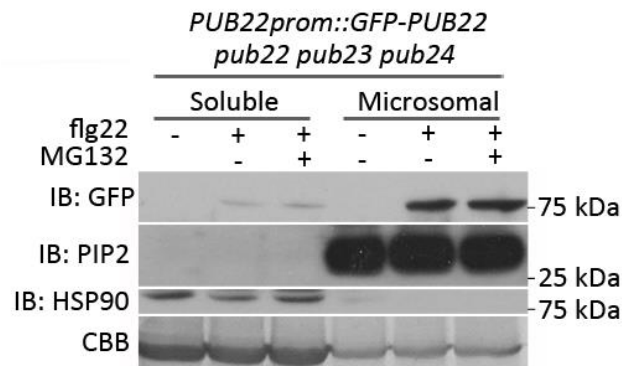
Figure 3-5 Microsomal fractionation analysis of *PUB22prom::GFP-PUB22* seedlings samples. Two-week-old seedlings expressing *PUB22prom::GFP-PUB22* grown on ½ MS solid medium, were treated for two hours with 50 µM MG132 and/or 1 µM flg22. Membrane fractions were separated by ultracentrifugation, analysed by SDS-PAGE and immunoblot together with soluble fractions using anti-GFP antibodies to detect GFP-PUB22, anti-PIP2 antibodies to confirm membrane enrichment and anti-HSP90 to label the soluble fractions. CBB was used as control for equal loading. Similar results were obtained in three independent experiments.

3.2 PUB22 autoubiquitination and its influence on protein stability

PUB22, as most of the single subunit E3 ligases, displays an inherent autoubiquitination activity *in vitro* (Trujillo et al. 2008). First evidences provided by the stability analyses of PUB22 in comparison to the PUB22[C13A] U-box inactive mutant, suggested that autoubiquitination may function as a mechanism of self-regulation through self-destruction (Stegmann et al. 2012). In order to further confirm the link between PUB22 autoubiquitination activity and its stability, I generated stable transgenic lines expressing GFP-PUB22 WT and one of its inactive mutants (previously published in

Trujillo et al. 2008) under the control of the *UBQ10* constitutive promoter, and analysed their functionality and stability *in planta*.

3.2.1 PUB22 possesses true autoubiquitination activity *in vitro*

Most of the single-unit E3 ligases can autoubiquitinate *in vitro*. In the previously published autoubiquitination experiments, PUB22 includes an affinity tag, which might deregulate its autoubiquitination activity or may serve as the substrate. To confirm the true autoubiquitination activity of PUB22, I performed an autoubiquitination assay using untagged PUB22 (Figure 3-6).

Untagged PUB22 was obtained by proteolytic cleavage of the GST tag. In presence of all the components required for ubiquitination, untagged PUB22 could efficiently autoubiquitinate (Figure 3-6). Controls lacking one of the essential components do not show activity.
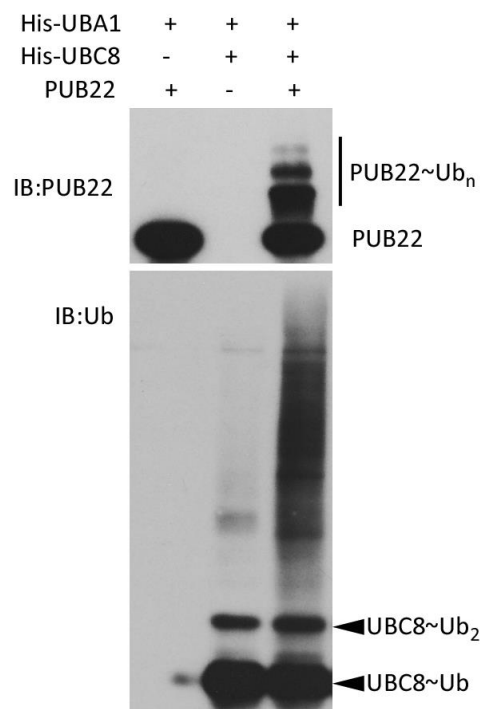

Figure 3-6 Autoubiquitination assay using untagged PUB22. Recombinant GST-PUB22 was bacterially expressed and purified. Untagged PUB22 was obtained after four hours incubation with thrombin protease. Purified untagged PUB22 was incubated together with the Arabidopsis His-UBA1 and His-UBC8 overnight at 30°C. Proteins were analysed by SDS-PAGE and immunoblot using anti-PUB22 and anti-ubiquitin antibodies.

3.2.2 PUB22 does not autoubiquitinate specific lysines

Because PUB22 possesses true autoubiquitination activity, I determined the ubiquitination sites with the purpose to characterize its autoubiquitination activity. Purified GST-PUB22 was used for an autoubiquitination assay and samples were resolved by SDS-PAGE and stained with CBB. Bands corresponding to ubiquitinated species of PUB22 were excised and analysed by LC-MS/MS in cooperation with Dr. Hirofumi Nakagami (RIKEN-Yokohama Japan) (Appendix Figure 7-2). The ubiquitination pattern indicated that PUB22 has no specificity towards a specific lysine (Figure 3-7). Nevertheless, a majority of the ubiquitination sites are concentrated at the N-terminal part of PUB22, suggesting that the UBC8~Ub conjugate has the best access to this region, potentially as a result of an extended conformation of the PUB22 ARM repeats.
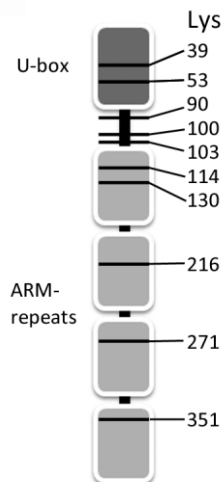

Figure 3-7 Schematic representation of PUB22 ubiquitination sites. LC-MS/MS analyses were performed on GST-PUB22 after *in vitro* autoubiquitination to identify ubiquitinated lysine residues.

3.2.3 PUB22 ubiquitination activity is required for complementation

The low level of PUB22 expression when under the control of its native promoter, precluded the biochemical analysis of its stabilization. Hence, for the stability analysis of PUB22 and its U-box inactive mutant, *UBQ10prom::GFP-PUB22* and *UBQ10prom::GFP-PUB22*[W40A] constructs were used to
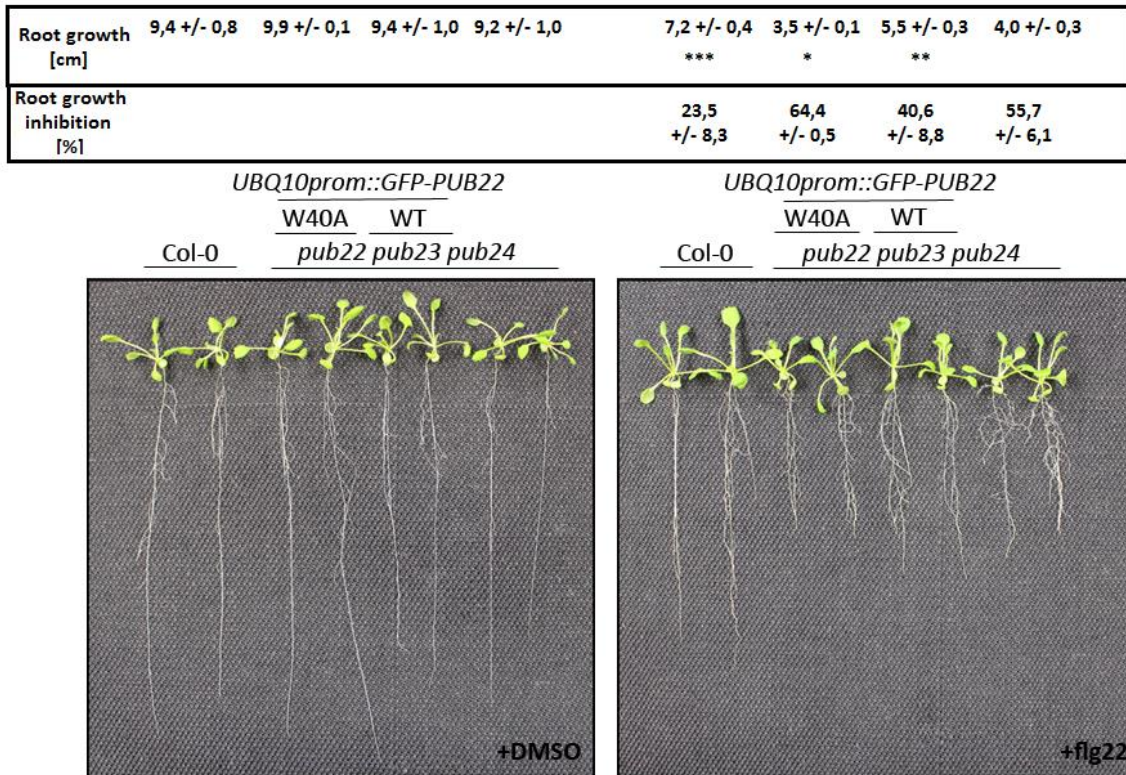
generate stable transgenic lines in the *pub22 pub23 pub24* mutant genetic background. The W40A mutation was my preferred choice, because it provides a more conservative alternative to C13A, because the W40A mutation is predicted to preserve the general structure of the U-box domain, while impairing E2 binding by affecting only the E2 interaction surface. Differently, the C13A mutation blocks the interaction with E2 by destabilizing the U-box hydrogen-bonding networks and destroying the U-box structure (Ohi et al. 2003) (Figure 3-8).
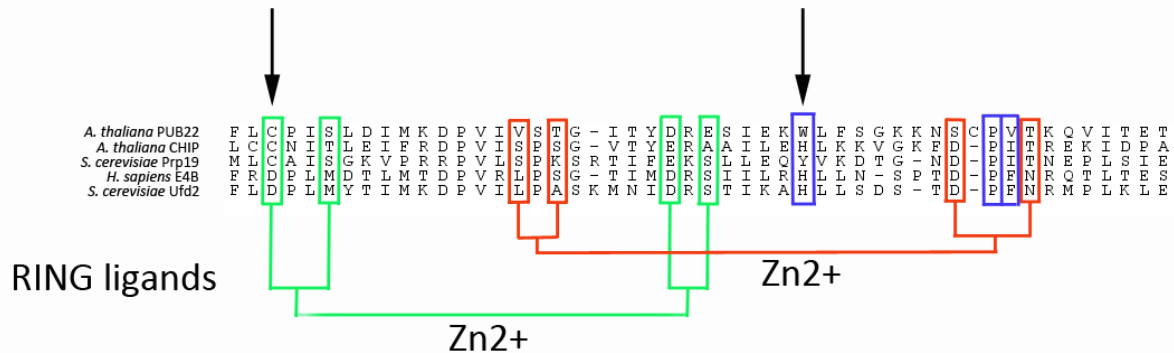
Figure 3-8 Alignment of various protein U-box domains. PUB22 U-box domain was aligned with the well-studied U-box sequences of the indicated proteins (Ohi et al. 2003) (accession numbers: *At*PUB22 OAP06343, *At*CHIP OAP04012, *Sc*Prp19 CAA97487, *Sc*Ufd2 CAA98767, *Hs*E4B AAH93696). RING ligands positions indicate zinc chelating residues in RING domains. U-box residues replacing zinc chelating amino acids and involved in the two hydrogen-bonding networks, are highlighted in red and green. Hydrophobic residues mediating E2 binding are highlighted in blue. Arrows indicate C13 and W40 residues of PUB22.

The functionality of the fusion proteins was tested employing the root growth inhibition assay, as described above. In presence of flg22, Col-0 seedlings displayed a 23,5 % root growth inhibition (Figure 3-9, right panel), whereas inhibition in the *pub22 pub23 pub24* triple mutants was 55,7 %. The *pub22 pub23 pub24* mutant plants carrying the *PUB22 WT* transgene presented an intermediate phenotype with 40,6 % inhibition, indicating a partial complementation. Whereas transgenic triple mutants transformed with the inactive *PUB22*[W40A] transgene responded with a comparable or even slightly increased inhibition (64,4 %) when compared to the triple mutant seedlings, indicating a potential dominant negative phenotype. Hence, ligase activity is necessary for PUB22 complementation. Under normal growth conditions, transgenic lines did not display any developmental phenotype (Figure 3-9, left panel).

| Root growth [cm]	9,4 +/- 0,8	9,9 +/- 0,1	9,4 +/- 1,0	9,2 +/- 1,0		7,2 +/- 0,4 ***	3,5 +/- 0,1 *	5,5 +/- 0,3 **	4,0 +/- 0,3
Root growth inhibition [%]						23,5 +/- 8,3	64,4 +/- 0,5	40,6 +/- 8,8	55,7 +/- 6,1

Figure 3-9 Root growth inhibition assay to test complementation of lines carrying *UBQ10prom::GFP-PUB22 WT* and *UBQ10prom::GFP-PUB22*[W40A] in the *pub22 pub23 pub24* genetic background (transgenic lines A). Measurements of root growth inhibition were performed on 20 days old seedlings grown for 14 days in 1 µM flg22 or DMSO containing ½ MS medium. Data is shown as mean of three independent experiments +/- S.E.M. (n=12). Statistical significance compared to *pub22 pub23 pub24* triple mutant plants is indicated by asterisks (Student's t-Test, *p < 0,05; **p < 0,01; ***p < 0,001). Similar results were obtained using an additional independent line for each construct.

3.2.4 PUB22 ubiquitination activity contributes to its own proteasomal degradation

It was proposed that the autoubiquitination activity of PUB22 may mediate its degradation, because the inactive PUB22[C13A] was more stable in comparison to PUB22 WT (Stegmann et al. 2012). In order to confirm these results, I analysed the stability of the inactive mutant PUB22[W40A] in a stable transgenic line. The GFP-PUB22[W40A] fusion protein under the control of the *UBQ10* promoter failed to complement the triple mutant phenotype, underlining the requirement of E2 binding for activity

and complementation (Figure 3-9). Moreover, I was able to confirm the previously reported loss of autoubiquitination activity (Trujillo et al. 2008) in an autoubiquitination assay (Figure 3-10). Purified MBP-PUB22 WT or MBP-PUB22^{W40A} were incubated with the Arabidopsis His-UBA1 as the E1 enzyme, His-UBC8 as the E2 enzyme, as well as ATP and ubiquitin for two hours. In presence of all the components required for ubiquitination, PUB22 WT efficiently autoubiquitinated as demonstrated by the appearance of the typical ubiquitination ladder detected with anti-PUB22 antibodies above the band corresponding to the unmodified MBP-PUB22 (Figure 3-10). On the other hand, the U-box mutant PUB22^{W40A} did not autoubiquitinate, validating its inactivity. Controls lacking His-UBC8 are shown.
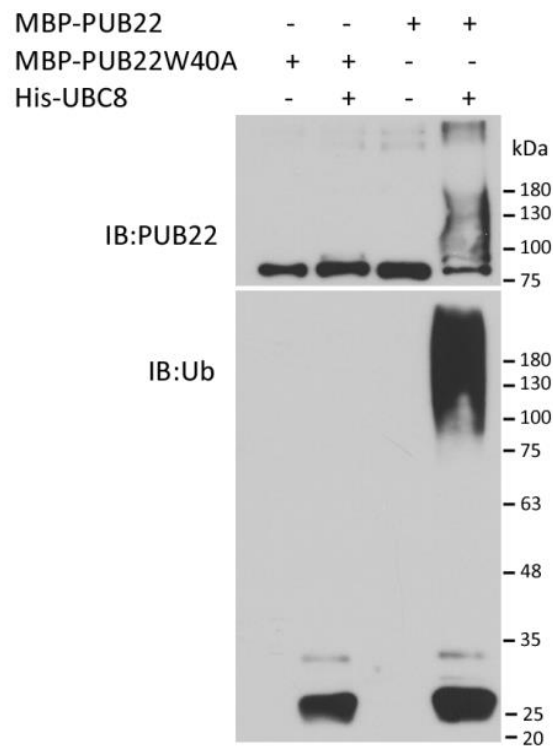

Figure 3-10 Autoubiquitination assay of PUB22 WT and PUB22^{W40A}. MBP-PUB22 WT and MBP-PUB22^{W40A} were purified. The E3 ligases were incubated together with His-UBA1 and His-UBC8 for two hours at 30°C. Proteins were analysed by SDS-PAGE and immunoblot using anti-PUB22 and anti-ubiquitin antibodies. Similar results were obtained in three independent experiments.

Analyses of the stability of the active and inactive PUB22 were performed in two independent transgenic lines per construct (lines A-B). Two-week-old seedlings were treated with CHX for the indicated time, harvested and analysed by immunoblot. In both independent lines, the inactive

mutant PUB22^{W40A} protein displayed enhanced stability in comparison to PUB22 WT (Figure 3-11, time 0), in agreement with the previous reports. CHX treatment resulted in the depletion of PUB22 WT at already 30 minutes after treatment, suggesting a high turnover. Surprisingly, also the levels of the inactive PUB22 were reduced over time in the presence of CHX. Tested lines displayed comparable levels of PUB22 transcripts, in RT-qPCR analysis (kindly performed by Kathrin Kowarschik, IPB-Halle, Appendix Figure 7-1).
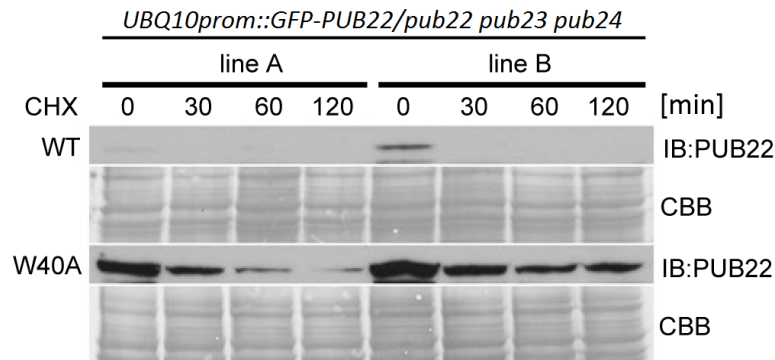
Figure 3-11 Stability analysis of PUB22 and PUB22^{W40A} in two independent stable transgenic lines upon CHX treatment. Two-week-old seedlings expressing *UBQ10prom::GFP-PUB22 WT* or *UBQ10prom::GFP-PUB22*^{W40A} of two transgenic lines A and B grown in ½ MS liquid medium, were treated for the indicated time with 50 µM CHX to inhibit protein translation. Total protein samples were analysed by SDS-PAGE and immunoblot using anti-PUB22 antibodies. CBB was used as control for equal loading. Similar results were obtained in three independent experiments.

The differential accumulation of WT and the inactive mutant variant of PUB22 at time 0 supports the previously proposed hypothesis that links PUB22 autoubiquitination activity to its degradation. Nevertheless, the reduction of PUB22^{W40A} levels upon CHX treatment suggests that this mutant may undergo proteasomal degradation as well.

To test this hypothesis, I treated two-week-old seedlings with the proteasome inhibitor MG132 and analysed PUB22 protein accumulation. Consistently with the presented results in the native promoter line, PUB22 WT was efficiently stabilized by proteasome inhibitor treatment (Figure 3-12). PUB22^{W40A} was more stable than the WT version, but also showed stabilization upon treatment. These results indicate that indeed the W40A inactive mutant of PUB22 is more stable, but also degraded by the 26S proteasome, suggesting the existence of a potential additional mechanism of degradation of PUB22, most likely independent from its own ubiquitination activity.
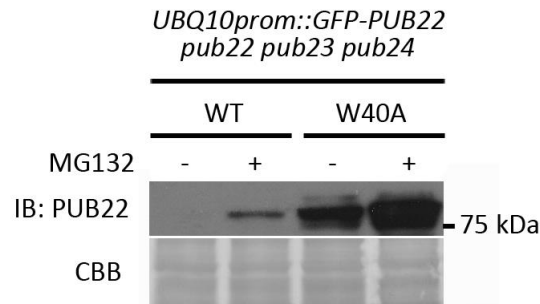
Figure 3-12 Stability analysis of PUB22 and PUB22^{W40A} upon MG132 treatment. Two-week-old seedlings expressing *UBQ10prom::GFP-PUB22 WT* or *UBQ10prom::GFP-PUB22^{W40A}* (transgenic lines B) grown in ½ MS liquid medium, were treated for two hours with 50 µM MG132 or the vehicle DMSO. Total protein samples were analysed by SDS-PAGE and immunoblot using anti-PUB22 antibodies. CBB was used as control for equal loading. Similar results were obtained in three independent experiments.

## 3.3 The regulation of PUB22 protein stability

Besides the transcriptional induction, PUB22 was shown to be posttranslationally regulated upon activation of immunity (Stegmann et al. 2012). The expression of PUB22 under the control of a constitutive promoter in protoplasts led to a modest accumulation of PUB22 protein, which was strongly stabilized by either proteasome inhibitor or flg22 treatments. To better characterize the stabilization of PUB22 during immunity, I examined several potential contributing factors.

3.3.1 PUB22 is stabilized by different PAMPs

Previous reports showed that PUB22 could be transiently stabilized in protoplasts by treatment with flg22. Time-course analyses showed that flg22-dependent stabilization is detectable already within five minutes after treatment, whereas the peak of protein stabilization is achieved after 30 minutes and maintained until 60 minutes (Figure 1-3 B). In order to confirm these results, I tested whether PUB22 could also be stabilized by flg22 treatment *in planta*. *UBQ10prom::GFP-PUB22* transgenic seedlings treated for one hour with 1 µM flg22 showed an increased accumulation of PUB22 (Figure 3-13), consistently with previous reports using protoplasts. Furthermore, to characterize the

dependency of PUB22 stabilization on the activation of specific PRRs, I included well described agonists, such as elf18 and pep1, and the fungal PAMP chitin, which are perceived by different receptors. Treatments with all elicitors led to the accumulation of PUB22 (Figure 3-13). Therefore, the stabilization of PUB22 during immunity does not depend on the activation of a specific receptor pathway, neither on the specific action of the co-receptor BAK1. While, BAK1 is required for the activation of receptors transducing the perception of flg22, elf18 and pep1, it is dispensable for chitin perception. This indicates that the stabilization of PUB22 depends on a downstream factor shared by all tested PRRs.
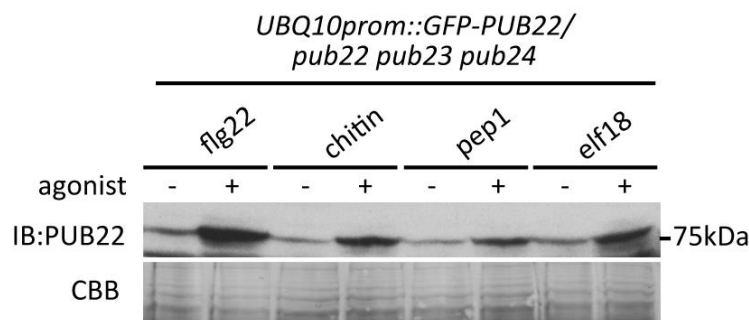
Figure 3-13 PUB22 stabilization analysis upon different elicitor treatments. Two-week-old seedlings expressing *UBQ10::GFP-PUB22 WT* (transgenic line A) grown in ½ MS liquid medium, were treated for one hour with 1 µM flg22, 200 µg/ml chitin, 1 µM pep1 or 1 µM elf18. Control seedlings were treated with water or the vehicle DMSO. Total protein samples were analysed by SDS-PAGE and immunoblot using anti-PUB22 antibodies. CBB was used as control for equal loading. Similar results were obtained in three independent experiments.

3.3.2 PUB22 ubiquitination and degradation is regulated by immune signalling

I could show that PUB22 possesses true autoubiquitination activity *in vitro* and that its ubiquitination activity is involved in its own degradation *in vivo*. Therefore, I hypothesized that autoubiquitination of PUB22 may cause the degradation of PUB22 via the 26S proteasome. Moreover, PUB22 was shown to stabilize during immunity raising the possibility that PUB22 stabilization may depend on immunity-triggered inhibition of its ubiquitination.

To test this and visualize PUB22 *in vivo* ubiquitination levels, I first treated *UBQ10prom::GFP-PUB22* transgenic seedlings for one hour with 1 µM flg22 to stabilize PUB22, I then rinsed the seedlings and

monitored PUB22 stability and ubiquitination over time in presence or absence of proteasome inhibitor (Figure 3-14). Stabilization of PUB22 prior to the analysis was necessary due to the low levels of PUB22 in naive plants precluding the detection of ubiquitinated protein.

PUB22 ubiquitination was weak at the initial time 0 (Figure 3-14, lane 2 upper panel). The levels of unmodified PUB22 together with ubiquitinated PUB22 increased two hours after removal of flg22 (lane 3), indicating a still ongoing stabilization probably due to residual flg22 in the plant tissue. Four hours after flg22 removal, unmodified PUB22 levels (lane 4 lower panel) decreased to the same extent as at time point 0 (lane 2 lower panel), in agreement with the transient nature of PUB22 stabilization. However, the levels of ubiquitinated PUB22 four hours after flg22 removal (lane 4 upper panel) are higher than at time point 0 (lane 2 upper panel), indicating an increase in PUB22 ubiquitination after the removal of flg22. Moreover, treatment with proteasome inhibitor led to the accumulation of both unmodified, and especially, ubiquitinated species of PUB22 (lane 5-6). This suggests that ubiquitination of PUB22 results in its degradation via the 26S proteasome.

Together, these results show that indeed PUB22 is ubiquitinated *in vivo*, potentially via autoubiquitination, causing its degradation via the 26S proteasome. Furthermore, the transient stabilization of PUB22 during immunity is mediated by the level of PUB22 ubiquitination. This suggests a mechanism dependent on immune signalling for the modulation of PUB22 ubiquitination and degradation.
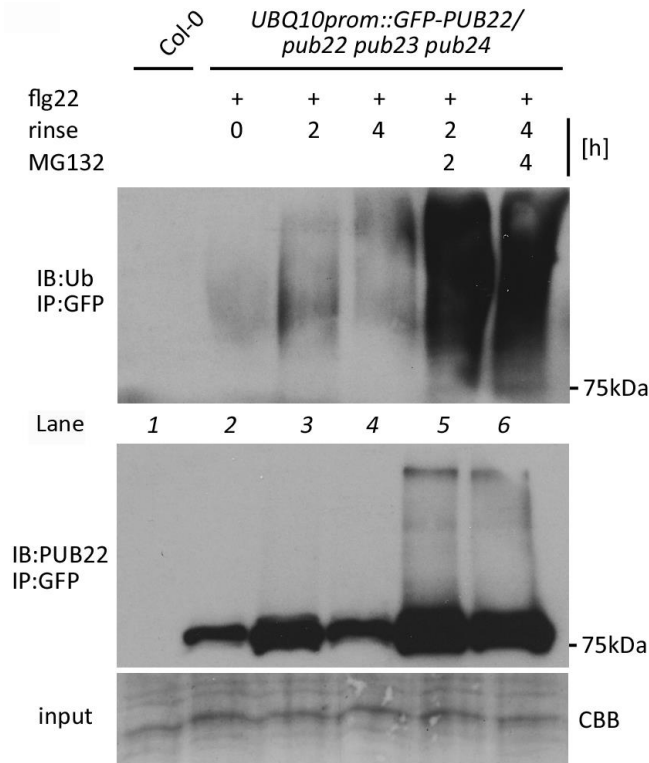
Figure 3-14 Analysis of *in vivo* ubiquitination of PUB22. Two-week-old seedlings expressing *UBQ10prom::GFP-PUB22 WT* (transgenic line B) grown in ½ MS liquid medium, were treated for one hour with 1 µM flg22. Seedlings were rinsed with fresh ½ MS medium and incubated for an additional period of time with or without 50 µM MG132 as indicated. After IP with GFP-trap beads, protein samples were analysed by SDS-PAGE and immunoblot using anti-PUB22 and anti-ubiquitin antibodies. Col-0 seedlings were used as control. CBB was used as control for equal loading of the input samples. Similar results were obtained in two independent experiments.

3.3.3 PUB22 homologues influence PUB22 stability

Because I showed that the activity of PUB22, as well as its ubiquitination levels, influence its stability, I investigated whether PUB22 ubiquitination is a consequence of direct intramolecular self-catalysed ubiquitination events, or is regulated by alternative mechanisms. For this purpose, I transiently expressed HA-PUB22 under the control of a 35S promoter in Arabidopsis mesophyll protoplasts derived from Col-0 or *pub22 pub23 pub24* triple mutant plants and examined protein levels. I hypothesised that if PUB22 is regulated by intramolecular self-catalysed ubiquitination events, the fusion protein HA-PUB22 would accumulate to the same extent in the two genotypes. One day after transformation, HA-PUB22 protein accumulated when expressed in *pub* triple knockout protoplasts, whereas in Col-0 protoplasts levels were undetectable (Figure 3-15). Notably,

in the Col-0 sample, anti-HA antibodies detected a high molecular weight smear, possibly corresponding to ubiquitinated forms of PUB22. These results suggest that intramolecular self-catalysed ubiquitination is unlikely to be the central mechanism regulating PUB22 stability, and supports the involvement of PUB23 and PUB24 in this process.
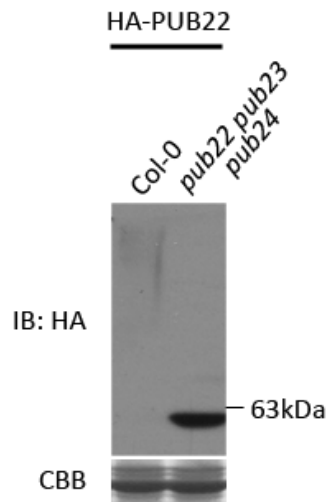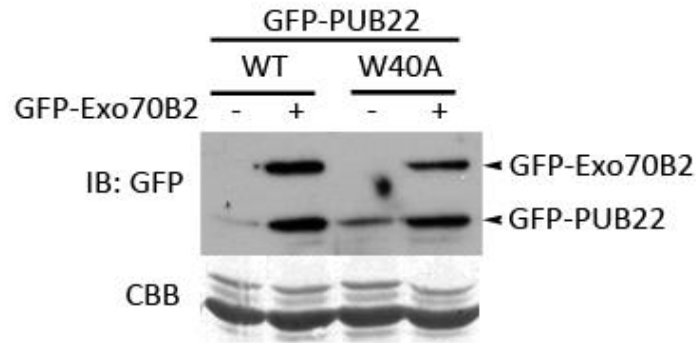

Figure 3-15 Stability analysis of PUB22 in Col-0 and *pub22 pub23 pub24* mutant genetic background. *35Sprom::HA-PUB22* construct was transformed into Arabidopsis mesophyll protoplasts derived from Col-0 or *pub22 pub23 pub24* mutant plants. One day after transformation, total protein samples were analysed by SDS-PAGE and immunoblot using anti-HA antibodies. CBB was used as control for equal loading. Similar results were obtained in three independent experiments.

## 3.3.4 Exo70B2 influences PUB22 stability

It has been shown that the binding of E3 ligases with their targets can influence their activity and stability (de Bie & Ciechanover 2011). Therefore, I investigated the potential role of Exo70B2, a *bona fide* target of PUB22, in its stabilization. Transient co-expression in protoplasts of GFP-Exo70B2 led to the stabilization of GFP-PUB22 WT and the more stable mutant variant GFP-PUB22^{W40A} (Figure 3-16).

Figure 3-16 Stability analysis of PUB22 WT and PUB22^W40A co-expressed with its substrate Exo70B2. *UBQ10prom::GFP-PUB22 WT* or *UBQ10prom::GFP-PUB22^W40A* and *35prom::GFP-Exo70B2* constructs were co-transformed into Arabidopsis mesophyll protoplasts derived from Col-0 plants. One day after transformation, total protein samples were analysed by SDS-PAGE and immunoblot using anti-GFP antibodies. CBB was used as control for equal loading. Similar results were obtained in three independent experiments.

Moreover, when HA-PUB22 was co-expressed with cMyc-Exo70B2 in protoplasts derived from *pub* triple mutant plants, both proteins displayed enhanced stability in comparison to when expressed in Col-0 derived protoplasts (Figure 3-17). This suggests that the reduced degradation of endogenous Exo70B2 in the *pub* triple mutant background may contribute to the stabilization of HA-PUB22. These results indeed indicate that Exo70B2 levels directly influence PUB22 stability.
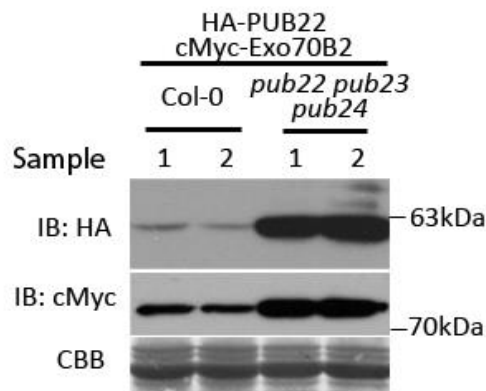
Figure 3-17 Stability analysis of PUB22 co-expressed with its substrate Exo70B2 in different genetic backgrounds. *35Sprom::HA-PUB22* and *35prom::cMyc-Exo70B2* constructs were co-transformed into Arabidopsis mesophyll protoplasts derived from Col-0 or *pub22 pub23 pub24* mutant plants. One day after transformation, total protein samples were analysed by SDS-PAGE and immunoblot using anti-HA and anti-cMyc antibodies. 1 and 2 indicate two independent samples. CBB was used as control for equal loading.
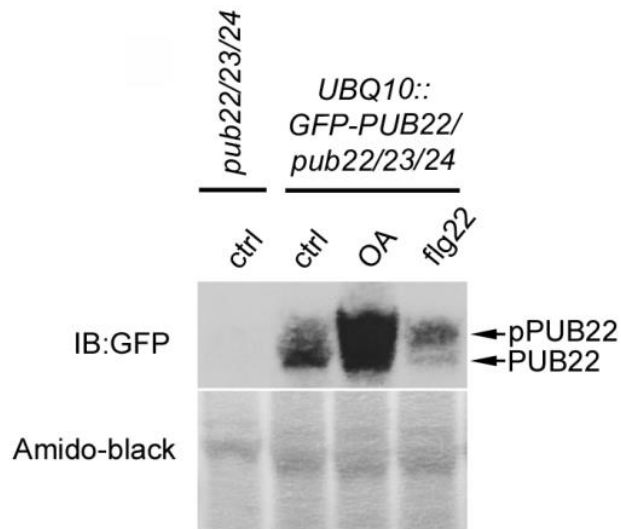
3.4 The phosphorylation of PUB22

PUB22 was shown to be stabilized within minutes upon activation of immunity, most likely by modulation of its autoubiquitination activity. Given that the posttranslational modification of enzymes is able to modify their activity, and as reported in the literature, a plethora of kinases are activated within the first minutes of the immune signal transduction, I attempted to elucidate whether PUB22 was phosphorylated.

3.4.1 Flg22 triggers PUB22 mobility shift

In order to assess PUB22 phosphorylation during the activation of the immune response, Phos-tag PAGE anaylsis were performed in collaboration with Xiyuan Jiang from the group of Dr. Justin Lee (IPB-Halle). Phos-tag PAGE allows to visualize phosphorylated proteins by their altered mobility.

Total protein was extracted from two-week-old transgenic seedlings expressing GFP-PUB22, treated for 90 minutes with the phosphatase inhibitor okadaic acid (OA), 30 minutes with flg22 or the vehicle DMSO as untreated control (Figure 3-18). 30 minutes after flg22 treatment, and within the time range of PUB22 stabilization, most of PUB22 was detected in an upper shifted band, possibly corresponding to the phosphorylated species of PUB22. By contrast, in the untreated seedling sample, it migrated faster (lower band). Treatment with OA, which strongly activates immune responses, led to a massive accumulation of both species of PUB22. These results suggest that PUB22 may be phosphorylated upon flg22 treatment and therefore, that phosphorylation may be involved in its stabilization.

Figure 3-18 *In vivo* **analysis of PUB22 phosphorylation by Phos-tag PAGE.** Two-week-old seedlings expressing *UBQ10prom::GFP-PUB22 WT* (transgenic line A) grown in ½ MS liquid medium, were treated for 90 min with 1 μM okadaic acid (OA) or for 30 min with 1 μM flg22 or the vehicle DMSO as control. The *pub22 pub23 pub24* seedlings were used as control. Total protein samples were analysed by Phos-tag PAGE and immunoblot using anti-GFP antibodies. Amido-black was used as control for equal loading. Similar results were obtained in two independent experiments.

3.4.2 PUB22 T62 and T88 are phosphorylated

To confirm the phosphorylation of PUB22 *in vivo* and to map the specific phosphosites, LC-MS/MS analyses were performed on immunopurified GFP-PUB22 protein in collaboration with Petra Majovsky from the group of Dr. Wolfgang Hoehenwarter (IPB-Halle). Two-week-old seedlings expressing *UBQ10prom::GFP-PUB22*[W40A] were incubated for 30 minutes with flg22 or the vehicle DMSO. GFP-PUB22[W40A] was purified using GFP-trap agarose beads, separated on a SDS-PAGE and stained before excision. After trypsin digestion, phosphorylated peptides were enriched using TiO_2 affinity chromatography. LC-MS/MS analyses confirmed phosphorylation of PUB22 in the flg22-treated seedlings at T62 and T88 (Appendix Table VI). Nevertheless, additional phosphosites on PUB22 may be present and not detected using this experimental constellation.

3.4.3 PUB22 and PUB24 are phosphorylated by MPK3 and MPK4 *in vitro*

The presented data demonstrated that PUB22 is phosphorylated at T62 and T88 upon activation of immune responses. T62 and T88 are followed by a proline creating a TP motif, typical for MAPKs phosphosite. Therefore, in collaboration with Dr. Lennart Eschen-Lippold from the group of Dr. Justin Lee (IPB-Halle), we tested whether MPK3, MPK4 and MPK6, which are the best-characterized MAPKs active in the early immune responses, could phosphorylate PUB22 *in vitro.*

Because the concentration of a recombinant kinase does not necessarily correlate with its activity towards a substrate, the activity of preactivated GST-MPK3, GST-MPK4 and untagged MPK6 towards the artificial kinase substrate myelin basic protein (MBP) was used for normalization (Figure 3-19, right panel). Normalized kinases were subsequently incubated together with MBP-PUB22 in presence of radioactive ATP for 30 minutes (Figure 3-19, left panel). High levels of radioactively labelled ATP were detected by autoradiography on MBP-PUB22 upon incubation with GST-MPK3. Weaker phosphorylation of MBP-PUB22 by GST-MPK4 was also detected. MBP-PUB24 was included in the *in vitro* phosphorylation assay and analysed. PUB24 was phosphorylated by GST-MPK3 and weakly by GST-MPK4 as well (Figure 3-19, middle panel). Neither MBP-PUB22 nor MBP-PUB24 displayed a signal after incubation with MPK6 upon autoradiography analysis.
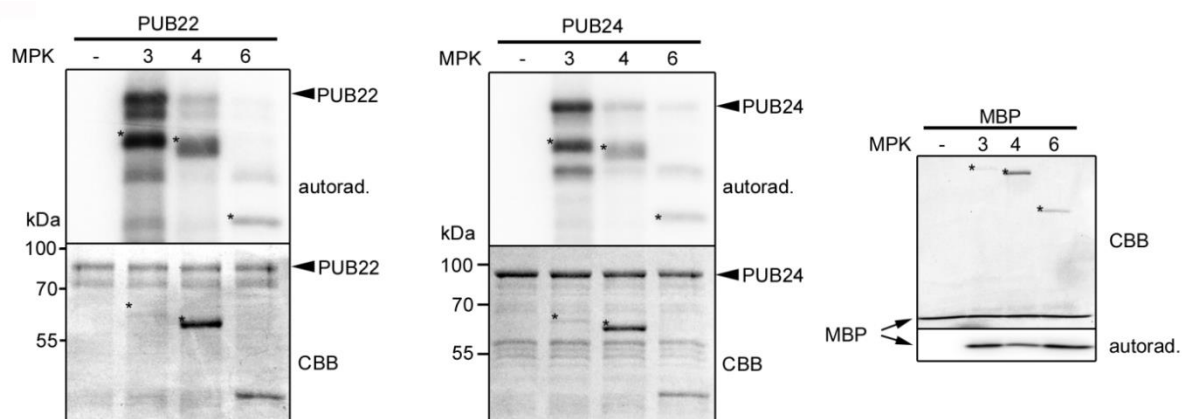
Figure 3-19 *In vitro* phosphorylation of PUB22 and PUB24 by MAPKs. Preactivated GST-MPK3, GST-MPK4 or untagged MPK6 (indicated by stars) were incubated together with purified MBP-PUB22, MBP-PUB24 or the artificial kinase substrate myelin basic protein (MBP) in presence of radioactive labelled ATP for 30 min at 37°C. Protein samples were analysed by SDS-PAGE and autoradiography. Similar results were obtained in two independent experiments.

In order to identify the residues phosphorylated by MPK3 and MPK4, Dr. Lennart Eschen-Lippold performed a non-radioactive *in vitro* phosphorylation assay and Petra Majovsky mapped the phosphosites by LC-MS/MS. Multiple phosphorylation sites by MPK3 and MPK4 were identified on TP/SP motifs, namely on T62, T88, and S422 (Appendix Table VII)(Figure 3-20). Hence, we could show that PUB22 and PUB24 are phosphorylated by MPK3 and MPK4 *in vitro* and we could confirm the previously found PUB22 phosphorylation sites at T62 and T88 as a MAPK phosphosite together with the newly identified S422.
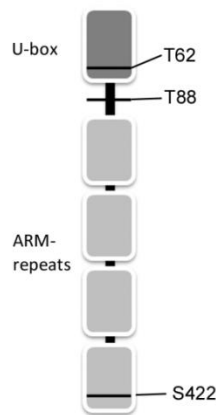
Figure 3-20 Schematic representation of the PUB22 phosphorylation sites identified from *in vitro* assays. LC-MS/MS analyses were performed on PUB22 after *in vitro* phosphorylation assay as described in 3.4.3 to identify phosphorylated residues.

3.5 The interaction of PUB22 with MAPKs

These data showed that PUB22 is phosphorylated *in vivo* upon flg22 treatment and *in vitro* by MPK3 and MPK4. Because substrate binding is a requirement for phosphorylation by kinases, several independent methods were employed to assay *in vivo* and *in vitro* interaction of PUB22 and MPK3/MPK4 and validate thus the above-presented data.

3.5.1 PUB22 interacts specifically with MPK3 in a BiFC assay

I first employed BiFC, also known as split-YFP, to test PUB22 interaction with MAPKs. This method consists in fusing the two halves of the fluorescent protein YFP to the putative interacting partners. When both proteins come into close proximity, YFP irreversibly complements, indicating that they belong to a protein complex or interact (Hu et al. 2002). To assay the interaction between PUB22 and MAPKs, I fused the C-terminal half of YFP (HA-cYFP) to the N-terminal end of the more stable and inactive PUB22^{W40A}. The *35Sprom::cMyc-nYFP-MPKs* constructs for *MPK3*, *MPK4*, *MPK6*, *MPK8*, and *MPK11* were provided by Dr. Justin Lee (IPB-Halle). Constructs were transiently transformed in Arabidopsis mesophyll protoplasts together with mCherry as a cytoplasmic and nuclear marker. YFP reconstitution was assessed by confocal laser scanning microscope one day after transformation.

Only co-expression of cMyc-nYFP-MPK3 and HA-cYFP-PUB22^{W40A} resulted in the reconstituted YFP fluorescent signal (Figure 3-21). Unspecific autofluorescence signal from chlorophyll could not be avoided due to the weak intensity of the specific YFP signal. Using the same microscopic settings, no signal was detected when HA-cYFP-PUB22^{W40A} was co-expressed with the MPK4, MPK6, MPK8 and MPK11 (Figure 3-21 and Appendix Figure 7-3), suggesting that MPK4-mediated *in vitro* phosphorylation of PUB22 may not take place under physiological conditions. In order to test whether any changes in the interaction between PUB22 and MPK3 occur during immunity, I treated the transformed protoplasts with flg22 and monitored the YFP fluorescence over time. No evident changes were detected within two hours after treatment (data not shown).
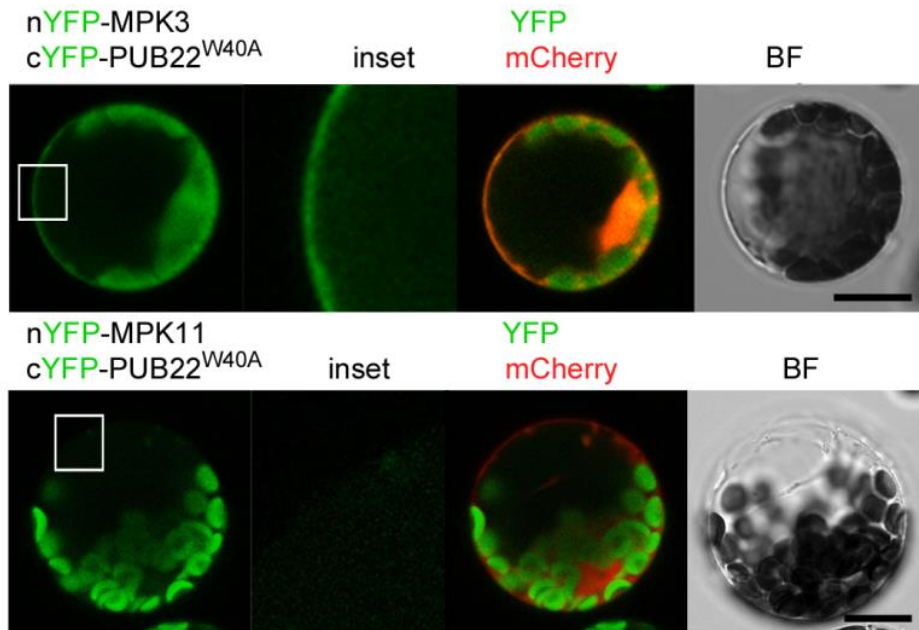
Figure 3-21 BiFC interaction analysis with PUB22^{W40A} and MPK3 or MPK11. *35Sprom::cMyc-nYFP-MPK3* or *MPK11* and *35Sprom::HA-cYFP-PUB22^{W40A}* constructs were co-expressed in Arabidopsis mesophyll protoplasts derived from *pub22 pub23 pub24* mutant plants together with a mCherry nuclear and cytoplasmic marker. One day after transformation, YFP reconstitution and mCherry fluorescence were analysed by confocal laser scanning microscope. Scale bar = 20 µm. Similar results were obtained in three independent experiments.

In order to confirm the expression of the fusion proteins, samples were harvested from protoplasts and analysed by immunoblot. Figure 3-22 shows that the fusion proteins HA-cYFP-PUB22^{W40A}, cMyc-nYFP-MPK3 and cMyc-nYFP-MPK11 were expressed. Additional protein expression analyses are presented in appendix Figure 7-4 and Figure 7-5, confirming the expression of the additional MAPKs. Interestingly, a mobility shift of PUB22 was detected upon flg22 treatment when co-expressed with MPK3, possibly indicating a flg22-dependent phosphorylation of PUB22. On the other hand, stabilization of PUB22 upon flg22 treatment could not be detected when co-expressed with MPK11, suggesting that MPK11 overexpression possibly interferes with PUB22 stabilization. YFP reconstitution indicates that PUB22 is found in close proximity to MPK3 and protein expression analyses revealed that co-expression of split-YFP PUB22 and MPK3 fusion proteins leads to a band shift of PUB22 upon activation of immune responses.
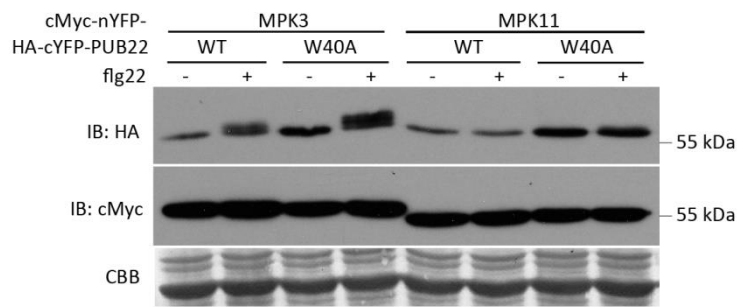
Figure 3-22 Expression analysis of PUB22^{W40A}, MPK3 and MPK11 used for BiFC. Total protein samples from BiFC experiments were analysed by SDS-PAGE and immunoblot using anti-HA and anti-cMyc antibodies. 1 μM flg22 was used for 30 min. CBB was used as control for equal loading. Similar results were obtained in three independent experiments.

3.5.2 PUB22 interacts *in planta* with MPK3 in a co-immunoprecipitation assay

The above results suggested that PUB22 interacts with MPK3. Nevertheless, the interaction was tested transiently in protoplasts via split-YFP using overexpression of the fusion proteins. I confirmed the interaction *in planta* employing a *UBQ10prom::GFP-PUB22* stable transgenic line.

Two-week-old seedlings expressing GFP-PUB22 were treated with flg22 and harvested at the indicated time points. GFP-PUB22 was purified by using GFP-trap agarose beads. Eluted proteins were analysed by immunoblot and co-immunoprecipitation of the endogenous MPK3 was assessed by using anti-MPK3 antibodies (Figure 3-23). PUB22 was immunoprecipitated in low amounts at the time point 0, consistently with previous experiments. Increasing protein levels were purified at 20 and 60 minutes after flg22 treatment due to its stabilization. Endogenous MPK3 co-immunoprecipitated strongest at 20 minutes, and was detectable in lower amounts at 0 and 60 minutes. A faint band was also detected in the Col-0 negative control, indicating a weak unspecific binding of MPK3 to the agarose beads. These results confirm that MPK3 interacts with or exists in the same complex as PUB22 *in planta*, also in the absence of immune signalling. Co-immunoprecipitated MPK3 levels are reduced at 60 minutes, suggesting a reduction of the PUB22 and MPK3 complex formation during the immune response.
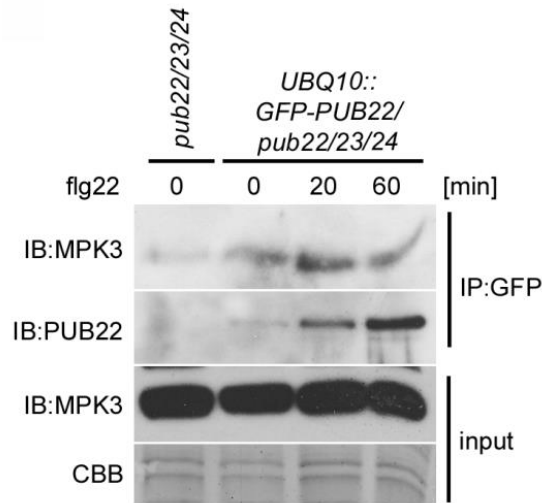
Figure 3-23 Co-immunoprecipitation of MPK3 by GFP-PUB22. Two-week-old seedlings expressing *UBQ10prom::GFP-PUB22 WT* (transgenic line A) grown in ½ MS liquid medium, were treated for the indicated time with 1 µM flg22. The *pub22 pub23 pub24* triple mutant seedlings were used as control. After immunoprecipitation with GFP-trap beads, protein samples were analysed by SDS-PAGE and immunoblot using anti-PUB22 and anti-MPK3 antibodies. CBB was used as control for equal loading of the input samples. Similar results were obtained in two independent experiments.

3.5.3 PUB22 physically interacts with MPK3

Results from the *in vitro* phosphorylation assay suggested that PUB22 and MPK3 physically interact. For studying their potential direct interaction, I performed a pull-down assay using recombinant MBP-PUB22, GST-MPK3 and GST-MPK6.

Free GST or recombinant GST-MPK3 or GST-MPK6 were immobilized on glutathione-agarose beads and subsequently incubated with bacterial lysate containing MBP-PUB22. After washing and eluting, proteins were analysed by immunoblot (Figure 3-24). MBP-PUB22 was detected only when added to the pull-down together with GST-MPK3 as bait, confirming a specific physical interaction between PUB22 and MPK3. PUB22 was not co-purified when using free GST or GST-MPK6 as baits.
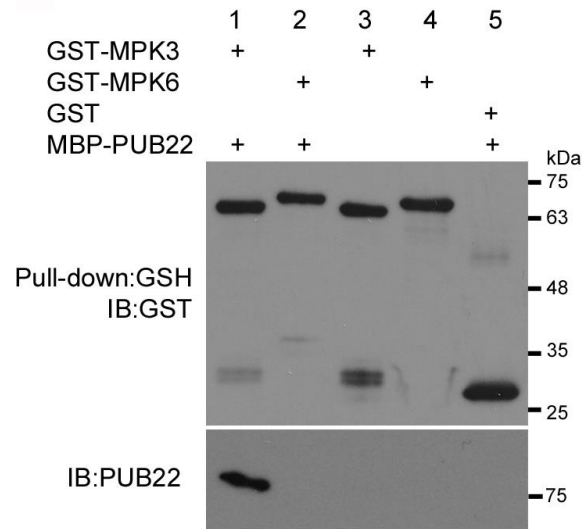
Figure 3-24 *In vitro* pull-down assay PUB22 in combination with MPK3 and MPK6. Recombinant GST-MPK3 and GST-MPK6 were immobilized on glutathione agarose beads. Free GST was used as control. GST fusion proteins were incubated with lysate containing MBP-PUB22. Elutions were analysed by SDS-PAGE and immunoblot using anti-GST and anti-PUB22 antibodies. Similar results were obtained in two independent experiments.

3.6 MPK3-dependent stabilization of PUB22

MPK3 is a key regulator of early immune responses and is activated within minutes upon perception of flg22. Considering that PUB22 binds and is phosphorylated by MPK3 *in vitro* and that PUB22 and MPK3 exist in a complex *in vivo*, I hypothesized that MPK3 may be responsible for the *in vivo* phosphorylation of PUB22 and potentially for its stabilization. Therefore, genetic approaches and gene mutation analyses were employed to test the dependency of PUB22 stabilization on MPK3 and/or its phosphorylation.

3.6.1 PUB22 stabilization is dependent on MPK3 activity

Since MPK3 interacted with PUB22, I assessed whether MPK3 is involved in the regulation of PUB22. To do so, I transiently expressed HA-PUB22 in mesophyll protoplasts derived from Col-0 or *mpk3* mutant plants and analysed PUB22 stabilization upon flg22 treatment (Figure 3-25). PUB22 was

stabilized after treatment with flg22 in Col-0 derived protoplasts, whereas the stabilization was lost in *mpk3* mutant derived protoplasts. When cMyc-MPK3 was co-expressed in Col-0 or *mpk3* mutant protoplasts, an increase in the basal level of PUB22 in both genetic backgrounds and stabilization after flg22 treatment were observed.
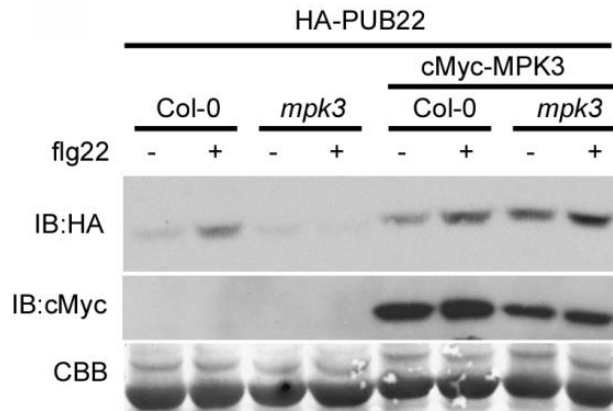
Figure 3-25 Analysis of the PUB22 stabilization dependence on MPK3. *35Sprom::HA-PUB22* and *35prom::cMyc-nYFP-MPK3* constructs were co-transformed into Arabidopsis mesophyll protoplasts derived from Col-0 or *mpk3* mutant plants. One day after transformation protoplasts were treated for 30 min with 1 µM flg22 and total protein samples were analysed by SDS-PAGE and immunoblot using anti-HA and anti-cMyc antibodies. CBB was used as control for equal loading. Similar results were obtained in three independent experiments.

Because the stabilization and phosphorylation time frame of PUB22 matches the MPK3 activation kinetics, I speculated that not only the binding with MPK3 but also the phosphorylation by MPK3 may be required for PUB22 stabilization. To test this hypothesis, I transiently expressed HA-PUB22 in mesophyll protoplasts together with either the cMyc-MKK5^{DD} constitutively active kinase or the cMyc-MKK5^{KR} inactive kinase from parsley (Lassowskat et al. 2014). MKK5 is the upstream MAPKK activating MPK3 and MPK6 (Meng & Zhang 2013) and *Pc*MKK5 has been successfully employed to activate Arabidopsis MPK3 and MPK6 (Lassowskat et al. 2014). PUB22 accumulated to higher levels upon co-expression with MKK5^{DD} than with MKK5^{KR} (Figure 3-26). Because also PUB24 could be phosphorylated *in vitro* by MPK3 (Figure 3-19), I tested whether it could also be stabilized *in vivo* in a similar manner as PUB22. Similarly to PUB22, co-expression with MKK5^{DD} led to higher accumulation of PUB24, than with MKK5^{KR} (Figure 3-26). Together these results indicate that MPK3 activation is required for PUB22 and PUB24 stabilization.
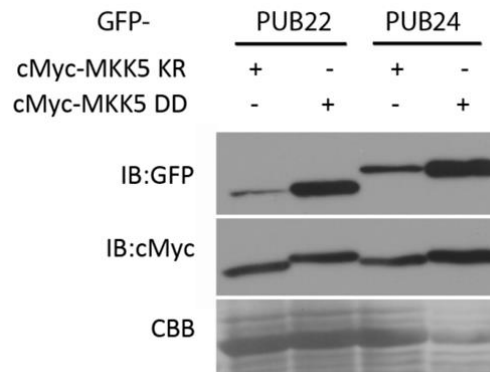
Figure 3-26 Analysis of the PUB22 stabilization dependence on the activity of MPK3. *UBQ10prom::GFP-PUB22 or UBQ10prom::GFP-PUB24* and *35Sprom::cMyc-MKK5^{DD}* or *35Sprom::cMyc-MKK5^{KR}* constructs were co-transformed into Arabidopsis mesophyll protoplasts derived from Col-0 plants. One day after transformation, total protein samples were analysed by SDS-PAGE and immunoblot using anti-GFP and anti-cMyc antibodies. CBB was used as control for equal loading. Similar results were obtained in three independent experiments.

3.6.2 Mimicking phosphorylation enhances PUB22 stability

Because MPK3 activation is necessary for the accumulation of PUB22, it is conceivable that MPK3-mediated phosphorylation of PUB22 contributes to its stabilization. To study the contribution of each phosphorylation event (identified in 3.4.3) to PUB22 stability, I mutated T62, T88 and S422 into alanine (A), a residue that cannot be phosphorylated to create a phosphonull mutant, or into glutamic acid (E), a negatively charged residue, to create a phosphomimetic mutant. Subsequently, I transiently expressed GFP-PUB22 WT, the inactive mutant, and phosphomutants in mesophyll protoplasts derived from *pub22 pub23 pub24* plants and analysed the stability of each mutant in two independent protoplast transformations (Figure 3-27).

As previously reported, PUB22 WT was highly unstable and weakly detectable, whereas PUB22^{W40A} accumulated to higher levels. PUB22^{T62A}, PUB22^{T88A}, and PUB22^{S422A} accumulated to a similar extent to PUB22 WT. Conversely, the corresponding phosphomimetic mutants presented a slightly higher stability. Therefore, also in the absence of immune signalling, mimicking phosphorylation by a glutamic acid substitution at any of the three phosphosites conferred enhanced stability to PUB22.

T62 is located in the U-box domain of PUB22, T88 in the linker region between the U-box domain and the ARM-repeats domain and S422 at the very end of the last ARM repeat (Figure 3-20). To test a potential additive effect, I created the double T62/88A phosphonull and T62/88E phosphomimetic mutants. Transient expression of GFP-PUB22$^{T62/88A}$ and GFP-PUB22$^{T62/88E}$ in mesophyll protoplasts resulted in the phosphonull mutant accumulating in low amounts contrary to the phosphomimetic mutant which displayed a higher stabilization phenotype (Figure 3-27). Because GFP-PUB22$^{T62/88E}$ accumulates to a higher extent than the respective single mutants with glutamic acid substitutions, it indicates that T62 and T88 phosphorylations possess non-redundant functions.
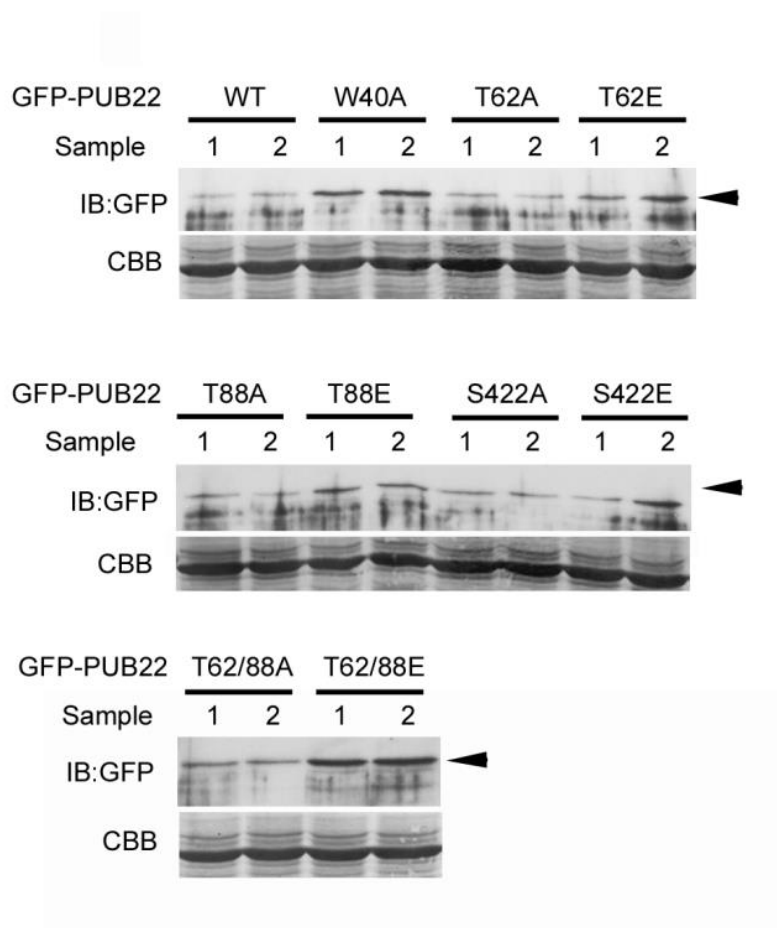
Figure 3-27 Analysis of PUB22 phosphomutants stability: *UBQ10prom::GFP-PUB22 WT*, *W40A*, *T62A*, *T62E*, *T88A*, *T88E*, *S422A*, *S422E, T62/88A and T62/88E* constructs were co-transformed into Arabidopsis mesophyll protoplasts derived from *pub22 pub23 pub24* mutant plants. One day after transformation total protein samples were analysed by SDS-PAGE and immunoblot using anti-GFP antibodies. 1 and 2 indicate two independent transformations. CBB was used as control for equal loading.

3.6.3 T62 and T88 phosphosites are required for PUB22 stabilization by flg22

To confirm these observations *in planta* and to check if phosphorylation at positions T62 and T88 are necessary for the stabilization of PUB22 during the immune responses, I generated stable transgenic lines. Because of the clear phenotype of the double mutant, *UBQ10prom::GFP-PUB22$^{T62/88A}$* and *UBQ10prom::GFP-PUB22$^{T62/88E}$* constructs were used to transform *pub22 pub23 pub24* triple mutant plants. Because my purpose was to compare protein stability, I selected lines with similar levels of transcription to the previously characterized *UBQ10prom::GFP-PUB22 WT* and *UBQ10prom::GFP-PUB22^{W40A}* lines (RT-qPCR analyses were kindly performed by Kathrin Kowarschik, IPB-Halle, appendix Figure 7-1). To assess the phosphomutants' stabilization after activation of the immune response, two-week-old seedlings were treated with flg22, and PUB22 stabilization was monitored over time (Figure 3-28). PUB22 WT was unstable and stabilized upon treatment, whereas PUB22^{W40A} displayed higher basal levels and stabilization. Importantly, PUB22$^{T62/88A}$ accumulated at lower basal levels than PUB22 WT and was unable to accumulate in response to flg22 treatment. This suggests that phosphorylation at positions T62 and T88 is strictly required to allow stabilization of PUB22. PUB22$^{T62/88E}$ displayed higher basal stability also *in planta*, as well as the ability to stabilize 60 minutes after flg22 treatment.
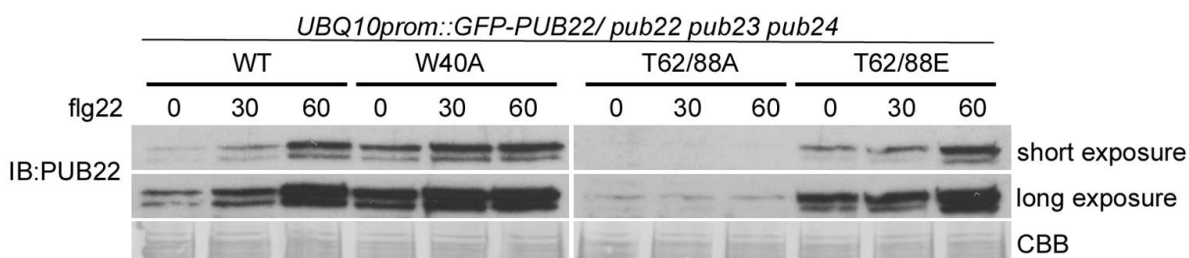
Figure 3-28 Analysis of PUB22 double phosphomutants stabilization upon flg22 treatment. Two-week-old seedlings expressing *UBQ10prom::GFP-PUB22 WT*, *W40A*, *T62/88A* and *T62/88E* (transgenic lines B) grown in ½ MS liquid medium, were treated for the indicated time with 1 μM flg22. Total protein samples were analysed by SDS-PAGE and immunoblot using anti-PUB22 antibodies. CBB was used as control for equal loading. Similar results were obtained in two independent experiments.

Next, I tested whether the high instability of the phosphonull mutant was caused by its degradation via the 26S proteasome. To do so, stable transgenic seedlings were treated with proteasome inhibitor MG132 (Figure 3-29). The otherwise undetectable PUB22 WT and PUB22$^{T62/88A}$ were rescued by the treatment, indicating a common turnover via the 26S proteasome, also true for the more stable PUB22^{W40A} and PUB22$^{T62/88E}$ which accumulated to a higher extent in presence of MG132. Notably, PUB22 and PUB22 mutants are consistently detected as two bands (Figure 3-28 and Figure 3-29), the upper one being stronger than the lower one, possibly corresponding to a modified and more stable form of PUB22 versus an unstable unmodified form. Moreover, an additional weaker upper band appeared on top in presence of proteasome inhibitor, suggestive of a form of PUB22 carrying a modification with potentially a degradative function such as ubiquitination.

In summary, these results indicate that phosphorylation at positions T62 and T88 by the action of MPK3 is required for PUB22 stabilization during the immune response, which is otherwise degraded by the 26S proteasome.
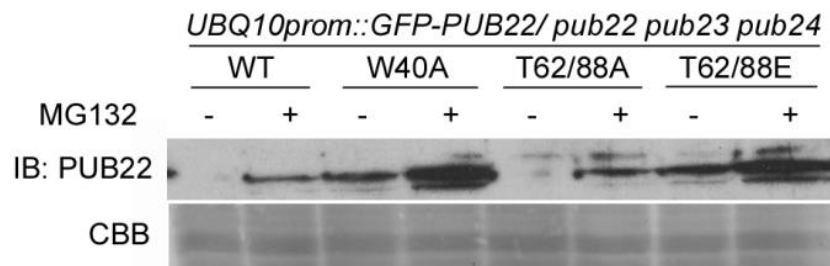

Figure 3-29 Analysis of PUB22 double phosphomutants stabilization by MG132. Two-week-old seedlings expressing *UBQ10prom::GFP-PUB22 WT*, *W40A*, *T62/88A* and *T62/88E* (transgenic lines B) grown in ½ MS liquid medium, were treated for two hours with 50 µM MG132. Total protein samples were analysed by SDS-PAGE and immunoblot using anti-PUB22 antibodies. CBB was used as control for equal loading. Similar results were obtained in two independent experiments.

## 3.7 The autoubiquitination activity of PUB22 phosphomutants

As hypothesised, phosphorylation by MPK3 is a stabilizing modification of PUB22 during the immune response. Moreover, the flg22 dependent modulation of PUB22 degradation correlated with the levels of ubiquitination. Changes in PUB22 ubiquitination and its stability are potentially the result of

changes in its autoubiquitination activity. Therefore, it seemed sensible to assume that phosphorylation increased the stability of PUB22 by attenuating its autoubiquitination activity. This hypothesis was tested by *in vitro* autoubiquitination assays, employing mutants of T62 and T88, located in and adjacent to the U-box. Because of its location in the ARM repeats domain, I hypothesized that S422 phosphorylation is unlikely to influence autoubiquitination, but rather regulates target binding.

3.7.1 PUB22$^{T62/88E}$ displays reduced autoubiquitination

In order to test if phosphorylation of PUB22 had an impact on the autoubiquitination activity, I analysed *in vitro* autoubiquitination activity of PUB22 phosphomimetic and phosphonull variants over time. Equal amounts of purified MBP-PUB22 WT, MBP-PUB22$^{T62/88A}$, and MBP-PUB22$^{T62/88E}$, were incubated in presence of His-UBA1, His-UBC8, ATP and ubiquitin for one or two hours. Subsequently, autoubiquitination activity was monitored by immunoblot. While PUB22 WT was strongly autoubiquitinated at one and two hours, the PUB22 phosphomimetic autoubiquitinated to a lower extent, as shown by the weaker ubiquitination signal detected by both the anti-PUB22 and anti-ubiquitin antibodies (Figure 3-30). This is in agreement with the premise that phosphorylation may reduce PUB22 autoubiquitination. However, in contrast to expectations, the PUB22 phosphonull variant did not display a PUB22 WT-like phenotype, but instead an autoubiquitination activity similar to PUB22 phosphomimetic. This indicates that alanine substitutions at positions 62 and 88 impaired the activity of PUB22 in a similar fashion as glutamic acid substitutions for *in vitro* assays. Nevertheless, ubiquitination detected by anti-ubiquitin showed a reduced signal in the phosphomimetic variant, especially at the earlier time point.
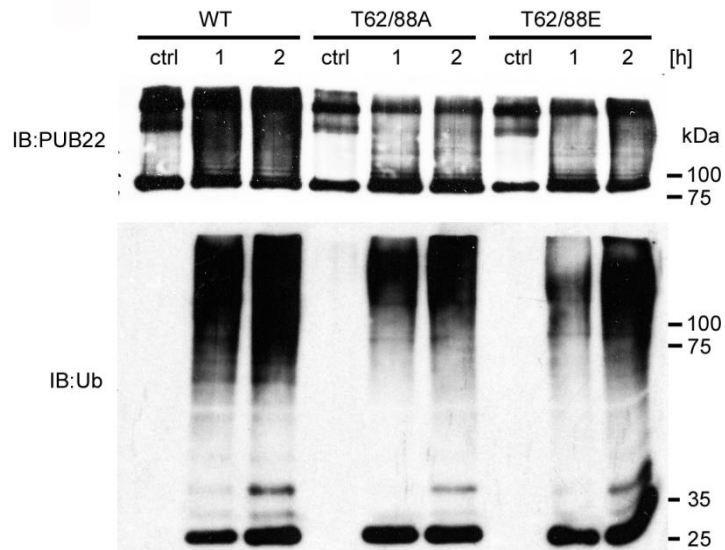
Figure 3-30 Autoubiquitination assay with PUB22 WT, PUB22$^{T62/88A}$, and PUB22$^{T62/88E}$. MBP-PUB22 WT, MBP-PUB22$^{T62/88A}$, and MBP-PUB22$^{T62/88E}$ were incubated together with His-UBA1 and His-UBC8 for the indicated time at 30°C. Proteins were analysed by SDS-PAGE and immunoblot using anti-PUB22 and anti-ubiquitin antibodies. Similar results were obtained in three independent experiments.

3.7.2 Exo70B2 ubiquitination is not impaired by PUB22 T62 and T88 mutations

PUB22 autoubiquitination activity was reduced by substitution of T62 and T88 by glutamic acid, yet surprisingly, also when mutated into alanine. In order to rule out the possibility that PUB22 mutations at these positions result in a general impairment of E3 activity, I investigated possible changes in the substrate ubiquitination. Exo70B2 was identified in previous reports as substrate of PUB22 (Stegmann et al. 2012). Therefore, I incubated purified His-Exo70B2 together with MBP-PUB22 WT, MBP-PUB22$^{T62/88A}$ or MBP-PUB22$^{T62/88E}$ in an *in vitro* ubiquitination assays to monitor substrate ubiquitination and E3 ligase autoubiquitination over time (Figure 3-31). As shown previously, PUB22 was able to ubiquitinate Exo70B2 *in vitro*. PUB22 phosphonull displayed a slightly reduced substrate ubiquitination, whereas PUB22 phosphomimetic a slight increase. This indicates that while mimicking phosphorylation results in a reduction of PUB22 autoubiquitination activity, it does not inhibit substrate ubiquitination.
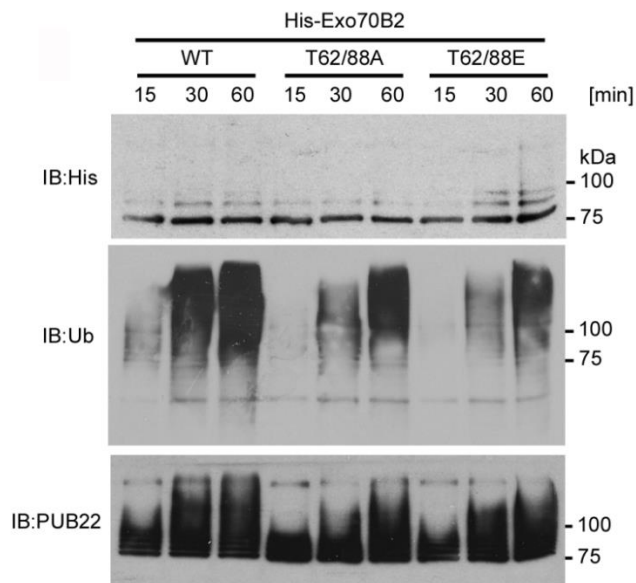
Figure 3-31 Exo70B2 ubiquitination by PUB22 WT, PUB22^T62/88A, and PUB22^T62/88E. MBP-PUB22 WT, MBP-PUB22^T62/88A, and MBP-PUB22^T62/88E were preincubated together with His-Exo70B2, His-UBA1 and His-UBC8. Ubiquitin was subsequently added and samples were incubated for the indicated time at 30°C. Proteins were analysed by SDS-PAGE and immunoblot using anti-His, anti-ubiquitin and anti-PUB22 antibodies. Similar results were obtained in two independent experiments.

3.7.3 T62 mediates the reduction in PUB22 autoubiquitination

Mimicking phosphorylation at position 62 and 88 had an additive effect *in vivo*, as revealed by the stronger stability presented by the double mutant. Because T62 and T88 are located in the U-box domain of PUB22 and in the linker region respectively, they may possess non-redundant functions influencing the activity of PUB22.

In order to analyse whether the two phosphomimetic mutations additively contribute to the reduction of PUB22 autoubiquitination activity, I generated single phosphonull and phosphomimetic mutants for PUB22. Subsequently, purified MBP-PUB22 WT, MBP-PUB22^T62A, MBP-PUB22^T62E, MBP-PUB22^T88A and MBP-PUB22^T88E were tested for *in vitro* autoubiquitination activity (Figure 3-32). Immunoblot analyses revealed that the autoubiquitination activity of PUB22^T88A and PUB22^T88E mutants was invariant from PUB22 WT. Whereas PUB22^T62A and PUB22^T62E displayed a reduced autoubiquitination activity. The phosphomimetic displayed a stronger impairment of its activity, similarly to what observed in the case of the double mutant (Figure 3-30).

In conclusion, these results suggest that phosphorylation at position 62 determines the reduction of the autoubiquitination activity of PUB22, resulting in its stabilization. By contrast, the phosphorylation at position 88, despite contributing to PUB22 stabilization *in vivo*, does not regulate autoubiquitination. Moreover, these results uncouple the regulation of PUB22 autoubiquitination activity, which is dependent on the phosphorylation status of residue T62, from the substrate ubiquitination, which was largely unaffected.

Figure 3-32 Autoubiquitination assay of PUB22 WT, PUB22^{T62A}, PUB22^{T62E}, PUB22^{T88A}, and PUB22^{T88E} single mutants. MBP-PUB22 WT, MBP-PUB22^{T62A}, MBP-PUB22^{T62E}, MBP-PUB22^{T88A}, and MBP-PUB22^{T88E} were incubated together with His-UBA1 and His-UBC8 for the indicated time at 30°C. Proteins were analysed by SDS-PAGE and immunoblot using anti-PUB22 and anti-ubiquitin antibodies. Similar results were obtained in three independent experiments.
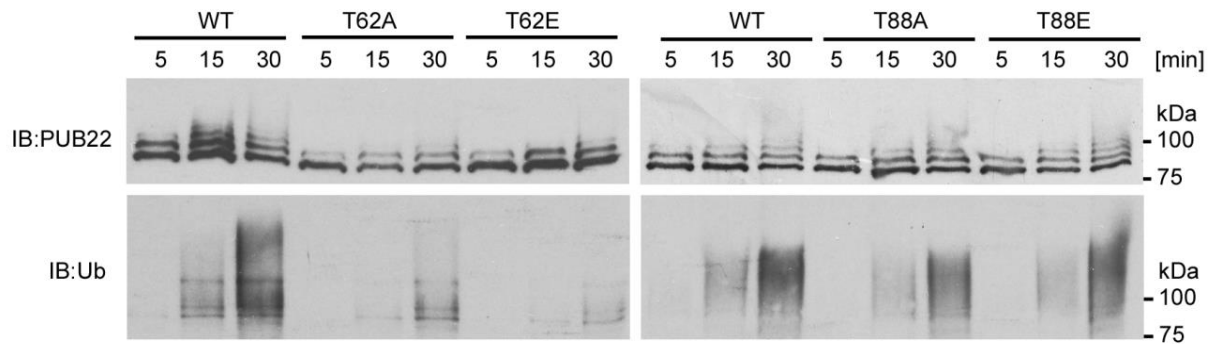
3.8 The role of T62 in PUB22 oligomerization

Results supported a role of T62 in the regulation of PUB22 autoubiquitination activity that is reflected on its stability. To dissect the molecular mechanism through which phosphorylation of T62 regulates the E3 ligase activity, I compared the PUB22 U-box sequence and structural model to dimeric and monomeric U-box E3 ligases. Starting from this point, I was able to extrapolate and demonstrate the molecular mode of action of PUB22.

3.8.1 T62 is located on a putative homodimerization surface of PUB22

The critical residue for the regulation of PUB22 autoubiquitination, T62, is located in the U-box domain. Because the structure of PUB22 U-box has not been yet resolved, a structural model was built by Dr. Marco Trujillo (IPB-Halle), using the zebrafish CHIP U-box crystal structure (PDB ID code 2F24) (Xu et al. 2006) (Figure 3-33). The model showed that T62 is exposed and therefore, accessible for phosphorylation. The residue was located opposite to the E2 interacting surface. W40, which mediates the interaction with E2s, was correctly predicted to be located at this interface. It is, therefore, unlikely that T62 regulates PUB22 autoubiquitination by affecting E2 binding.
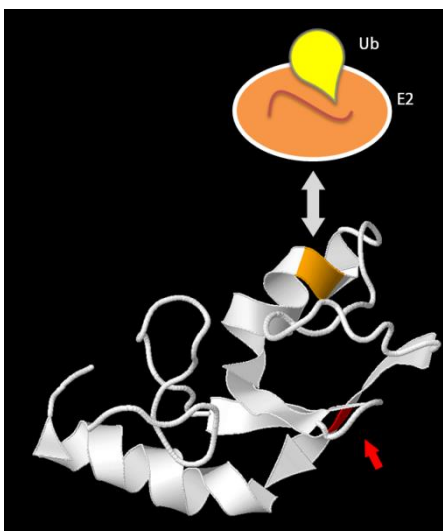
Figure 3-33 PUB22 U-box structural model. PUB22 U-box structural model (5-80 aa) was generated by using the web-based SWISS-MODEL for protein structure homology modelling using the zebrafish CHIP (PDB ID code 2F42) as template. W40 is highlighted in orange and T62 is highlighted in red. A schematic illustration of Ub~E2 illustrates the E2 interaction orientation.

The crystal structure of several yeast and animal U-box-containing E3 ligases has been determined, including the dimeric *M. musculus* CHIP (accession number NP_062693) and the monomeric *H. sapiens* E4B (accession number AAH93696) (Zhang et al. 2005, Benirschke et al. 2010). In order to clarify PUB22's mode of action, I performed an alignment of the U-box domains including *Mm*CHIP, *At*CHIP, *Sc*Prp19, *Hs*E4B and *Sc*Ufd2. Highlighted in violet and red are the four hydrophobic residues crucial for the homodimerization of *Mm*CHIP: Y231, I246, I282 and A286 (Figure 3-34). N284, additionally forms hydrogen bonds with the same residue on the complementary protomer (Zhang

et al. 2005). In the monomeric *Hs*E4B, the hydrophobic residues are substituted by charged residues and the aspartate with a valine. In PUB22, the first two hydrophobic residues are conserved (F10 and I25), as well as the hydrogen bond forming N64 (violet). However, the other two hydrophobic residues are substituted by threonines (red), the first one corresponding to T62.
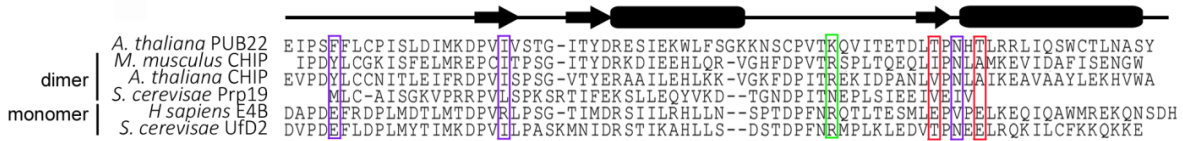
Figure 3-34 Sequence alignment of diverse U-box domains: Sequence alignment of U-box domains from different E3 ligases highlighting key conserved residues in PUB22 which are required for CHIP dimerization (violet) and variants including T62 (red) or such that may play a role in the activation of the E2-ubiquitin conjugate (green) (accession numbers: *At*PUB22 OAP06343, *Mm*CHIP NP_062693, *At*CHIP OAP04012, *Sc*Prp19 CAA97487, *Hs*E4B AAH93696, *Sc*Ufd2 CAA98767).

In order to acquire more information about the similarities between PUB22 U-box and dimeric or monomeric U-box E3 ligases, an electrostatic surface potentials map of PUB22 U-box model was generated and the available structures of *Mm*CHIP or *Hs*E4B were used for comparison (Figure 3-35). The five residues previously mentioned, residing at the CHIP dimer interface, are highlighted together with the corresponding residues on E4B and PUB22. The hydrophobic dimerization interface is characterized by the absence of electrostatic charges in CHIP. By contrast, E4B displays large acidic regions at the equivalent surface, which is likely to preclude dimer formation.

The electrostatic surface potentials on the corresponding surface of PUB22 U-box model resemble to a certain extent those of CHIP. Mimicking phosphorylation at position 62, resulted in the enlargement of the adjacent acidic patch, resembling E4B in this region. This suggests that PUB22 may dimerize via hydrophobic interaction through its U-box domain, similarly to CHIP. Whereas phosphorylation of T62 may affect the dimer formation via disturbing the hydrophobic interaction established by the nearby I25 and the hydrogen bond formed by N64. This would result in an increase of the monomeric status.
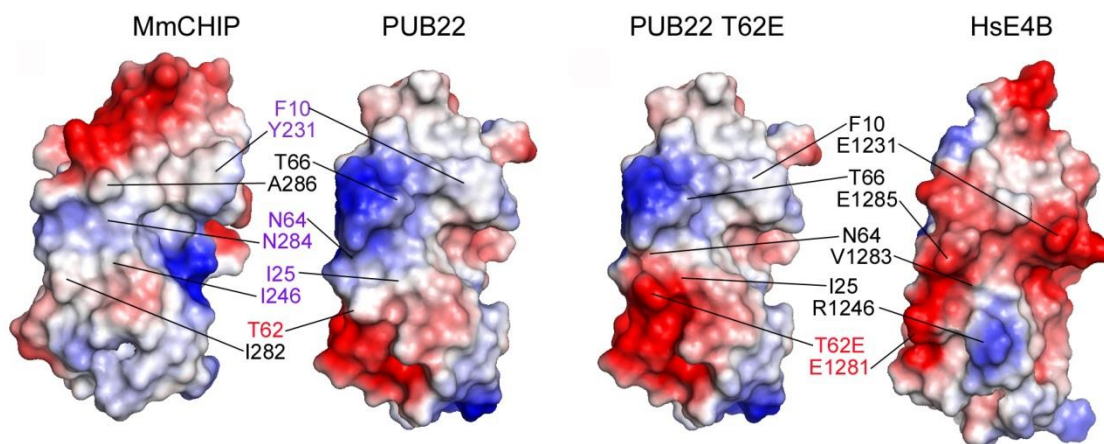
Figure 3-35 Electrostatic surface potentials of PUB22, CHIP and E4B U-box domains: Electrostatic surface potentials of mouse CHIP (PDB ID code 2C2V), the structural model of PUB22 and PUB22^{T62E} phosphomimetic mutant, and human E4B (PDB ID code 3L1X) showing the residues important for dimerization. PUB22 U-box structural model (5-80 aa) was generated by using the web-based SWISS-MODEL for protein structure homology modelling using the zebrafish CHIP (PDB ID code 2F24).

3.8.2 PUB22 oligomerizes via its U-box domain

In view of the above-mentioned similarities between PUB22 U-box and the homodimerizing CHIP U-box, I tested whether PUB22 also formed homooligomers by performing a pull-down assay using its U-box domain. Because it is not possible to know the number of molecules involved in the interaction, the term "oligomer" is employed, instead of dimer. Recombinant GST-PUB22^{U-box} was expressed and immobilized on glutathione agarose beads; free GST was used as control. Loaded beads were then incubated in a bacterial lysate containing His-PUB22^{U-box}. After washing, eluates were analysed by immunoblot (Figure 3-36). A band corresponding to His-PUB22^{U-box} was detected when using GST-PUB22^{U-box} as bait, but not when using free GST, indicating that PUB22 U-box can homooligomerize *in vitro*.
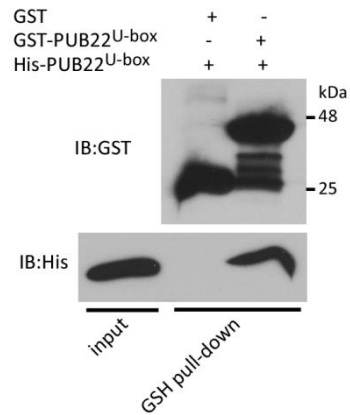
Figure 3-36 *In vitro* **pull-down assay to test U-box homooligomerization:** Recombinant GST-PUB22[U-box] was immobilized on glutathione agarose beads. Free GST was used as control. GST fusion proteins were incubated with lysate containing His-PUB22[U-box]. Eluates were analysed by SDS-PAGE and immunoblot with anti-GST and anti-His antibodies.

A similar experiment was performed to test heterooligomerization of the U-box domain of PUB22 with PUB24. PUB22[W40A] mutant was also included. The W40A mutation blocks the interaction with the E2 and is located opposite to the putative oligomerization surface. It was therefore employed to validate the putative orientation of the oligomer formation, which was predicted to be via the backside of the E2 interacting surface. Recombinant GST-PUB22[U-box] or free GST were used as baits on glutathione agarose beads to co-precipitate recombinant MBP-PUB22 WT, MBP-PUB22[W40A], or MBP-PUB24. In all cases, the full length ligase was co-purified exclusively in presence of GST-PUB22[U-box], and not of the GST control (Figure 3-37). Hence, W40 is not involved in dimerization and PUB22 U-box can form heterodimers *in vitro*.
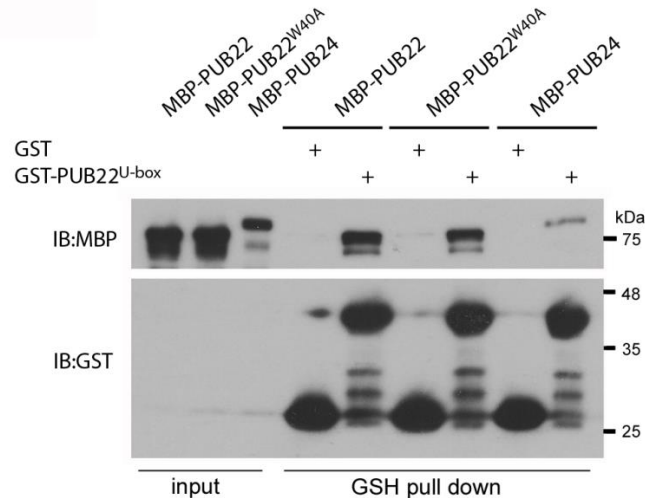
Figure 3-37 *In vitro* **pull-down assay to analyse U-box homo- and heterooligomerization:** Recombinant GST-PUB22[U-box] was immobilized on glutathione agarose beads. Free GST was used as control. GST fusion proteins were incubated with lysates containing MBP-PUB22, MBP-PUB22[W40A] or MBP-PUB24. Elutions were analysed by SDS-PAGE and immunoblot with anti-MBP and anti-GST antibodies.

3.8.3 T62 determines the oligomerization status

In vitro analyses demonstrated that PUB22 formed homooligomers and heterooligomers with PUB24 via its U-box domain. To confirm the ability of PUB22 to form oligomers, I performed *in vivo* oligomerization studies using a split-luciferase assay with each half of luciferase fused to two independent U-box domains of PUB22. The split-luciferase assay allows the dynamic and quantifiable analysis of protein-protein interaction. This enables both the analysis of PUB22 oligomerization and the effect of the T62 mutation. However, to overcome the unequal accumulation of full-length PUB22 phosphomutants *in vivo* (Figure 3-27), the U-box domain only was cloned in order to obtain comparable expression of the split luciferase U-box fusion proteins.

The N-terminal or the C-terminal part of the luciferase enzyme (nLUC or cLUC) was cloned at the C-terminus of PUB22[U-box] WT and mutants to generate the *U-box-nLUC* and *U-box-cLUC* constructs. Constructs were transiently transformed in mesophyll protoplasts and upon addition of the luciferase substrate, luciferin, luminescence was quantified in a plate-reader (Figure 3-38). Co-expression of WT U-boxes resulted in a strong luminescence signal, which was normalized to 100. The expression of the phosphomimetic U-box[T62E] displayed a significant reduction of the

luminescence signal, which reflects a reduction of the oligomerization status, in agreement with the model of the electrostatic potentials. The expression of the U-box^{T62A} phosphonull mutant also displayed a reduced signal. However, the effect of the T62E mutation was stronger.

Because the previous analysis of PUB22$^{U\text{-}box}$ model suggested a potential oligomerization via hydrophobic interactions, I mutagenized T62 into an isoleucine and tested U-box^{T62I} oligomerization (Figure 3-38). Co-expression of U-box^{T62I}-nLUC with U-box^{T62I}-cLUC showed a significant increase in luminescence in comparison to the U-box WT, suggesting that the isoleucine substitution at position 62 stabilizes the oligomer formation.
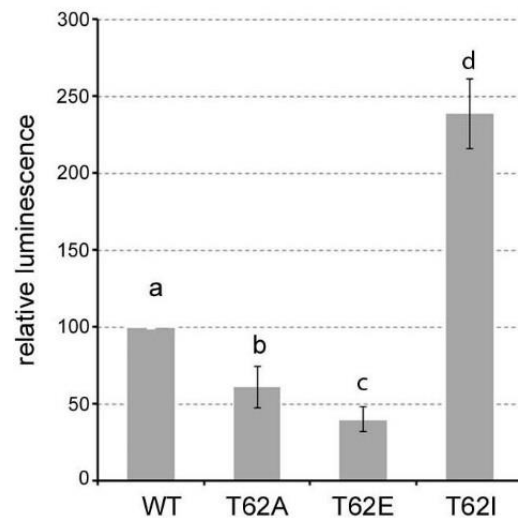
Figure 3-38 Split luciferase assay to analyse U-box *in vivo* oligomerization. *35Sprom::PUB22$^{U\text{-}box}$-nLUC* and *35Sprom::PUB22$^{U\text{-}box}$-cLUC* constructs were co-transformed into Arabidopsis mesophyll protoplasts derived from *pub22 pub23 pub24* mutant plants. Constructs carrying T62A, T62E or T62I mutation were included. One day after transformation samples were incubated 10 min with 1 mM D-luciferin and luminescence was measured in a plate reader. Shown is the normalized mean signal intensity +/- S.D. of three independent biological replicates. Letters indicate significantly different values between WT and mutant variants of at least three independent biological replicates at p < 0,05 (one way ANOVA, Tukey post hoc test).

The comparable levels of expression of the U-box split luciferase fusion proteins for WT, T62A, T62E and T62I mutants was assessed by immunoblot using a polyclonal anti-luciferase antibody which recognized both halves of luciferase. As shown in Figure 3-39, all the split luciferase fusion proteins accumulate equally.
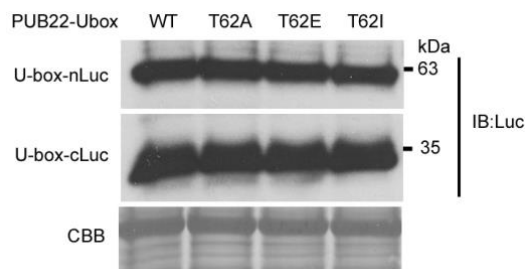
Figure 3-39 Analysis of the expression levels of split luciferase fusion proteins. Total protein samples from split luciferase experiments in Figure 3-38 were analysed by SDS-PAGE and immunoblot using anti-luciferase antibodies. CBB was used as control for equal loading.

3.8.4 Hydrophobic residues mediate PUB22 oligomerization

The increase in the oligomerization status displayed by T62I suggested that oligomerization occurs via hydrophobic interactions. Moreover, the sequence alignment of PUB22 and CHIP U-box domains indicated that the conserved F10 and I25 hydrophobic residues may contribute to oligomerization. In order to validate their importance, the model of PUB22 U-box was used to predict the U-box dimer (Figure 3-40). F10 and I25, highlighted in magenta, as well as T62 in red, are indeed located at the predicted interface between the protomers. While T62 and I25 face a hydrophobic region of the interacting protomer, F10 resides over a positively charged patch (blue).
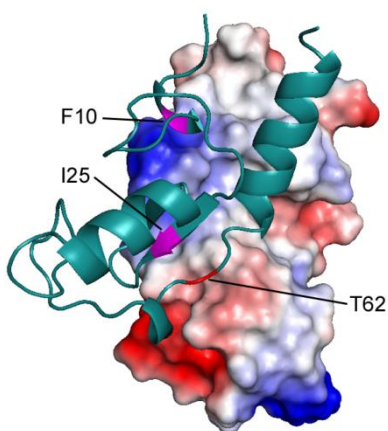
Figure 3-40 Model of PUB22^{U-box} dimer. Structural model of PUB22^{U-box} dimer. Residues F10 and I25 are highlighted in magenta and T62 in red. Dimer model was generated by SwissModel.

To assess their importance in the oligomer formation and the accuracy of the model, I mutated I25 into an arginine (R), to destabilize the hydrophobic interactions and reduce oligomerization. F10 was substituted by a glutamic acid creating an ionic interaction with the positive patch of the other protomer, which is expected to increase oligomerization. Split luciferase constructs carrying *U-box*^{I25R} or *U-box*^{F10E} were generated and transformed into mesophyll protoplasts for split luciferase assay as described above. *U-box*^{W40A} was included as control, since the position of W40 should not affect the interaction.

Indeed, the W40A mutation did not significantly alter the luminescence signal and hence, the oligomerization (Figure 3-41). Whereas the expression of U-box^{I25R} or U-box^{F10E} split luciferase constructs resulted in a reduction and an enhancement of the luminescence signal respectively (Figure 3-41). These results support the accuracy of the generated models and a role for I25 and F10 in the mediation of oligomer formation via hydrophobic interactions.
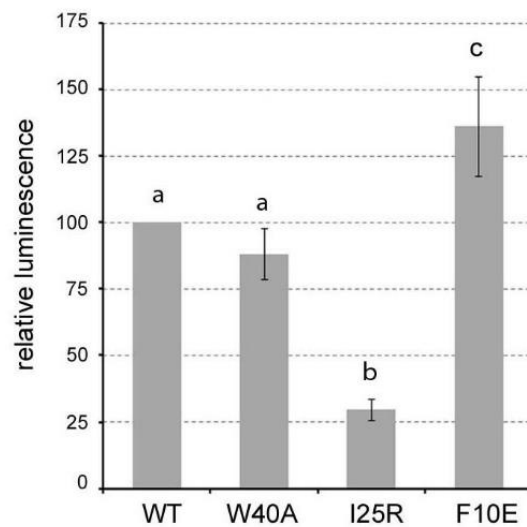
Figure 3-41 Split luciferase assay to analyse U-box-mediated oligomerization and the role of conserved residues. *35Sprom::PUB22*$^{U-box}$*-nLUC* and *35Sprom::PUB22*$^{U-box}$*-cLUC* constructs were co-transformed into Arabidopsis mesophyll protoplasts derived from *pub22 pub23 pub24* mutant plants. Constructs carrying W40A, I25R or F10E mutation were included. One day after transformation samples were incubated 10 min with 1 mM D-luciferin and luminescence was measured in a plate reader. Shown are the normalized mean signal intensities +/- S.D. of three independent biological replicates. Letters indicate significantly different values between WT and mutant variants of at least three independent biological replicates at p < 0,05 (one way ANOVA, Tukey post hoc test).

The equal expression of the U-box split luciferase fusion proteins for WT, W40A, I25R and F10E mutants was assessed by immunoblot using the anti-luciferase antibody and showed that all variants were expressed to similar levels (Figure 3-42).
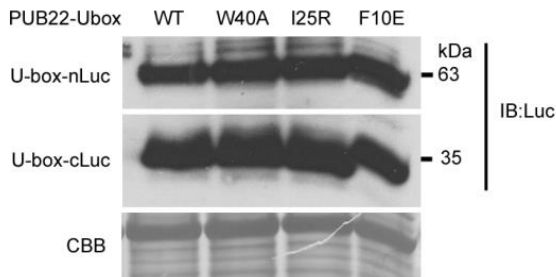
Figure 3-42 Split luciferase fusion proteins expression analysis: Total protein samples from split luciferase experiments in Figure 3-41 were analysed by SDS-PAGE and immunoblot using anti-luciferase antibodies. CBB was used as control for equal loading.

3.9 The link between oligomerization and autoubiquitination

The latter results showed that PUB22 oligomerizes via its U-box domain. Mimicking phosphorylation at T62 decreases oligomer formation in favor of the monomeric conformation. Moreover, T62E mutation reduces the ability of PUB22 to autoubiquitinate *in vitro*, which correlates with its enhanced stability *in vivo*. Therefore, in order to confirm the connection between oligomerization and autoubiquitination activity, the autoubiquitination activity of additional PUB22 mutants, displaying altered oligomerization, was characterized. Furthermore, I explored whether PUB22 autoubiquitination occurs *in cis* or *trans*.

3.9.1 The oligomerization status influences the autoubiquitination activity

Mimicking phosphorylation at T62 reduced PUB22$^{U\text{-box}}$ oligomerization status and additionally the autoubiquitination activity of PUB22 *in vitro*. On the other hand, T62I substitution stabilized the

oligomer. If oligomer formation correlates with autoubiquitination activity, as suggested by the phosphonull and phosphomimetic analyses, PUB22^{T62I} should present increased autoubiquitination activity. To test this, I purified MBP-PUB22^{T62I} and tested its autoubiquitination activity by *in vitro* autoubiquitination assay. Immunoblot analysis with anti-PUB22 antibodies revealed that indeed PUB22^{T62I} possesses enhanced autoubiquitination activity (Figure 3-43).
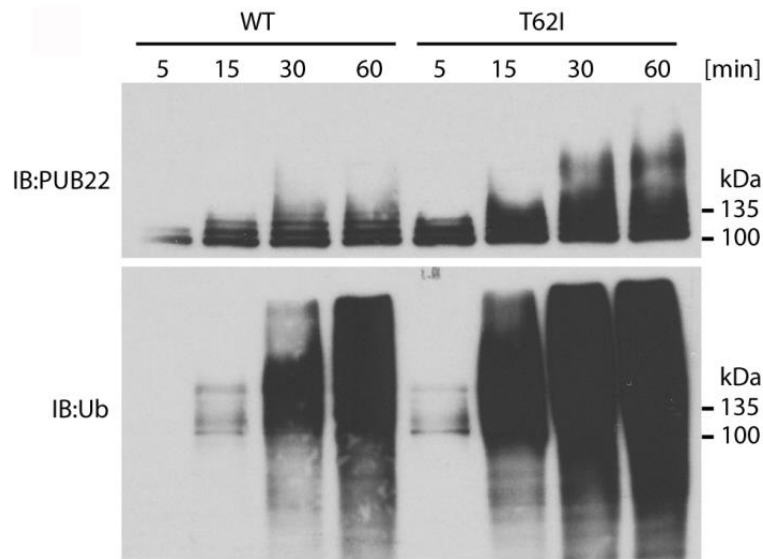
Figure 3-43 Autoubiquitination assay of PUB22 WT and PUB22^{T62I}. MBP-PUB22 WT and MBP-PUB22^{T62I} were incubated together with His-UBA1 and His-UBC8 for the indicated time at 30°C. Proteins were analysed by SDS-PAGE and immunoblot using anti-PUB22 and anti-ubiquitin antibodies. Similar results were obtained in three independent experiments.

Two additional mutations, I25R and F10E, were shown to also affect oligomerization, with reducing and enhancing effects respectively. Purified MBP-PUB22^{I25R} and MBP-PUB22^{F10E} displayed reduced and enhanced activity respectively (Figure 3-44), confirming the correlation between the oligomerization status and autoubiquitination.
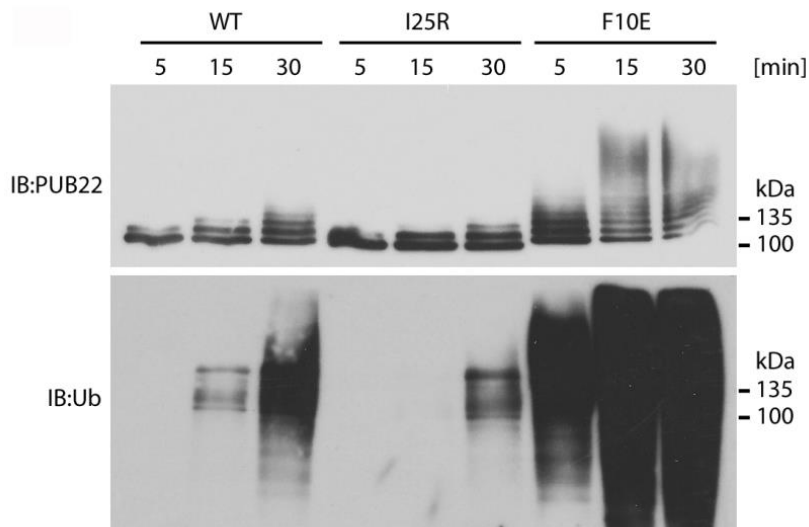
Figure 3-44 Autoubiquitination assay of PUB22 WT, PUB22^{I25R}, and PUB22^{F10E}. MBP-PUB22 WT, MBP-PUB22^{I25R}, and MBP-PUB22^{F10E} were incubated together with His-UBA1 and His-UBC8 for the indicated time at 30°C. Proteins were analysed by SDS-PAGE and immunoblot using anti-PUB22 and anti-ubiquitin antibodies. Similar results were obtained in two independent experiments.

3.9.2 PUB22 autoubiquitinates *in trans*

The mutational analysis of the amino acids at the oligomerization interface proved the direct correlation between oligomerization and autoubiquitination. I reasoned that autoubiquitination *in trans* would be a prerequisite for the oligomerization to directly influence the autoubiquitination (Figure 3-45), because evidently *trans*-ubiquitination is dependent on dimer/oligomerization. In contrast, ubiquitination *in cis* would be theoretically independent of oligomerization. Nevertheless, oligomerization may conceivably result in conformational changes, affecting activity.
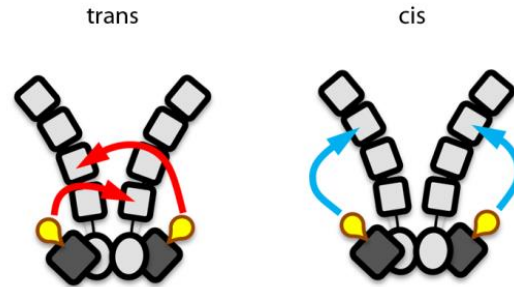
Figure 3-45 Schematic representation of autoubiquitination mechanisms. Schematic illustrations depict potential mechanisms of self-catalysed ubiquitination by PUB22 dimer occurring *in trans* or *cis*.

To test whether PUB22 *trans*-ubiquitinates, I set up a *trans*-ubiquitination assay consisting of full-length MBP-PUB22^{W40A} as a substrate for *trans*-ubiquitination by GST-PUB22^{U-box} (Figure 3-46 cartoon). Because the full-length W40A mutant variant is inactive, its modification can only be the result of *trans*-ubiquitination by the catalytically active U-box (Figure 3-46). The inactive mutant W40A did not display any autoubiquitination activity, as previously shown. Whereas in presence of the active U-box domain, PUB22^{W40A} became ubiquitinated, as demonstrated by the appearance of high molecular weight species.

In summary, these results unveil *trans*-ubiquitination as a mode of action of PUB22 autoubiquitination. This is consistent with the autoubiquitination activity being dependent on the oligomerization status, which was demonstrated by the mutational analysis of the amino acids exposed on the oligomerization interface, including T62. Moreover, phosphorylation of T62 is probably involved in the regulation of this molecular mechanism during immunity, through the reduction of the oligomerization, which results in reduced autoubiquitination and finally stabilization.
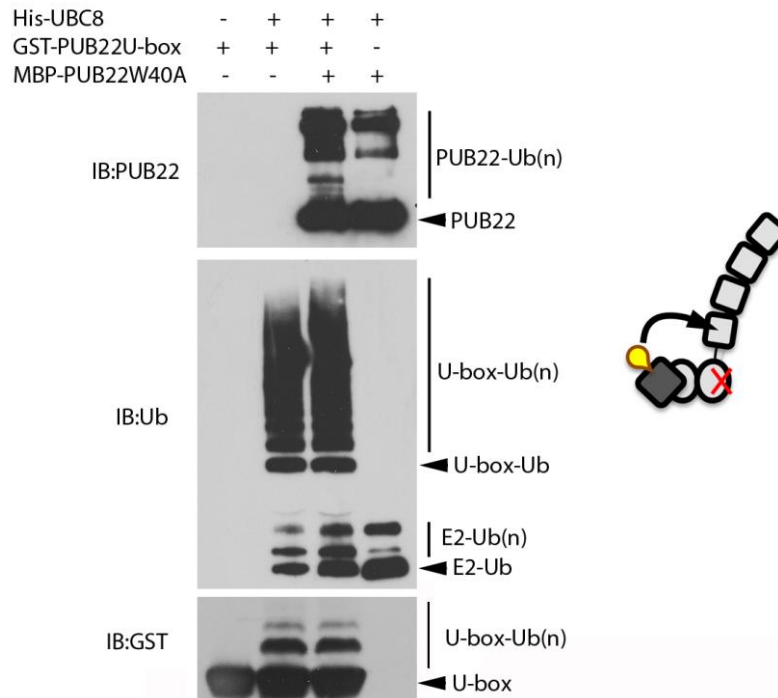
Figure 3-46 PUB22 *trans*-ubiquitination assay. The truncated catalytically active GST-PUB22$^{U\text{-box}}$ was preincubated with full-length catalytically inactive MBP-PUB22^{W40A}, His-UBA1 and His-UBC8. Ubiquitin was subsequently added and samples were incubated for two hours at 30°C. Proteins were analysed by SDS-PAGE and immunoblot using anti-PUB22 (recognizes C-term), anti-ubiquitin and anti-GST antibodies. Schematic illustration of the *trans*-ubiquitination assay.

3.10 Functional analysis of PUB22 variants

The biochemical data indicates that in order for PUB22 to carry out its function during the immune response, it must undergo an initial stabilization process triggered by phosphorylation. In order to verify a loss of functionality of PUB22$^{T62/88A}$ during immunity, I performed various assays to analyse the functional complementation. The *UBQ10::GFP-PUB22$^{T62/88A}$* and *UBQ10::GFP-PUB22$^{T62/88E}$* lines were generated in the *pub22 pub23 pub24* triple mutant background, and hence, I was able to assess the complementation of immunity-related phenotypes. *UBQ10::GFP-PUB22 WT* and *UBQ10::GFP-PUB22^{W40A}* were used as controls together with Col-0 and *pub22 pub23 pub24* mutant plants.

In agreement with my previous results, the inhibition of triple mutants root growth was significantly stronger than Col-0 (67,8 % vs 33,8 %) (Figure 3-47). The expression of PUB22 WT, but not

PUB22^{W40A}, partially complemented the enhanced growth inhibition phenotype (53,3 % vs 67,3 %), as reported before. PUB22$^{T62/88A}$ phosphonull expressing seedlings displayed a similar inhibition to the triple mutants (63,7 %), indicating a loss of the complementation. In contrast to expectations, the PUB22$^{T62/88E}$ phosphomimetic also failed to complement this phenotype (64,4 %).

| | | *pub22 pub23* | *pub22 pub23 pub24/UBQ10prom::GFP-PUB22* | | | |
	Col-0	*pub24*	WT	W40A	T62/88A	T62/88E
Root growth DMSO [cm]	8,4 +/- 1,6	8,4 +/- 1,3	8,6 +/- 1,5	8,4 +/- 1,2	8,3 +/- 1,6	8,8 +/- 1,2
Root growth flg22 [cm]	5,4 +/- 0,6 ***	2,7 +/- 0,4	4,0 +/- 0,7 ***	2,7 +/- 0,4	3,0 +/- 0,6	3,0 +/- 0,5
Root growth inhibition [%]	33,8 +/- 10,6	67,8 +/- 4,3	53,3 +/- 6,6	67,3 +/- 2,7	63,7 +/- 5,4	64,4 +/- 6,4

Figure 3-47 Root growth inhibition complementation assay for *UBQ10prom::GFP-PUB22 WT, W40A, T62/88A, and T62/88E* (transgenic lines A): Measurements of root growth inhibition were performed in 20 days old seedlings grown for 14 days in 1 μM flg22 or DMSO containing ½ MS medium. Data is shown as mean of three independent experiments +/- S.E.M. (n=12). Statistical significance compared to *pub22 pub23 pub24* triple mutant plants is indicated by asterisks (Student's t-Test, *p < 0,05; **p < 0,01; ***p < 0,001). Similar results were obtained using an additional independent line (line B) per each construct.

Next, MAPKs activation was analysed. Phosphorylated forms of MPK3 and MPK6 upon flg22 treatment could be detected by immunoblot using anti-pERK1/2 antibody in the Col-0 WT seedlings 20 minutes after flg22 treatment (Figure 3-48). In line with their enhanced resistance phenotype, *pub* triple mutants displayed a stronger and prolonged activation of MPK3 and MPK6, in comparison to Col-0. MAPKs activation was attenuated by PUB22 WT. Signal attenuation was additionally increased by the expression of the PUB22$^{T62/88E}$ phosphomimetic, indicating a stronger dampening of the *pub22 pub23 pub24* enhanced responsiveness phenotype. Whereas, the expression of the inactive PUB22^{W40A} mutant or PUB22$^{T62/88A}$ phosphonull displayed a weaker but still prolonged activation of MAPKs, more similar to the triple mutants.
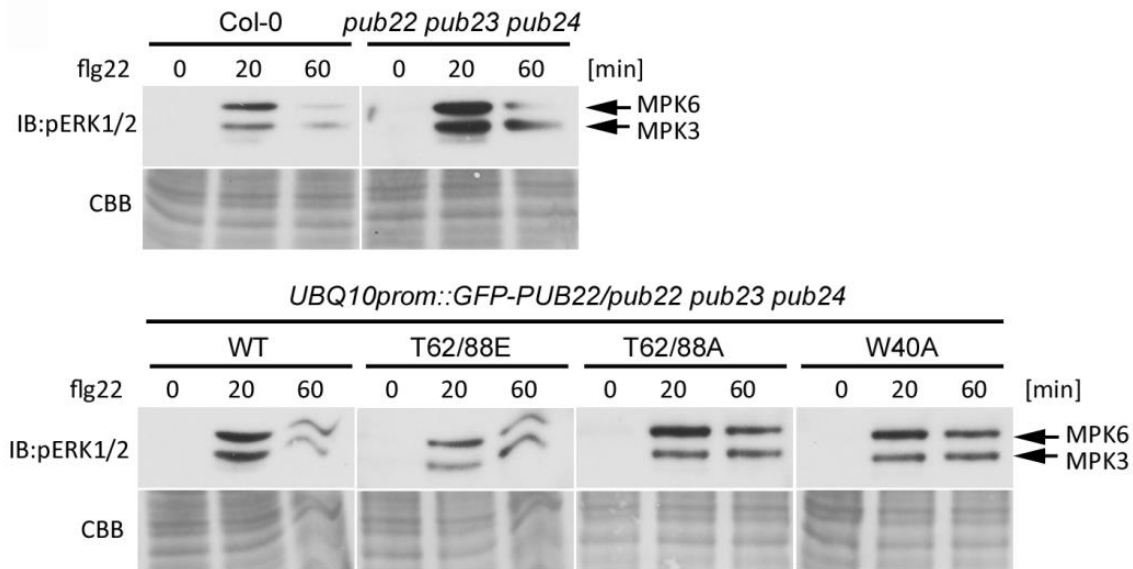
Figure 3-48 Analysis of MAPK activation in transgenic lines expressing mutant variants of PUB22. Two-week-old seedlings of the indicated genotypes (transgenic lines A) grown on ½ MS solid medium, were treated for the indicated time with 100 nM flg22. Total protein samples were analysed by SDS-PAGE and immunoblot using anti-pERK1/2 antibodies. Similar results were obtained in two independent experiments.

Finally, to further assess the biological significance of PUB22 phosphorylation, I examined the disease resistance phenotypes using the virulent pathogen *Pseudomonas syringae* pv *tomato* DC3000 *ΔavrPto/ΔavrPtoB*. This less virulent *P. syringae* mutant is impaired in PTI suppression and therefore, more suitable for the distinction of mild resistance phenotypes. Leaves were infiltrated with a needle-less syringe and the bacterial growth was measured two days after infiltration (Figure 3-49). The expression of PUB22 WT rendered the plants significantly more susceptible in comparison to the *pub22 pub23 pub24* mutant. The same phenotype was measured for the PUB22[T62/88E] phosphomimetic, suggesting that the phosphorylated form of PUB22 is the active form. On the other hand, the expression of PUB22[W40A] inactive mutant and PUB22[T62/88A] phosphonull led to a slightly higher, although not significantly different, bacterial growth in comparison to the triple mutants. This indicates that phosphorylation of T62 and T88 is required for the PUB22-mediated dampening of the immune responses.
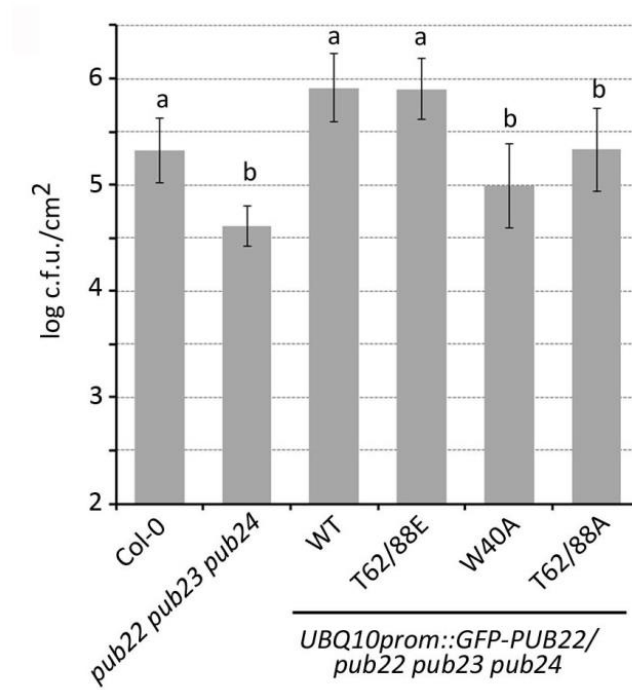
Figure 3-49 Analysis of disease resistance in transgenic lines expressing mutant variants of PUB22. Six-week-old plants of the indicated genotypes (transgenic lines B) were syringe infiltrated with a 1×10^5 c.f.u./ml bacterial suspension of *Pst DC3000 ΔAvrPto/ΔAvrPtoB*. Bacterial growth was assessed two days after infection. Shown is the mean value +/- S.D. (n = 5). Similar results were obtained in three independent experiments. Letters indicate signicantly different values $p < 0,05$ compared to *pub22 pub23 pub24* (one-way ANOVA and Tukey post hoc test).

4. Discussion

PUB22 is one of the most extensively studied PUB proteins. Its importance became clear when genetic analyses revealed its function in the dampening of the immune signalling. Triple knockout plants for *PUB22* and its homologs displayed stronger and prolonged responses to various elicitors. Enhanced responsiveness results in enhanced resistance against pathogens. Because mutants do not display a developmental phenotype, PUB22, PUB23 and PUB24 are proposed to exclusively mediate the downregulation of activated immune signalling. Subsequent studies showed that they fulfil this function, at least in part, by targeting the exocyst subunit Exo70B2. Unpublished data confirms that PUB22 and PUB24 interact with additional components of the intracellular transport. These observations suggest that the triplet mediates the reorganization of the vesicular trafficking during immunity.

Besides being transcriptionally induced, PUB22 was shown to be rapidly stabilized upon activation of immunity, potentially via attenuation of its self-catalysed constant turnover. This puzzling trait provided the first clue to the existence of a post-translationally regulated process acting on PUB22 activity. In order to shed light on the mode-of-action of single unit E3 ligases, this work aimed at deciphering the molecular mechanisms regulating PUB22 activity, using its instability as a starting point.

4.1 Dynamics of PUB22 expression and stabilization

PUB22 transcriptional induction was broadly examined in the work of Trujillo and colleagues (2008). *PUB22* transcripts were verified to be up-regulated upon PAMP treatments, as well as upon application of *Pst* bacterial pathogens and *Hpa* an oomycete pathogen. Moreover, promoter-GUS fusion experiments showed that the 2 kb region upstream of *PUB22* indeed contained the functional promoter elements for PAMP responsiveness. The time point chosen for the mentioned *PUB22*

induction by PAMPs, was 60 minutes after treatment, common for monitoring transcriptional changes.

In this work, using a functional native promoter line (Figure 3-1), I could directly confirm PUB22 protein expression 60 minutes after flg22 treatment, as well as at the following time points (Figure 3-2), in agreement with the previously shown promoter induction results. Nevertheless, early immune signalling response analyses, such as the measurement of ROS production and of MAPKs activity, had demonstrated that already within the first few minutes, *pub22 pub23 pub24* mutant plants respond with a faster and enhanced activation of the immune response in comparison to Col-0 plants (Trujillo et al. 2008). This phenotype suggested a role for the endogenous *PUB22*, *PUB23* and *PUB24* in the regulation of the signalling output already in naive plants, and therefore before of *PUB22* promoter induction and *de novo* protein synthesis, in addition to a role in signal downregulation after the activation of the immune responses. Indeed, my immunoprecipitation experiments reveal a low concentration of PUB22 present in naive plants (Figure 3-3), indicating low basal promoter activity. In addition, I showed that the basal pool of PUB22 protein undergoes continuous proteasomal turnover (Figure 3-4), keeping PUB22 levels low. Low levels of PUB22 were only detectable after immunopurification. This is consistent with the minimal accumulation of PUB22 even when overexpressed by the 35S promoter (Figure 3-11, Figure 3-12, Stegmann et al. 2012).

PUB22's rapid stabilization after activation of immune responses is suggestive of a regulatory mechanism. Stabilization already takes place 5 minutes after flg22 treatment (Figure 1-3 B) (Stegmann et al. 2012), largely precluding any transcriptional effect. PUB22 accumulation peaks at 30 and 60 minutes after treatment, and returns to initial levels after 180 minutes. Because PUB22 is stabilized already within the first minutes after pathogen perception, I inferred that the stabilization mechanism impinges on the stability of the existing protein pools by enabling them to escape degradation. This regulatory system may consent PUB22 to establish an initial prompt response in the downregulation of immune signalling, which precedes its transcriptional induction and is crucial to fine tune the activation of rapid responses. In addition, the importance of PUB22 stabilization is evidenced by the inability of transgenic lines overexpressing the PUB22$^{T62/88A}$ mutant, which is not stabilized by the activation of immune responses (Figure 3-28), to complement the pathogen resistance phenotype as efficiently as the WT or the phosphomimetic variant (Figure 3-49). This indicates that stabilization of PUB22 mediated by T62/88 phosphorylation is required for its full

functionality in response to pathogen attack. Interestingly, overexpression of neither of the PUB22 phosphomutant variants complemented the increased inhibition of root growth phenotype presented by the *pub* triple mutant seedlings grown in presence of flg22 (Figure 3-47). This supports a specialized function for the phosphorylation of PUB22 in the regulation of only certain defence-related responses.

By contrast, the expression of *PUB22prom::GFP-PUB22* in the transgenic line conveyed nearly full complementation of the *pub22 pub23 pub24* enhanced root growth inhibition phenotype (Figure 3-1). Because the expression of PUB22 alone in the *PUB22prom::GFP-PUB22* line achieves full complementation of a triple *pub* knockout genotype, it is likely that PUB22 is transcribed to a higher extent than in the Col-0 genotype. In fact, while the GFP-PUB22 fusion protein could be detected by immunoblot (Figure 3-2), endogenous PUB22 could never be detected using the same experimental conditions and treatments (data not shown). This suggests a lower abundance of the endogenous PUB22. Indeed, insertional effects have to be taken into account, which may influence the level of transcription. Alternatively, it is conceivable that the absence of PUB23 and PUB24 alters *PUB22* transcription in the *PUB22prom::GFP-PUB22* line. For future experiments, in order to estimate the relative contribution of *PUB22* transcription in combination with PUB22 stabilization, native promoter lines for the expression of PUB22 phosphomutants could be generated.

4.2 Reciprocal downregulation of PUB22 and MPK3 activity in a negative feedback loop

Negative feedback loops are inherent to all signalling networks. Homeostatic systems make use of negative feedback loops to accelerate their stabilization into steady state conditions (Ferrell 2013). This work revealed that the stabilization of PUB22 is regulated through a negative feedback loop, activated by MPK3. MPK3 was identified as an upstream signalling component phosphorylating PUB22 at T62 and T88, leading to its stabilization (3.4, 3.6). Consequently, the stable variant of PUB22, namely the phosphomimetic mutant PUB22$^{T62/88E}$, was shown to downregulate immune signalling, including the downregulation of the activation of MPK3 itself (Figure 3-48). In this way, PUB22 and MPK3 create reciprocal regulatory loops, acting on each other's activity.

Through the stabilization of PUB22, MPK3 contributes to the attenuation of PTI. Accordingly, despite being long considered a positive regulator of immunity, together with MPK6, recent transcriptomic and genetic studies revised its role, and brought to light a negative regulatory function for MPK3 (Frei dit Frey et al. 2014, Ranf et al. 2011). Therefore, MPK3 and MPK6 appear to be far more functionally distinct than previously thought. These observations are in agreement with the reported specific phosphorylation of PUB22 by MPK3 and not by MPK6 (Figure 3-19). *mpk3* mutants do not have a constitutively active immunity phenotype, suggesting that MPK3 is probably dedicated to the downregulation of activated immune responses in a similar way as PUB22 and its homologs. In line with this, *mpk3* phenocopies the *pub22 pub23 pub24* triple mutant. Both display increased ROS production upon flg22 and elf18 treatment (Ranf et al. 2011, Trujillo et al. 2008) and increased resistance to *Pst* DC3000 (Frei dit Frey et al. 2014, Trujillo et al. 2008). Accordingly, *mpk3* mutant plants lack the ability to stabilize PUB22 (Figure 3-25), suggesting that PUB22 and potentially other functionally redundant homologs such as PUB24, may be further key components targeted in MPK3-mediated signal dampening. Indeed, PUB24 was also phosphorylated by MPK3 *in vitro* (Figure 3-19) and stabilized upon co-expression with MKK5^{DD} (Figure 3-26). Notably, T62 and T88 are conserved in 40 % and 21 % of class II and class III PUBs respectively (appendix Figure 7-6).

On the other hand, *pub22 pub23 pub24* triple mutants display prolonged activation of MPK3 (Trujillo et al. 2008). Because the *pub22 pub23 pub24* triple mutants are highly resistant against pathogens, this phenotype supports the importance of PUB22, PUB23, and PUB24 as targets of MPK3 in the attenuation of the immune signal. Furthermore, the specific prolonged activation of MPK3 hints towards a possible direct and specific feedback regulation of MPK3 by PUB22. However, despite interacting with each other, MPK3 was not ubiquitinated by PUB22 in an *in vitro* ubiquitination assay (appendix Figure 7-7). Therefore, the prolonged activation of MPK3 present in *pub22 pub23 pub24* apparently is indirect. A constellation which would allow such an indirect effect was reported for the cellular inhibitor of apoptosis protein 1 (cIAP1) and XIAP RING E3 ligases. In combination with UbcH5a, cIAP1 and XIAP ubiquitinate MEKK2 and MEKK3 with K63-linked chains to regulate cell differentiation (Takeda et al. 2014). The chains anchored on MEKK2 and MEKK3 were proposed to directly impede the MEK5-ERK5 interaction, in this way downregulating downstream MAPK signalling. Whether PUB22 can influence the activation of MPK3 by ubiquitinating the upstream MKK5 is an interesting possibility that remains to be tested.

It is possible that MPK3 regulation by PUB22 originates from a different mechanism involving Exo70B2, the confirmed target of PUB22. Also, in *exo70b2* mutant plants, the activation of MPK3 specifically, is lower, opposite to *pub22 pub23 pub24* triple mutant plants (Stegmann et al. 2012). These results support the involvement of Exo70B2 in the negative feedback loop of PUB22 on MPK3 activity. In the signalling cascade, MPK3 is placed at a convergence point shared by different receptors, thereby explaining PUB22's stabilization by treatment with multiple elicitors (Figure 3-13). Hypothetically, Exo70B2 may contribute to PRRs intracellular trafficking and influence the levels of PM-localized receptors and thus the downstream signal intensity, including MPK3 activation. However, it seems unlikely that changes in PRR levels are responsible for the specific prolonged activation of one specific MAPK.

4.3 PUB22 autoubiquitination and self-degradation

Autoubiquitination is a feature common to most single unit E3 ligases *in vitro*. While assessing autoubiquitination activity *in vitro* is a straight forward task, to prove autoubiquitination activity *in vivo* is hampered by many obstacles, such as protein half-life and the action of DUBs. Moreover, other E3 ligases may contribute *in vivo* to the ubiquitination of the E3 ligase in question, disturbing the evaluation of autoubiquitination.

I could demonstrate that PUB22 possesses true autoubiquitination activity *in vitro* (Figure 3-6), independently of the purification tag. In some cases, the purification tag may serve as a ubiquitination substrate producing false positives or activates the otherwise inhibited E3 ligase autoubiquitination activity as in the case of Parkin (Burchell et al. 2012). LC-MS/MS analyses led to the identification of multiple ubiquitinated sites on PUB22 (Figure 3-7, appendix Figure 7-2), underlining that PUB22 can undergo autoubiquitination *in vitro*. In this regard, the attempts to supply the best proof of PUB22 autoubiquitination by comparing *in vivo* ubiquitination levels between PUB22 and PUB22^{W40A} was precluded by the drastic disparity in protein accumulation between the two variants.

4. Discussion

Self-destructing ligases: regulation of their autoubiquitination

This work revealed that PUB22 can oligomerize via its U-box domain (Figure 3-36, Figure 3-38) and that PUB22 autoubiquitination occurs *in trans* (Figure 3-46) on the PUB22 oligomer. In line with this, the degree of autoubiquitination directly correlates to the oligomeric status (3.9), indicating that oligomerization influences autoubiquitination. In addition, I revealed that the oligomerization status itself is regulated by the phosphorylation event at T62 (Figure 3-38) (discussed in 4.4). Interestingly, PUB22 could not only homooligomerize, but also heterooligomerize with PUB24 *in vitro* (Figure 3-37), raising the possibility that PUB22 is *trans*-ubiquitinated by PUB24 and other heterologous E3 ligases by forming heterooligomers. PUB22 displayed enhanced stability when expressed in *pub22 pub23 pub24* triple mutant genetic background compared to the Col-0 genotype, supporting the hypothesis of PUB heterooligomers formation, consequent *trans*-ubiquitination, and degradation. In the homologs PUB12 and PUB13, besides PUB23 and PUB24, the T62 residue is conserved (appendix Figure 7-6), adding them to the list of PUB22 potential heterooligomerizing partners. In support of this, preliminary data showed that the inactive PUB22^{W40A} expressed in a *pub22 pub23 pub24* triple mutant genetic background was ubiquitinated *in vivo* (data not shown). Furthermore, PUB22^{W40A} displayed the ability to stabilize upon flg22 treatment (Figure 3-28) and to accumulate upon proteasome inhibitor treatment (Figure 3-29). Therefore, despite PUB22 autoubiquitination being crucial for its regulation, additional mechanisms, including heterooligomer formation, and *trans*-ubiquitination, are likely to be in place to ensure PUB22 degradation. Such interactions give a first glimpse at a highly interconnected circuitry, based on homo- and hetero-oligomerization of its components to regulate their own stability.

Several E3 ligases were proposed to mediate their own degradation through autoubiquitination, because inactivation of their ligase activity led to increased stability. One example is the U-box E3 ligase CMPG1, a homolog of PUB22 involved in INF1-triggered cell death (ICD) in potato (Bos et al. 2010). *P. infestans* effector Avr3a binds and stabilizes CMPG1. This was proposed to allow *P. infestans* early biotrophic growth preceding the necrotrophic phase. Similar to PUB22, CMPG1 autoubiquitination activity is required for its own degradation, since inactive CMPG1 mutants are more stable. Therefore, Avr3a was proposed to negatively interfere with the autoubiquitination activity of CMPG1 in order to reduce its degradation. Importantly, also CMPG1 inactive mutants could be stabilized by co-expression with Avr3a, indicating that Avr3a may additionally protect CMPG1 from being targeted by heterologous ligases. CMPG1 shares 67 % of similarity with PUB22 in

regards to their U-box domain, and may thus also form homo- and heterooligomers contributing to its degradation. In this scenario, Avr3a may stabilize CMPG1 by binding to the backside of the U-box and inhibiting oligomer formation. In support of this hypothesis, Avr3a was found to bind (appendix Figure 7-8) and stabilize PUB22 too (appendix Figure 7-9).

In animals, Mdm2 stands out as probably one of the best studied E3 ligases, because of its unquestionable relevance in targeting and regulating the levels of the tumor suppressor protein p53. Mdm2 is constitutively active and mediates the ubiquitination and degradation of both itself and p53 (Fang et al. 2000). This maintains p53 levels low, whereas upon genotoxic stress p53 degradation is suppressed, its levels rise and ultimately lead to cell apoptosis. Importantly, Mdm2 forms homodimers through its RING domain, suggesting that its autoubiquitination may occur *in trans*, as in the case of PUB22. Because of its critical role, the regulation of Mdm2 stabilization and activity occurs at many levels (Y. Zhao et al. 2014). For example, the expression of MdmX, a closely related protein, stabilizes Mdm2. This is accomplished by heterodimerization with Mdm2, in this way reducing the frequency of Mdm2 homodimerization. MdmX lacks E3 ligase activity, hence it competes with Mdm2 for dimer formation and presumably for ubiquitination, resulting in Mdm2 reduced autoubiquitination and enhanced p53 ubiquitination (Okamoto et al. 2009).

The binding of the substrate protein may result in reduced E3 ligase autoubiquitination. For example, it was shown that the presence of the substrate Exo70B2 reduces the autoubiquitination levels of PUB22 *in vitro* (Stegmann et al. 2012). In agreement with this, overexpression of Exo70B2 *in vivo* leads to the accumulation of PUB22 (Figure 3-16, Figure 3-17). Possibly, Exo70B2 stabilizes PUB22 by competing with PUB22 itself for ubiquitination or obstructing oligomerization.

In contrast to PUB22 and Mdm2, other ligases require a stimulus to activate their autoubiquitination and consequent degradation. In Arabidopsis, KEG is a RING ligase involved in ABA signalling (Stone et al. 2006). KEG continuously targets the Abscissic acid Insensitive 5 (ABI5) TF to proteasomal degradation in order to repress ABA signalling, and KEG itself is stable under basal conditions (Liu and Stone 2010). However, KEG autoubiquitination and degradation is induced by ABA, resulting in ABI5 stabilization and the activation of the ABA signalling pathway. This suggests that KEG autoubiquitination activity is actively inhibited. Indeed, phosphorylation of the KEG kinase domain is required for KEG destabilization, which suggests a possible intramolecular inhibition of the unphosphorylated kinase domain towards the adjacent RING domain, or alternatively, a

phosphorylation-dependent inhibition of DUB binding. Similarly, in animals, Parkin, which belongs to the novel RING-in-between-RING (RBR) type of E3 ligases, requires a conformational change to activate its autoubiquitination (Trempe et al. 2013). Its five domains are packed in a compact arrangement in which the RING0 domain occludes the active site cysteine of the RING2 domain. RING2 mediates an HECT-like ubiquitination process. The RING1 domain, which mediates the E2 binding, is also blocked by a repressor element. Up to date, the identity of the molecular trigger necessary to unblock Parkin's activity is still unknown. Also cIAP1 is a stable RING ligase, which is necessary to inhibit apoptosis through the binding and inhibition of caspases (Roy et al. 1997). The elucidation of cIAP1 crystal structure revealed that cIAP1 RING ligase exists as an inactive monomer, with its RING domain sequestered within cIAP1's compact structure (Dueber et al. 2011). cIAP1 activation requires the binding of its antagonist to trigger a conformational change, which allows dimerization through the RING domain. Dimerization results in cIAP1 autoubiquitination, its degradation via the 26S proteasome and the release of the associated caspases to activate apoptosis (Varfolomeev et al. 2007).

Alternative modes of PUB22 degradation

In most of the reported cases, such as in the examples mentioned above, ligase autoubiquitination possesses a self-degradatory function. These include PUB22, as I could show that PUB22 oligomerization and consequent *trans*-ubiquitination leads to its proteasomal degradation. Proteasomes are located throughout the cytoplasm and nucleus, and their regulatory subunit can recognize soluble ubiquitinated proteins for degradation in its catalytic core. Despite a comprehensive description of PUB22, its intracellular localization has not been studied. Cho and colleagues reported in 2008, that PUB22 is located in the cytosol when overexpressed in mesophyll protoplasts. PUB22 does not possess any membrane binding domains or merystilation sites, supporting its cytoplasmic localization and therefore, it should be accessible to proteosomal degradation.

On the other hand, several putative targets of PUB22, including the *bona fide* target Exo70B2, are components of the vesicular traffic, which contain modules for membrane binding. In particular, Exo70B2 includes a putative phospholipid binding domain targeting it to the PM, as revealed by cell biological analyses on stably transformed seedlings (Dr. Ooi-Kock Teh, personal communication).

Upon different treatments resulting in protein stress (proteotoxicity), Exo70B2 undergoes degradation via the 26S proteasome (Stegmann et al. 2012) and via autophagocytosis (Dr. Ooi-Kock Teh, personal communication). In some cases, E3 ligases can be degraded along with their targets. The E3s belonging to the casitas B-lineage leukemia (Cbl) family target RTKs including the epidermal growth factor receptor (EGFR). Ubiquitination of EGFR by Cbl results in the vacuolar degradation of both E3 and receptor (Ryan et al. 2006). Therefore, an alternative degradation pathway, as in the case of Exo70B2, may exist for PUB22. Studies found PUB22 to be located at the PM in stable transgenic lines and also to accumulate upon concanamycin A treatment, an inhibitor of vacuolar degradation (Dr. Ooi-Kock Teh, personal communication). These observations are in agreement with the detection of PUB22 in the microsome-enriched fraction, in addition to the cytosol (Figure 3-5). Therefore, it is possible that the cytosolic PUB22 protein pool undergoes proteasomal degradation, while the PUB22 pool bound to membrane-localized substrates is transported with them to the vacuole for degradation after ubiquitination.

Type and site of PUB22 ubiquitination

In addition to the potential non-proteasomal degradation of PUB22 inferred from its association to membranes, clues can be gained through the identification of the linkage type of ubiquitin chains with which PUB22 is modified. Although LC-MS/MS analysis of *in vitro* ubiquitinated proteins is a prompt and convenient approach, the use of a selected E2 may bias the assessment of the true linkage type. In this work, I employed the promiscuous and highly processive E2 enzyme UBC8 to perform PUB22 *in vitro* autoubiquitination assays. However, the investigation of chain linkage type was not addressed. Importantly, UBC8 was shown to interact with PUB22 under physiological conditions (Marco Trujillo, personal communication).

In parallel, the site of ubiquitin attachment on the E3 ligase plays a crucial role. The TRAF6 E3 RING ligase requires autoubiquitination through a single K63-linked polyubiquitin peptide on K124 in order to activate downstream kinases such as TAK1 and IKK (Deng et al. 2000, Lamothe et al. 2007), which ultimately activate TFs as NF-κB during immunity (Wang et al. 2001). The K124 site was recognized as the main ubiquitination site, and its mutation impairs signal transduction. In some cases, the formation of proteolytic chains demands site-specific ubiquitination events. For instance, mutation of XIAP K322 and K328 into arginines drastically reduces its autoubiquitination activity *in*

vitro and *in vivo* (Shin et al. 2003). Nevertheless, the XIAP[K322/328R] double mutant does not present altered stability or functionality, conflicting with the importance of the general ubiquitination activity of XIAP. In my work, PUB22 ubiquitination sites were mapped onto multiple lysine residues based on an *in vitro* ubiquitination assay in combination with UBC8 (Figure 3-7, appendix Figure 7-2). Despite the apparent lack of specificity of PUB22 ubiquitination, seven of the ten lysines detected (K39, K53, K90, K100, K103, K114, K130, K216, K271, and K351), are located at the N-terminal portion of PUB22. This observation is in line with the retained ability to autoubiquitinate of the truncated PUB22[U-box] (Figure 3-46). These results are also suggestive of the most accessible area to the UBC8~ubiquitin conjugate to mediate autoubiquitination within the oligomer. The ubiquitination sites K39 and K53 are located in the U-box domain. By using the generated PUB22[U-box] model, I predicted the positions of these lysines to be on the E2 interacting surface, in agreement with the observation that PUB22 autoubiquitinates *in trans* through oligomerization. K39 is very proximal to W40, which contacts the E2 enzyme. This implies a unidirectional *trans*-ubiquitination from one PUB22~E2 complexed protomer towards an uncomplexed PUB22. One may hence speculate that PUB22 forms an asymmetrical dimer, such as in the case of CHIP. CHIP is a U-box E3 ligase implicated in the clearance of misfolded proteins, which forms homodimers via hydrophobic patches that mediate U-box to U-box interaction (Zhang et al. 2005). Because the helical hairpins located in the central region between the U-box and the TPR domains also mediate the dimer formation, CHIP dimer is asymmetric, with protomers adopting different conformations rendering only one U-box domain available for E2 binding.

Additional potential modifications of PUB22

It is important to mention that PUB22 was frequently detected as a double band of unequal intensities *in vivo* (Figure 3-23, Figure 3-28, Figure 3-29). The upper band, with a size increase of about 5-10 kDa, is stronger than the lower band, which is often faint. Interestingly, the intensity of both bands increases upon flg22 treatment (Figure 3-28). Since it was shown that phosphorylation is a prerequisite for stabilization, one can infer that both bands are phosphorylated species by MPK3. Judging by the considerable shift in migration, it is unlikely that this is a result of phosphorylation. Also, no changes in migration were detected in *in vitro* reactions in which PUB22 was phosphorylated by MPK3 (data not shown). On the other hand, PUB22 double band might be

explained by monoubiquitination or by a post-translational modification by an ubiquitin-like protein, such as Nedd8. The role of monoubiquitination has been well characterized in the context of histone regulation and endocytosis of PM located proteins (Hicke 2001), but only few examples exist for E3 ligases. One of these rare examples is the monoubiquitination of CHIP. CHIP monoubiquitination is mediated by Ube2w on K2, at its N-terminal extension, and it is required for CHIP *in vivo* activity (Scaglione et al. 2011). The function of CHIP monoubiquitination is non-proteolytic, and serves instead in stabilizing the interaction of CHIP with the DUB enzyme Ataxin-3. Ataxin-3 protects CHIP from the action of additional E2 enzymes, which could polyubiquitinate it. Subsequently, after the completion of a substrate ubiquitination round, Ataxin-3 deubiquitinates CHIP. In the case of CHIP, monoubiquitination is transient and highly dynamic, so that the *in vivo* visualization through band shift results difficult. On the contrary, most of PUB22 protein exists as a gel-shifted protein and therefore, potentially in its modified form. Hypothetically, PUB22 monoubiquitination might help the recruitment of proteins, as in the case of CHIP, and/or may have an impact on its subcellular localization. However, PUB22 *in vivo* ubiquitination experiments do not support the possibility of its monoubiquitination, because anti-ubiquitin antibodies fail to detect a clear band corresponding to the immunopurified PUB22 (Figure 3-14). Instead, a uniform ubiquitination smear, distinctive of polyubiquitination, was observed. In order to achieve a complete characterization of PUB22 ubiquitination, challenging *in vivo* studies are required to identify the type of ubiquitin chains built and their attachment sites.

4.4 Oligomerization and E3 ligase activity

RING and U-box proteins multimerize in countless ways (Deshaies & Joazeiro 2009). In addition to homo- and heterodimerization, supramolecular structures can be formed through additional interfaces and thereby, introduce higher order of complexity. E3 ligase oligomerization was shown to impinge on its functionality in different ways.

In my work, I showed that PUB22 oligomerizes through its U-box domain both *in vitro* (Figure 3-36) and *in vivo* (Figure 3-38). Through to the generation of the PUB22 U-box model (Figure 3-35), I could hypothesize that its dimerization may occur via hydrophobic interactions, in a similar way as CHIP.

Indeed, I was able to confirm most of the interactions predicted by the model experimentally. Mimicking of phosphorylation at T62 by replacement with a glutamic acid, reduced oligomerization (Figure 3-38). This strongly suggested that T62 phosphorylation is engaged in the regulation of dimer formation, potentially via disturbing the contacts in the hydrophobic interface between protomers. Indeed, substitution with an isoleucine residue strengthened the oligomeric interaction, as it was predicted (Figure 3-38). Surprisingly, the substitution of T62 with an alanine also determined the reduction of oligomerization, however to a lower extent than glutamic acid (Figure 3-38). The PUB22^{T62A} autoubiquitination activity was also reduced to an intermediate level in between the WT and PUB22^{T62E} (Figure 3-32). Considering the electrostatic surface potentials in the predicted model of PUB22 U-box domain (Figure 3-35), I hypothesized that the replacement of threonine with alanine, a smaller amino acid, may not be sufficient to confine the influence of the adjoining negatively charged patch. This could result in a phosphorylation-like phenotype, even though weaker. This nicely correlates with the homooligomerization and autoubiquitination phenotypes of PUB22 phosphomutants. However, the stability profile of PUB22$^{T62/88A}$, which cannot stabilize, differs completely from the more stable PUB22$^{T62/88E}$ (Figure 3-28). Potentially, the T62A mutation does not affect the *in vivo* heterooligomerization of PUB22 with endogenous E3 ligases, as it does instead in the homooligomer, resulting in its maintained heterologous *trans*-ubiquitination and degradation. Alternatively, phosphorylation may be required for the recognition of PUB22 by an additional stabilizing factor, such as a ubiquitin-specific protease, as shown in the case of TRIM25 and TRAF6 (Pauli et al. 2014, D. Lin et al. 2015).

A role for phosphorylation in the regulation of E3 oligomerization and activity was reported for a few animal E3s. For instance, TRAF6 is phosphorylated by the kinase MST4, in order to downregulate TLR signalling during the immune response (Jiao et al. 2015). TRAF6 can homodimerize through its N-terminal RING and first zinc finger domain (Yin et al. 2009), and form homotrimers through its C-terminal coiled-coil and TRAF-C domain (Ye et al. 2002). Two phosphorylation sites, in T463 and T486, were identified, which are adjacent to the trimer interface of a model of TRAF6-C domain (Jiao et al. 2015). Because TRAF6-C phosphomimetic mutant displayed reduced homooligomerization, phosphorylation probably disturbs the trimer formation. This results in the inhibition of TRAF6 autoubiquitination and therefore, in the reduction of TRAF6-mediated signalling.

Interestingly, in some instances, E3 ligases can form higher order oligomers. This is usually the case when oligomerization is mediated by multiple domains, as in the case of TRAF6. Fluorescence

resonance energy transfer analysis showed that full-length TRAF6 exists in oligomers of higher order (Yin et al. 2009). Therefore, TRAF6 was proposed to create infinite oligomers in a concentration-depedent manner. Preliminary biochemical analysis, intended to measure the affinity of PUB22 oligomerization (Dr. Ilona Turek, personal communication), hint towards a probable supramolecular structure formed by multimers of PUB22. Also, ambiguous high molecular weight species of PUB22 (>245 kDa, the upper ladder band) were often detected on SDS-PAGE from *in vitro* (Figure 3-10) (Figure 3-46) and *in vivo* (data not shown) samples. Recently, the ARM repeats domain of the UND-PUB-ARM PUB10, a regulator of JA signalling, was suggested to mediate its homooligomerization (Jung et al. 2016). *In vitro* pull-down experiments showed that the GST tagged ARM domain of PUB10 could interact directly with the MBP-ARM recombinant protein. Interestingly, no U-box oligomerization was detected for PUB10. In the light of this report, an additional potential oligomerization surface may be present in the ARM repeats domain of PUB22 as well.

Ubiquitin priming in dimeric and monomeric E3 ligases

Ubiquitin priming is mediated by the E3 ligase and consists in the conformational restriction of the E2~ubiquitin conjugate (Berndsen & Wolberger 2014). RING and U-box domains are not inert scaffolds but can contact the donor ubiquitin, complexed with the E2, and place it in the correct orientation towards the target lysine to promote efficient ubiquitination.

Insights into the mechanisms of dimeric RING-mediated ubiquitination were first provided by Plechanovová and colleagues (2011) by studying the mammalian RING finger protein 4 (RNF4) ligase, which regulates the homeostasis of SUMOylated proteins (Tatham et al. 2008). RNF4 can homodimerize, and both protomers were shown to participate together in the priming of ubiquitin (Plechanovová et al. 2011). Indeed, RNF4 monomeric mutants are inactive. Dimerization is therefore required for the general activity of RNF4, in which ubiquitination is either directed towards the substrate (substrate-ubiquitination) or itself (autoubiquitination). While the UbcH5a E2 enzyme binds only one protomer of the RNF4 dimer, the donor ubiquitin is contacted and coordinated by the Y193 residue residing on the second protomer. Y193 is located at the dimer interface and is essential for dimer formation. Interestingly, the RNF4[Y193H] mutant, which retains the ability to form a dimer, is inactive towards the substrate, indicating the importance of ubiquitin coordination. Similarly, the donor ubiquitin in the UbcH5b~ubiquitin conjugate is coordinated by the baculoviral

IAP repeat containing 7 (BIRC7) dimer (Dou et al. 2012). BIRC7 is a human dimeric RING E3 ligase which negatively regulates cell death. The elucidation of its structure in complex with Ubc5Hb identified extensive non-covalent interactions between the RING domains of both BIRC7 protomers and the donor ubiquitin. This results in the stabilization of the globular body and the C-terminal tail of ubiquitin.

It was suggested that monomeric E3 ligases, such as the U-box E3 ligase E4B, may also conformationally restrict the E2~ubiquitin conjugate. In E4B, the loss of the hydrogen bond through R1143 mutation into alanine, critically affects the ability to activate ubiquitin transfer, while not affecting the E2 binding affinity (Pruneda et al. 2012). Notably, the equivalent residue is conserved and critical for E2 binding in the dimeric RNF4 (R181) (Plechanovová et al. 2011). This suggests that, despite sharing elements required for effective ubiquitination, monomeric and dimeric ligases may rely on different mechanisms for the proper conformational restriction of the E2~ubiquitin conjugate onto the E3.

I demonstrated that the levels of PUB22 oligomerization correlate proportionally with its autoubiquitination efficiency. Hence, PUB22 may require oligomerization to prime ubiquitin in a similar fashion as RNF4. However, mutants of PUB22 that are impaired in their oligomerization, such as PUB22$^{T62/88A}$ and PUB22$^{T62/88E}$, are not significantly affected in substrate ubiquitination efficiency (Figure 3-31). Moreover, PUB22$^{T62/88E}$ complements the *pub22 pub23 pub24* triple mutation to a comparable extent as PUB22 WT (Figure 3-49). This indicates that, differently from the monomeric mutants of RNF4, which are inactive, PUB22$^{T62/88E}$ is functional and contributes to the dampening of the immune response. Therefore, both oligomeric and monomeric forms of PUB22 are biochemically active (activity being defined as either auto- or substrate ubiquitination), and in consequence, both must be capable of ubiquitin priming. This suggests that PUB22 mechanism of ubiquitin priming is uncoupled from its oligomerization status. Therefore, PUB22 is likely to rely on a priming mechanism utilized by monomeric E3s. In line with this, the previously mentioned R1143 residue in E4B is conserved in PUB22 (Figure 3-34, green box).

Because PUB22 can autoubiquitinate *in trans*, it seems reasonable to hypothesize that the function of oligomer formation serves mainly the purpose of enabling *trans*-ubiquitination by providing spatial proximity between the protomers, or to provoke a conformational change that favours *trans*-ubiquitination. Alternatively, PUB22 oligomerization may affect the binding affinity to specific E2s. A

change in the affinity to a specific E2, as for instance the used UBC8, may allow alternative E2 to replace UBC8 and in this way determine the formation of alternative chain types. Examples for such a mechanism of regulation have not been reported up to date. For this work, the E2 UBC8 was used for all experiments and it remains to be demonstrated whether mutant variants are affected in their activity in alternative PUB22~E2 combinations.

4.5 Phosphorylation of PUB22 and U-box-type E3 ligases

Interaction between U-box-type E3 ligases and kinases is a common theme in the regulation of diverse processes such as symbioses, self-incompatibility, and immunity (Mbengue et al. 2010, Gu et al. 1998, Lu et al. 2011). Despite the high recurrence of this phenomenon, the molecular function of E3 ligase phosphorylation has not been elucidated.

The dynamic of the PUB22-MPK3 interaction

By means of an *in vitro* pull-down assay, I demonstrated that PUB22 interacts directly and specifically with MPK3 (Figure 3-24). The interaction with MPK3 occurred without its prior activation, suggesting that the interaction may be constitutive. Further, Co-IP assays revealed that they exist in a complex *in vivo* (Figure 3-23). Time-course analyses indicated that their association may be transient and decrease over time after flg22 treatment, because PUB22 accumulation does not correspond to an increase in interacting MPK3. This is in agreement with the rational of a rapid response, in which kinase and substrate are continuously maintained in close proximity to maximize the speed of reaction upon signal activation. Possibly, upon flg22 treatment, PUB22-MPK3 interaction is reduced due to a reduction of the affinity of phosphorylated PUB22 to MPK3. Importantly, PUB22 rapid stabilization coincides with the time frame of MPK3 activation, namely within the first minutes of the immune response. Although being phosphorylated also by MPK4 *in vitro* (Figure 3-19), PUB22 did not interact with MPK4 in a BiFC assay (appendix Figure 7-3), suggesting that they are probably not a physiological pair. However, potential phosphorylation and stabilization of PUB22 at later time points by means of alternative kinases certainly account for a

probable scenario. Indeed, unpublished results from our group infer the involvement of additional kinases as regulators of PUB22.

Functions of phosphorylation

Because PUB22 was found to be phosphorylated *in vivo* (Figure 3-18), I tested and confirmed the MPK3-mediated phosphorylation of PUB22 in an *in vitro* phosphorylation assay (Figure 3-19). The PUB22 phosphorylation sites targeted by MPK3 were mapped on T62, T88, and S422 (Figure 3-20). PUB22 protein is predicted in a number of plant species in which T62, T88, and S422 are conserved, including: soybean *Glycine max*, tomato *Solanum lycopersicum*, wild tomato *Solanum Pennellii* and potato *Solanum tuberosum* (Figure 4-1). The rice *Os*SPL11, homolog of *At*PUB13, shows conservation of T62. The tomato *Sl*CMPG1 and the mais *Zm*CMPG1, homologs of *At*PUB20 instead, show T88 conservation.

Figure 4-1 Alignment of *At*PUB22 nearest homologs of different species: Alignment of *At*PUB22 T62, T88 and S422 phosphosites with predicted PUB22 sequences of the soybean *Glycine max* (*Gm*), the tomato *Solanum lycopersicum* (*Sl*), the wild tomato *Solanum pennellii* (*Sp*) and the potato *Solanum tuberosum* (*St*). Confirmed proteins homologs of PUB22 in other species are *Oryza sativa* (*Os*) SPL11, *Sl*CMPG1 and *Zea mays* (*Zm*) CMPG1.

Individual substitutions of the phosphosites with a glutamic acid to mimic phosphorylation determined an increase in PUB22 stability (Figure 3-27). Also, the simple overexpression of MPK3 resulted in PUB22 stabilization (Figure 3-25), conceivably due to an enhanced amount of basally-activated MPK3. Since T62 and T88 are located in and adjacent to the U-box domain, whereas S422 is located at the C-terminal end of the ARM repeats domain, I hypothesized that their phosphorylation affects different aspects of the regulation of PUB22. I demonstrated that

phosphorylation of T62 regulates autoubiquitination and contributes to the stabilization of PUB22, which has been discussed in 4.4. Instead, T88 phosphomutants autoubiquitination activity is invariant (Figure 3-32). Accordingly, phosphorylation of T88 additively contributes to PUB22 stabilization (Figure 3-27). Therefore, the effect on the stability of PUB22 is likely to function through a different mechanism.

Phosphorylation has been reported in many instances to modulate the conformational organization of disordered proteins (Wright & Dyson 2015). Phosphorylation modifies the electrostatic properties of a domain, leading for example to enhanced target binding. In the case of p53, phosphorylation at multiple sites of its intrinsically disordered N-terminal transactivation domain results in increasingly efficient binding to CREB-binding protein (CBP) and p300, which controls the extent of p53 activation (Lee et al. 2010). T88 is found in a predicted disordered region (aa 81-92), located between the U-box domain and the ARM repeats-like domain. Phosphorylation may trigger a transition to a structured form. This may alter the geometry of the molecule so that it is less prone to self-modification. Alternatively, the re-structuring of a disordered domain can have implications on its proteasomal degradation. Indeed, Prakash and colleagues (2004) revealed that ubiquitination is not sufficient for efficient degradation of folded ("ordered") proteins, and that proteasomal degradation is enhanced by the presence of an unstructured site, such as disordered regions (Prakash et al. 2004). These regions are used as the initiation site for degradation. In light of this, PUB22 phosphorylation at T88 and the potential organization of the disordered domain may result in PUB22 being a less suitable substrate for the proteasome.

S422 is located in the ARM repeats domain at the C-terminal end. Because ARM repeats mediate substrate interaction, phosphorylation at this position may be involved in the regulation of substrate recruitment. The previously described PUB13 is phosphorylated by BAK1 after activation of immune responses (Lu et al. 2011). Experiments with kinase inhibitors supported the importance of PUB13 phosphorylation in the binding with its substrate FLS2. Interestingly, BAK1 could strongly phosphorylate the ARM domain of PUB13 and at multiple sites (Zhou et al. 2015). Therefore, it was proposed that PUB13 phosphorylation enhances its association to its substrate FLS2. Similarly, PUB22 phosphorylation at S422 may result in increased substrate binding. This may have a stabilizing effect on PUB22, given that overexpression of Exo70B2 leads to the accumulation of PUB22 (Figure 3-16, Figure 3-17). Accordingly, the PUB22^{S422E} phosphomimetic mutant displays increased stability in comparison to the WT (Figure 3-27). However, because PUB22$^{T62/88A}$ is

incapable of flg22-triggered stabilization, phosphorylations at T62 and T88 are probably dominant over S422. A possible scenario requires the initial phosphorylation of T62 and T88 to switch the ubiquitination activity, impinging on oligomerization and molecule conformation respectively, and subsequent phosphorylation of S422 to increase substrates binding affinity.

4.6 Working model for the mechanistic function of PUB22 phosphorylation

In this work, I identified MPK3 as an upstream signalling component controlling PUB22 activity to trigger a negative feedback loop. In parallel to the contribution of gene induction, the molecular basis for PUB22 rapid stabilization was elucidated (Figure 4-2). Data indicates that in its basal state PUB22 exists as an autoubiquitinating and therefore unstable oligomer (Figure 4-2, 1). Upon pathogen perception, MAPK signalling cascades are triggered leading to the activation of MPK3 (in red colour, 2). MPK3 subsequently phosphorylates PUB22 at three sites (3), contributing to PUB22 stabilization via different mechanisms. Phosphorylation of T62 inhibits PUB22 oligomerization, and consequently, PUB22 stability is increased by inhibition of autoubiquitination (4). Stabilized PUB22 can then engage substrates for ubiquitination and dampen the immune signalling (5). Finally, upon substrate depletion and potentially de-phosphorylation, PUB22 returns to its initial dimerized state and becomes unstable (6).
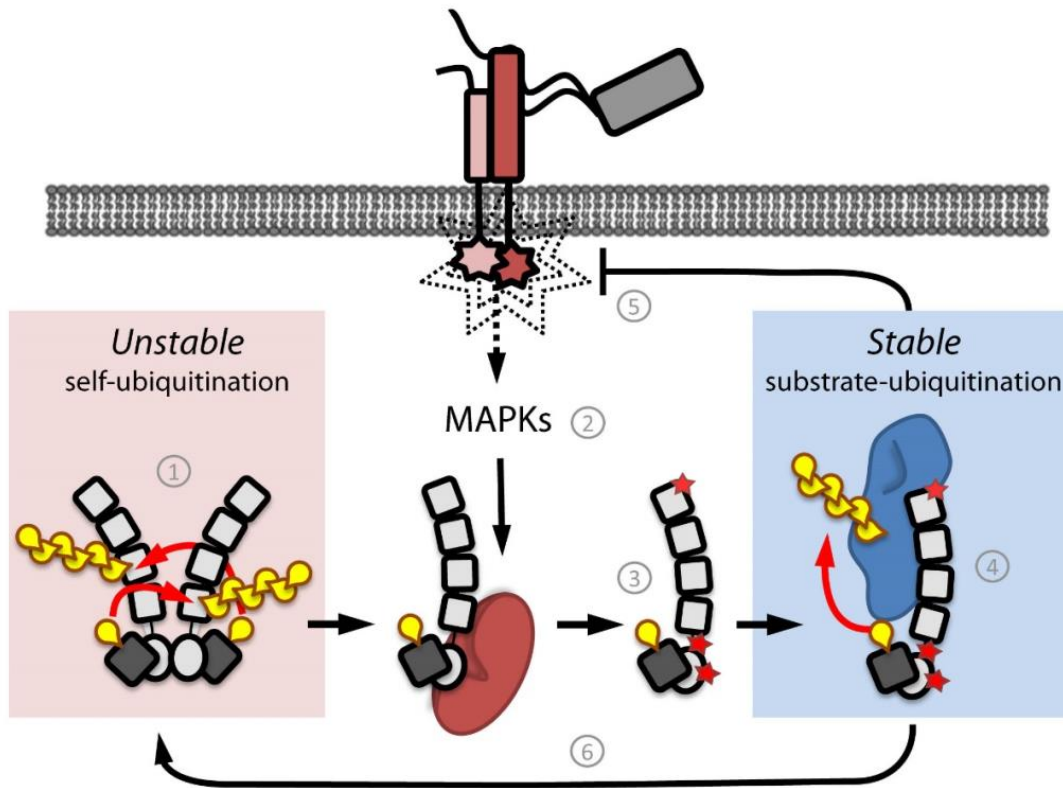
Figure 4-2 Model of PUB22 regulation and dampening of the immune response. (1) PUB22 continuously dimerizes and autoubiquitinates *in trans*. (2) Upon pathogen perception, MAPKs are activated. (3) MPK3 (in red colour) phosphorylates PUB22 at three residues T62, T88 and S422 (red stars). (4) Phosphorylation of PUB22 inhibits dimerization resulting in a monomeric and stable form less prone to autoubiquitinate. PUB22 accumulates and engages and ubiquitinates substrates. (5) Ubiquitination of PUB22 substrates leads to dampening of the immune response. (6) Upon termination of signalling, PUB22 returns to its initial autoubiquitinating and unstable state.

5. Summary

Signalling circuits are continuously being triggered and the intensity, as well as the duration of signalling events, must be tightly controlled to ensure homeostasis. Negative regulation is essential for that. During the immune response, the U-box-type E3 ligase PUB22 was shown to negatively regulate immune signalling by targeting components of the vesicular trafficking. However, in spite of the importance of ubiquitination, little is known about the molecular mechanisms controlling the activity of single unit E3 ligases, as PUB22.

Here, I showed that PUB22 is regulated via ubiquitination, which determines its continuous degradation. However, upon activation of the immune response PUB22 is stabilized. I discovered that PUB22's stabilization is controlled by MPK3-mediated phosphorylation. Mimicking phosphorylation resulted in increased stability of PUB22 *in vivo*, correlating with a reduced autoubiquitination activity *in vitro*. Autoubiquitination is dependent on the oligomerization of PUB22, which is inhibited by phosphorylation. The importance of PUB22 phosphorylation was shown by complementation analysis, demonstrating that phosphomimetic mutants, however not phosphonull mutants, efficiently dampen the immune response.

I propose a model in which MPK3-mediated phosphorylation of PUB22 determines an activity switch by disrupting oligomerization, rescuing PUB22 from degradation and allowing it to engage targets to dampen cellular signalling during immunity. This novel regulatory mechanism suggests that autoubiquitination, which is inherent to most single unit E3s *in vitro*, can function as a self-regulatory mechanism *in vivo*. Furthermore, this work uncovers a previously unknown negative feedback loop of MPK3 via PUB22 to dampen the immune response, elucidating MPK3 dual role in immunity and the crosstalk between ubiquitination and phosphorylation in the immune signalling.

6. Bibliography

Antignani, V. et al., 2015. Recruitment of PLANT U-BOX13 and the PI4Kβ1/β2 Phosphatidylinositol-4 Kinases by the Small GTPase RabA4B Plays Important Roles during Salicylic Acid-Mediated Plant Defense Signaling in Arabidopsis. *The Plant cell*, 27(1), pp.243–61.

Asai, S. & Shirasu, K., 2015. Plant cells under siege: plant immune system versus pathogen effectors. *Current opinion in plant biology*, 28, pp.1–8.

Asai, T. et al., 2002. MAP kinase signalling cascade in Arabidopsis innate immunity. *Nature*, 415, pp.977–83.

Bakshi, M. & Oelmüller, R., 2014. WRKY transcription factors, Jack of many trades in plants. *Plant signaling & behavior*, 9(2), p.e27700.

Barlow, P.N. et al., 1994. Structure of the C3HC4 Domain by H-nuclear Magnetic Resonance Spectroscopy. *Journal of Molecular Biology*, 237, pp.201–211.

Beck, M. et al., 2012. Spatio-temporal cellular dynamics of the Arabidopsis flagellin receptor reveal activation status-dependent endosomal sorting. *The Plant cell*, 24(10), pp.4205–19.

Bedford, L. et al., 2010. Assembly, Structure and Function of the 26S proteasome. *Trends in cell biology*, 20(7), pp.391–401.

Benirschke, R.C. et al., 2010. Molecular basis for the association of human E4B U box ubiquitin ligase with E2-conjugating enzymes UbcH5c and Ubc4. *Structure*, 18(8), pp.955–65.

Berndsen, C.E. & Wolberger, C., 2014. New insights into ubiquitin E3 ligase mechanism. *Nature structural & molecular biology*, 21(4), pp.301–7.

de Bie, P. & Ciechanover, A., 2011. Ubiquitination of E3 ligases: self-regulation of the ubiquitin system via proteolytic and non-proteolytic mechanisms. *Cell death and differentiation*, 18(9), pp.1393–402.

Bigeard, J., Colcombet, J. & Hirt, H., 2015. Signaling Mechanisms in Pattern-Triggered Immunity (PTI). *Molecular Plant*, 8(4), pp.521–539.

Boller, T. & Felix, G., 2009. A renaissance of elicitors: perception of microbe-associated molecular patterns and danger signals by pattern-recognition receptors. *Annual review of plant biology*, 60, pp.379–406.

Bos, J.I.B. et al., 2010. Phytophthora infestans effector AVR3a is essential for virulence and manipulates plant immunity by stabilizing host E3 ligase CMPG1. *PNAS*, 107(21), pp.9909–14.

Brock, A.K. et al., 2010. The Arabidopsis Mitogen-Activated Protein Kinase Phosphatase PP2C5 Affects Seed Germination, Stomatal Aperture, and Abscisic Acid-Inducible Gene Expression. *Plant Physiology*, 153, pp.1098–1111.

Budhidarmo, R., Nakatani, Y. & Day, C.L., 2012. RINGs hold the key to ubiquitin transfer. *Trends in biochemical sciences*, 37(2), pp.58–65.

Burchell, L., Chaugule, V.K. & Walden, H., 2012. Small, N-Terminal Tags Activate Parkin E3 Ubiquitin Ligase Activity by Disrupting Its Autoinhibited Conformation. *PloS one*, 7(4), p.e34748.

Cao, F.Y., Yoshioka, K. & Desveaux, D., 2011. The roles of ABA in plant – pathogen interactions. *The Journal of Plant Research*, 124, pp.489–499.

Cao, Y. et al., 2014. The kinase LYK5 is a major chitin receptor in Arabidopsis and forms a chitin-induced complex with related kinase CERK1. *eLife*, 3, p.e03766.

Chanarat, S. & Sträßer, K., 2013. Splicing and beyond: The many faces of the Prp19 complex. *Biochimica et Biophysica Acta*, 1833(10), pp.2126–2134.

Chang, L. & Karin, M., 2001. Mammalian MAP kinase signalling cascades. *Nature*, 410, pp.37–40.

Chen, H. et al., 2008. Firefly luciferase complementation imaging assay for protein-protein interactions in plants. *Plant physiology*, 146(2), pp.368–76.

Chen, Z.J., 2012. Ubiquitination in signaling to and activation of IKK. *Immunological reviews*, 246(1), pp.95–106.

Chinchilla, D. et al., 2007. A flagellin-induced complex of the receptor FLS2 and BAK1 initiates plant defence. *Nature*, 448(7152), pp.497–500.

Chinchilla, D. et al., 2006. The Arabidopsis Receptor Kinase FLS2 Binds flg22 and Determines the Specificity of Flagellin Perception. *The Plant cell*, 18(2), pp.465–476.

Cho, S.K. et al., 2008. Arabidopsis PUB22 and PUB23 are homologous U-Box E3 ubiquitin ligases that play combinatory roles in response to drought stress. *The Plant cell*, 20(7), pp.1899–914.

Choi, C.M. et al., 2014. Composition, Roles, and Regulation of Cullin-based Ubiquitin E3 Ligases. *The Arabidopsis book*, 11, p.e0175.

Coates, J.C., 2003. Armadillo repeat proteins: beyond the animal kingdom. *Trends in Cell Biology*, 13(9), pp.463–471.

Deng, L. et al., 2000. Activation of the IκB Kinase Complex by TRAF6 Requires a Dimeric Ubiquitin-Conjugating Enzyme Complex and a Unique Polyubiquitin Chain. *Cell*, 103(2), pp.351–361.

Deshaies, R.J. & Joazeiro, C.A.P., 2009. RING domain E3 ubiquitin ligases. *Annual Review of Biochemistry*, 78, pp.399–434.

Després, C. et al., 2000. The Arabidopsis NPR1/NIM1 Protein Enhances the DNA Binding Activity of a Subgroup of the TGA Family of bZIP Transcription Factors. *The Plant cell*, 12(2), pp.279–290.

Dharmasiri, N., Dharmasiri, S. & Estelle, M., 2005. The F-box protein TIR1 is an auxin receptor. *Nature*, 435(7041), pp.441–445.

Disch, E. et al., 2016. Membrane-Associated Ubiquitin Ligase SAUL1 Suppresses Temperature- and Humidity-Dependent Autoimmunity in Arabidopsis. *MPMI*, 29(1), pp.69–80.

Donnelly, M.A. & Steiner, T.S., 2002. Two Nonadjacent Regions in Enteroaggregative Escherichia coli Flagellin Are Required for Activation of Toll-like Receptor 5. *The Journal of biological chemistry*, 277(43), pp.40456–40461.

Dou, H. et al., 2012. BIRC7–E2 ubiquitin conjugate structure reveals the mechanism of ubiquitin transfer by a RING dimer. *Nature structural & molecular biology*, 19(9), pp.876–883.

Downes, B. & Vierstra, R.D., 2005. Post-translational regulation in plants employing a diverse set of polypeptide tags. *Biochemical Society transactions*, 33(2), pp.393–399.

Dubiella, U. et al., 2013. Calcium-dependent protein kinase/NADPH oxidase activation circuit is required for rapid defense signal propagation. *PNAS*, 110(21), pp.8744–8749.

Duda, D.M. et al., 2008. Structural Insights into NEDD8 Activation of Cullin-RING Ligases: Conformational Control of Conjugation. *Cell*, 134(6), pp.995–1006.

Dueber, E.C. et al., 2011. Antagonists Induce a Conformational Change in cIAP1 That Promotes Autoubiquitination. *Science*, 334(6054), pp.376–380.

Ehlert, A. et al., 2006. Two-hybrid protein-protein interaction analysis in Arabidopsis protoplasts: establishment of a heterodimerization map of group C and group S bZIP transcription factors. *The Plant Journal*, 46(5), pp.890–900.

Engelhardt, S. et al., 2012. Relocalization of late blight resistance protein R3a to endosomal compartments is associated with effector recognition and required for the immune response. *The Plant cell*, 24(12), pp.5142–5158.

Erpapazoglou, Z., Walker, O. & Haguenauer-tsapis, R., 2014. Versatile Roles of K63-Linked Ubiquitin Chains in Trafficking. *Cells*, 3(4), pp.1027–1088.

Eulgem, T. & Somssich, I.E., 2007. Networks of WRKY transcription factors in defense signaling. *Current opinion in plant biology*, 10(4), pp.366–71.

Fang, S. et al., 2000. Mdm2 Is a RING Finger-dependent Ubiquitin Protein Ligase for Itself and p53. *The Journal of biological chemistry*, 275(12), pp.8945–8951.

Feilner, T. et al., 2005. High throughput identification of potential Arabidopsis mitogen-activated protein kinases substrates. *Molecular & cellular proteomics: MCP*, 4(10), pp.1558–68.

Ferrell, J.E.J., 2013. Feedback loops and reciprocal regulation: recurring motifs in the systems biology of the cell cycle. *Current Opinion in Cell Biology*, 25(6), pp.676–86.

Freemont, P.S., Hanson, I.M. & Trowsdale, J., 1991. A Novel Cysteine-Rich Sequence Motif. *Cell*, 64, pp.483–484.

Frei dit Frey, N. et al., 2014. Functional analysis of Arabidopsis immune-related MAPKs uncovers a role for MPK3 as negative regulator of inducible defences. *Genome biology*, 15(87), pp.1–22.

Frye, C.A. & Innes, R.W., 1998. An Arabidopsis Mutant with Enhanced Resistance to Powdery Mildew. *The Plant cell*, 10(6), pp.947–956.

Fu, H. et al., 1998. Multiubiquitin chain binding and protein degradation are mediated by distinct

domains within the 26 S proteasome subunit Mcb1. *Journal of Biological Chemistry*, 273(4), pp.1970–1981.

Fu, Z.Q. & Dong, X., 2013. Systemic Acquired Resistance: Turning Local Infection into Global Defense. *Annual review of plant biology*, 64, pp.839–863.

Furlan, G., Klinkenberg, J. & Trujillo, M., 2012. Regulation of plant immune receptors by ubiquitination. *Frontiers in plant science*, 3(238), pp.1–6.

Gallagher, E. et al., 2006. Activation of the E3 ubiquitin ligase Itch through a phosphorylation-induced conformational change. *PNAS*, 103(6), pp.1717–1722.

Gao, M. et al., 2008. MEKK1, MKK1/MKK2 and MPK4 function together in a mitogen-activated protein kinase cascade to regulate innate immunity in plants. *Cell research*, 18(12), pp.1190–1198.

Gimenez-Ibanez, S., Hann, D.R., et al., 2009. AvrPtoB targets the LysM receptor kinase CERK1 to promote bacterial virulence on plants. *Current Biology*, 19, pp.423–429.

Gimenez-Ibanez, S. et al., 2014. The bacterial effector HopX1 targets JAZ transcriptional repressors to activate jasmonate signaling and promote infection in Arabidopsis. *PLoS biology*, 12(2), p.e1001792.

Gimenez-Ibanez, S., Ntoukakis, V. & Rathjen, J.P., 2009. The LysM receptor kinase CERK1 mediates bacterial perception in Arabidopsis. *Plant signaling & behavior*, 4(6), pp.539–41.

Göhre, V. et al., 2008. Plant pattern-recognition receptor FLS2 is directed for degradation by the bacterial ubiquitin ligase AvrPtoB. *Current biology*, 18(23), pp.1824–32.

Goldenberg, S.J. et al., 2004. Structure of the Cand1-Cul1-Roc1 Complex Reveals Regulatory Mechanisms for the Assembly of the Multisubunit Cullin-Dependent Ubiquitin Ligases. *Cell*, 119(4), pp.517–528.

Gómez-Gómez, L., Bauer, Z. & Boller, T., 2001. Both the extracellular leucine-rich repeat domain and the kinase activity of FSL2 are required for flagellin binding and signaling in Arabidopsis. *The Plant cell*, 13(5), pp.1155–63.

González-Lamothe, R. et al., 2006. The U-box protein CMPG1 is required for efficient activation of defense mechanisms triggered by multiple resistance genes in tobacco and tomato. *The Plant cell*, 18(4), pp.1067–83.

Gosti, F. et al., 1999. ABI1 Protein Phosphatase 2C Is a Negative Regulator of Abscisic Acid Signaling. *The Plant cell*, 11(10), pp.1897–1909.

Grefen, C. et al., 2010. A ubiquitin-10 promoter-based vector set for fluorescent protein tagging facilitates temporal stability and native protein distribution in transient and stable expression studies. *The Plant journal*, 64(2), pp.355–65.

Gu, T. et al., 1998. Binding of an arm repeat protein to the kinase domain of the S-locus receptor kinase. *PNAS*, 95(1), pp.382–7.

Gu, Y. & Innes, R.W., 2011. The KEEP ON GOING protein of Arabidopsis recruits the ENHANCED DISEASE RESISTANCE1 protein to trans-Golgi network/early endosome vesicles. *Plant physiology*, 155(4), pp.1827–38.

Gudesblat, G.E., Iusem, N.D. & Morris, P.C., 2007. Guard cell-specific inhibition of Arabidopsis MPK3 expression causes abnormal stomatal responses to abscisic acid and hydrogen peroxide. *New Phytologist*, 173(4), pp.713–721.

Gust, A. a et al., 2007. Bacteria-derived peptidoglycans constitute pathogen-associated molecular patterns triggering innate immunity in Arabidopsis. *The Journal of biological chemistry*, 282(44), pp.32338–48.

Halter, T. et al., 2014. The leucine-rich repeat receptor kinase BIR2 is a negative regulator of BAK1 in plant immunity. *Current Biology*, 24(2), pp.134–143.

Hatakeyama, S. et al., 2001. U Box Proteins as a New Family of Ubiquitin-Protein Ligases. *The Journal of biological chemistry*, 276(35), pp.33111–33120.

Den Herder, G. et al., 2012. Lotus japonicus E3 ligase SEVEN IN ABSENTIA4 destabilizes the symbiosis receptor-like kinase SYMRK and negatively regulates rhizobial infection. *The Plant cell*, 24(4), pp.1691–707.

Hershko, A. et al., 1983. Components of Ubiquitin-Protein Ligase System. *The Journal of biological chemistry*, 258(13), pp.8206–8214.

Hicke, L., 2001. Protein regulation by monoubiquitin. *Nature reviews. Molecular cell biology*, 2(3), pp.195–201.

Hofmann, R.M. & Pickart, C.M., 1999. Noncanonical MMS2-Encoded Ubiquitin-Conjugating Enzyme Functions in Assembly of Novel Polyubiquitin Chains for DNA repair. *Cell*, 96(5), pp.645–653.

Hoth, S. et al., 2002. Genome-wide gene expression profiling in Arabidopsis thaliana reveals new targets of abscisic acid and largely impaired gene regulation in the abi1-1 mutant. *Journal of Cell Science*, 115(24), pp.4891–4900.

Hu, C., Chinenov, Y. & Kerppola, T.K., 2002. Visualization of Interactions among bZIP and Rel Family Proteins in Living Cells Using Bimolecular Fluorescence Complementation. *Molecular cell*, 9(4), pp.789–798.

Huffaker, A., Pearce, G. & Ryan, C.A., 2006. An endogenous peptide signal in Arabidopsis activates components of the innate immune response. *PNAS*, 103(26), pp.10098–103.

Ichimura, K. et al., 2006. MEKK1 Is Required for MPK4 Activation and Regulates Tissue-specific and Temperature-dependent Cell Death in Arabidopsis. *The Journal of biological chemistry*, 281(48), pp.36969–36976.

Ikeda, F. et al., 2011. SHARPIN forms a linear ubiquitin ligase complex regulating NF-κB activity and apoptosis. *Nature*, 471(7340), pp.637–41.

Ishihama, Y. et al., 2002. Microcolumns with self- assembled particle frits for proteomics. *Journal of Chromatography A*, 979(1-2), pp.233–39.

Jacobson, A.D. et al., 2009. The Lysine 48 and Lysine 63 Ubiquitin Conjugates Are Processed Differently by the 26 S Proteasome. *The Journal of biological chemistry*, 284(51), pp.35485–35494.

Jiao, S. et al., 2015. The kinase MST4 limits inflammatory responses through direct phosphorylation of the adaptor TRAF6. *Nature immunology*, 16(3), pp.246–57.

Jones, J.D.G. & Dangl, J.L., 2006. The plant immune system. *Nature*, 444(7117), pp.323–9.

Jung, C. et al., 2016. PLANT U-BOX PROTEIN10 Regulates MYC2 Stability in Arabidopsis. *The Plant cell*, 27(7), pp.2016–2031.

Katagiri, F., Thilmony, R. & He, S.Y., 2002. The Arabidopsis thaliana-pseudomonas syringae interaction. *The Arabidopsis book*, 1, p.e0039.

Kato, K. et al., 2011. Protein kinase C stabilizes X-linked inhibitor of apoptosis protein (XIAP) through phosphorylation at Ser87 to suppress apoptotic cell death. *Psychogeriatrics*, 11, pp.90–97.

Kim, D.-Y. et al., 2013. Advanced proteomic analyses yield a deep catalog of ubiquitylation targets in Arabidopsis. *The Plant cell*, 25(5), pp.1523–40.

Kim, H.-S. et al., 2005. The Pseudomonas syringae effector AvrRpt2 cleaves its C-terminally acylated target, RIN4, from Arabidopsis membranes to block RPM1 activation. *PNAS*, 102(18), pp.6496–501.

Kinkema, M., Fan, W. & Dong, X., 2000. Nuclear Localization of NPR1 Is Required for Activation of PR Gene Expression. *The Plant cell*, 12(12), pp.2339–2350.

Kirisako, T. et al., 2006. A ubiquitin ligase complex assembles linear polyubiquitin chains. *The EMBO journal*, 25(20), pp.4877–4887.

Koegl, M. et al., 1999. A Novel Ubiquitination Factor, E4, Is Involved in Multiubiquitin Chain Assembly. *Cell*, 96(5), pp.635–644.

Komander, D., Clague, M.J. & Urbé, S., 2009. Breaking the chains: structure and function of the deubiquitinases. *Nature reviews. Molecular cell biology*, 10(8), pp.550–63.

Kong, L. et al., 2015. Degradation of the ABA co-receptor ABI1 by PUB12/13 U-box E3 ligases. *Nature Communications*, 6(8630), pp.1–13.

Kunze, G. et al., 2004. The N Terminus of Bacterial Elongation Factor Tu Elicits Innate Immunity in Arabidopsis Plants. *The Plant cell*, 16(12), pp.3496–3507.

Kwak, J.M. et al., 2003. NADPH oxidase AtrbohD and AtrbohF genes function in ROS-dependent ABA signaling in Arabidopsis. *The EMBO journal*, 22(11), pp.2623–2633.

Lamothe, B. et al., 2007. Site-specific Lys-63-linked Tumor Necrosis Factor Is a Critical Determinant of IkB Kinase Activation. *The Journal of biological chemistry*, 282(6), pp.4102–4112.

Lassowskat, I. et al., 2014. Sustained mitogen-activated protein kinase activation reprograms defense metabolism and phosphoprotein profile in Arabidopsis thaliana. *Frontiers in plant science*, 5(554), pp.1–20.

Lauwers, E., Jacob, C. & André, B., 2009. K63-linked ubiquitin chains as a specific signal for protein sorting into the multivesicular body pathway. *The Journal of cell biology*, 185(3), pp.493–502.

Lee, C.W. et al., 2010. Graded enhancement of p53 binding to CREB-binding protein (CBP) by multisite phosphorylation. *PNAS*, 107(45), pp.19290–19295.

Lee, J. et al., 2004. Dynamic changes in the localization of MAPK cascade components controlling pathogenesis-related (PR) gene expression during innate immunity in parsley. *The Journal of biological chemistry*, 279(21), pp.22440–8.

Leitner, J. et al., 2012. Lysine63-linked ubiquitylation of PIN2 auxin carrier protein governs hormonally controlled adaptation of Arabidopsis root growth. *PNAS*, 109(21), pp.8322–8327.

Li, W. et al., 2012. The U-Box/ARM E3 ligase PUB13 regulates cell death, defense, and flowering time in Arabidopsis. *Plant physiology*, 159(1), pp.239–50.

Lin, D. et al., 2015. Induction of USP25 by viral infection promotes innate antiviral responses by mediating the stabilization of TRAF3 and TRAF6. *PNAS*, 112(36), pp.11324–29.

Lin, N. & Martin, G.B., 2005. An avrPto/avrPtoB Mutant of Pseudomonas syringae pv . tomato DC3000 Does Not Elicit Pto-Mediated Resistance and Is Less Virulent on Tomato. *MPMI*, 18(1), pp.43–51.

Lin, Z.-J.D. et al., 2015. PBL13 is a serine/threonine protein kinase that negatively regulates Arabidopsis immune responses. *Plant Physiology*, 169(4), pp.2950–2962.

Liu, H. & Stone, S.L., 2010. Abscisic acid increases Arabidopsis ABI5 transcription factor levels by promoting KEG E3 ligase self-ubiquitination and proteasomal degradation. *The Plant cell*, 22(8), pp.2630–41.

Liu, J. et al., 2015. The RhoGAP SPIN6 associates with SPL11 and OsRac1 and negatively regulates programmed cell death and innate immunity in rice. *PLoS pathogens*, 11(2), p.e1004629.

Lu, D. et al., 2010. A receptor-like cytoplasmic kinase, BIK1, associates with a flagellin receptor complex to initiate plant innate immunity. *PNAS*, 107(1), pp.496–501.

Lu, D. et al., 2011. Direct ubiquitination of pattern recognition receptor FLS2 attenuates plant innate immunity. *Science*, 332(6036), pp.1439–42.

Luna, E. et al., 2011. Callose deposition: a multifaceted plant defense response. *MPMI*, 24(2), pp.183–93.

Mackey, D. et al., 2003. Arabidopsis RIN4 Is a Target of the Type III Virulence Effector AvrRpt2 and Modulates RPS2-Mediated Resistance. *Cell*, 112(3), pp.379–389.

Mackey, D. et al., 2002. RIN4 interacts with Pseudomonas syringae type III effector molecules and is required for RPM1-mediated resistance in Arabidopsis. *Cell*, 108(6), pp.743–754.

Mandadi, K.K. & Scholthof, K.G., 2013. Plant Immune Responses Against Viruses : How Does a Virus Cause Disease? *The Plant cell*, 25(5), pp.1489–1505.

Mao, G. et al., 2011. Phosphorylation of a WRKY transcription factor by two pathogen-responsive

MAPKs drives phytoalexin biosynthesis in Arabidopsis. *The Plant cell*, 23(4), pp.1639–53.

Maor, R. et al., 2007. Multidimensional protein identification technology (MudPIT) analysis of ubiquitinated proteins in plants. *Molecular & cellular proteomics*, 6(4), pp.601–10.

Maraschin, F.D.S., Memelink, J. & Offringa, R., 2009. Auxin-induced, SCF(TIR1)-mediated poly-ubiquitination marks AUX/IAA proteins for degradation. *The Plant journal*, 59(1), pp.100–9.

Martins, S. et al., 2015. Internalization and vacuolar targeting of the brassinosteroid hormone receptor BRI1 are regulated by ubiquitination. *Nature communications*, 6, p.6151.

Mbengue, M. et al., 2010. The Medicago truncatula E3 ubiquitin ligase PUB1 interacts with the LYK3 symbiotic receptor and negatively regulates infection and nodulation. *The Plant cell*, 22(10), pp.3474–88.

Melotto, M. et al., 2006. Plant Stomata Function in Innate Immunity against Bacterial Invasion. *Cell*, 126(5), pp.969–980.

Meng, X. & Zhang, S., 2013. MAPK cascades in plant disease resistance signaling. *Annual review of phytopathology*, 51, pp.245–66.

Miller, G. et al., 2009. The Plant NADPH Oxidase RBOHD Mediates Rapid Systemic Signaling in Response to Diverse Stimuli. *Science signaling*, 2(84), p.ra45.

Monaghan, J. et al., 2014. The calcium-dependent protein kinase CPK28 buffers plant immunity and regulates BIK1 turnover. *Cell host & microbe*, 16(5), pp.605–15.

Moore, J.W., Loake, G.J. & Spoel, S.H., 2011. Transcription dynamics in plant immunity. *The Plant cell*, 23(8), pp.2809–20.

Mou, Z., Fan, W. & Dong, X., 2003. Inducers of Plant Systemic Acquired Resistance Regulate NPR1 Function through Redox Changes. *Cell*, 113(7), pp.935–944.

Mudgil, Y. et al., 2004. A Large Complement of the Predicted Arabidopsis ARM Repeat Proteins Are Members of the U-Box E3 Ubiquitin Ligase Family. *Plant physiology*, 134(1), pp.59–66.

Nakagami, H. et al., 2006. A Mitogen-activated Protein Kinase Kinase Kinase Mediates Reactive Oxygen Species Homeostasis in Arabidopsis. *The Journal of biological chemistry*, 281(50), pp.38697–38704.

Nakagami, H. et al., 2010. Large-Scale Comparative Phosphoproteomics Identifies Conserved Phosphorylation Sites in Plants. *Plant physiology*, 153(7), pp.1161–1174.

Nakatani, Y. et al., 2013. Regulation of ubiquitin transfer by XIAP, a dimeric RING E3 ligase. *The Biochemical journal*, 450(3), pp.629–38.

Nakhaei, P. et al., 2012. IκB kinase ε-dependent phosphorylation and degradation of X-linked inhibitor of apoptosis sensitizes cells to virus-induced apoptosis. *Journal of virology*, 86(2), pp.726–37.

Nathan, J.A. et al., 2013. Why do cellular proteins linked to K63-polyubiquitin chains not associate with proteasomes? *The EMBO Journal*, 32(4), pp.552–565.

Navarro, L. et al., 2004. The Transcriptional Innate Immune Response to flg22. Interplay and Overlap with Avr Gene-Dependent Defense Responses and Bacterial Pathogenesis. *Plant physiology*, 135(6), pp.1113–1128.

Nishimura, M.T. & Dangl, J.L., 2010. Arabidopsis and the Plant Immune System. *Plant Journal*, 61(6), pp.1053–1066.

Oerke, E.-C., 2006. Crop losses to pests. *Journal of Agricultural Science*, 144, pp.31–43.

Ohi, M.D. et al., 2003. Structural insights into the U-box, a domain associated with multi-ubiquitination. *Nature structural biology*, 10(4), pp.250–5.

Okamoto, K., Taya, Y. & Nakagama, H., 2009. Mdmx enhances p53 ubiquitination by altering the substrate preference of the Mdm2 ubiquitin ligase. *FEBS Letters*, 583(17), pp.2710–2714.

Olsen, J. V et al., 2005. Parts per Million Mass Accuracy on an Orbitrap Mass Spectrometer via Lock Mass Injection into a C-trap. *Molecular & cellular proteomics*, 4(12), pp.2010–2021.

Olsen, J. V, Ong, S. & Mann, M., 2004. Trypsin Cleaves Exclusively C-terminal to Arginine and Lysine Residues. *Molecular & cellular proteomics*, 3(6), pp.608–614.

Palm-Forster, M. a T., Eschen-Lippold, L. & Lee, J., 2012. A mutagenesis-based screen to rapidly identify phosphorylation sites in mitogen-activated protein kinase substrates. *Analytical biochemistry*, 427(2), pp.127–9.

Paul, I. & Ghosh, M.K., 2014. The E3 ligase CHIP: insights into its structure and regulation. *BioMed research international*, 2014, p.918183.

Pauli, E. et al., 2014. The Ubiquitin-Specific Protease USP15 Promotes RIG-I – Mediated Antiviral Signaling by Deubiquitylating TRIM25. *Science signaling*, 7(307), p.ra3.

Pecher, P. et al., 2014. The Arabidopsis thaliana mitogen-activated protein kinases MPK3 and MPK6 target a subclass of " VQ-motif "-containing proteins to regulate immune responses. *New Phytologist*, 203(2), pp.592–606.

Petersen, M. et al., 2000. Arabidopsis MAP kinase 4 negatively regulates systemic acquired resistance. *Cell*, 103(7), pp.1111–20.

Petutschnig, E.K. et al., 2010. The lysin motif receptor-like kinase (LysM-RLK) CERK1 is a major chitin-binding protein in Arabidopsis thaliana and subject to chitin-induced phosphorylation. *The Journal of biological chemistry*, 285(37), pp.28902–11.

Pickart, C.M. & Eddins, M.J., 2004. Ubiquitin: Structures, functions, mechanisms. *Biochimica et Biophysica Acta*, 1695(1-3), pp.55–72.

Pickart, C.M. & Fushman, D., 2004. Polyubiquitin chains: polymeric protein signals. *Current Opinion in Chemical Biology*, 8(6), pp.610–616.

Plechanovová, A. et al., 2011. Mechanism of ubiquitylation by dimeric RING ligase RNF4. *Nature structural & molecular biology*, 18(9), pp.1052–9.

Popescu, S.C. et al., 2009. MAPK target networks in Arabidopsis thaliana revealed using functional

protein microarrays. *Genes & development*, 23(1), pp.80–92.

Prakash, S. et al., 2004. An unstructured initiation site is required for efficient proteasome-mediated degradation. *Nature structural & molecular biology*, 11(9), pp.830–837.

Pruneda, J.N. et al., 2012. Structure of an E3:E2~Ub complex reveals an allosteric mechanism shared among RING/U-box ligases. *Molecular cell*, 47(6), pp.933–942.

Qiu, J.-L. et al., 2008. Arabidopsis MAP kinase 4 regulates gene expression through transcription factor release in the nucleus. *The EMBO journal*, 27(16), pp.2214–2221.

Ramonell, K. et al., 2005. Loss-of-Function Mutations in Chitin Responsive Genes Show Increased Susceptibility to the Powdery Mildew Pathogen Erysiphe cichoracearum. *Plant physiology*, 138(2), pp.1027–1036.

Ranf, S. et al., 2015. A lectin S-domain receptor kinase mediates lipopolysaccharide sensing in Arabidopsis thaliana. *Nature immunology*, 16(4), pp.426–33.

Ranf, S. et al., 2011. Interplay between calcium signalling and early signalling elements during defence responses to microbe- or damage-associated molecular patterns. *The Plant journal*, 68(1), pp.100–13.

Rappsilber, J., Ishihama, Y. & Mann, M., 2003. Stop and go extraction tips for matrix- assisted laser desorption/ionization, nanoelectrospray, and LC/MS sample pretreatment in proteomics. *Analytical chemistry*, 75(3), pp.663–70.

Rentel, M.C. et al., 2004. OXI1 kinase is necessary for oxidative burst-mediated signalling in Arabidopsis. *Nature*, 427(6977), pp.858–61.

Robatzek, S., Chinchilla, D. & Boller, T., 2006. Ligand-induced endocytosis of the pattern recognition receptor FLS2 in Arabidopsis. *Genes & development*, 20(5), pp.537–42.

Roux, M. et al., 2011. The arabidopsis leucine-rich repeat receptor-like kinases BAK1/SERK3 and BKK1/SERK4 are required for innate immunity to Hemibiotrophic and Biotrophic pathogens. *The Plant cell*, 23(6), pp.2440–2455.

Roy, N. et al., 1997. The c-IAP-1 and c-IAP-2 proteins are direct inhibitors of specific caspases. *The EMBO journal*, 16(23), pp.6914–6925.

Ryan, P.E. et al., 2006. Regulating the regulator: negative regulation of Cbl ubiquitin ligases. *Trends in biochemical sciences*, 31(2), pp.79–88.

Salt, J.N. et al., 2011. Altered germination and subcellular localization patterns for PUB44/SAUL1 in response to stress and phytohormone treatments. *PloS one*, 6(6), p.e21321.

Samuel, M.A. et al., 2009. Cellular pathways regulating responses to compatible and self-incompatible pollen in Brassica and Arabidopsis stigmas intersect at Exo70A1, a putative component of the exocyst complex. *The Plant cell*, 21(9), pp.2655–71.

Scaglione, K.M. et al., 2011. Ube2w and ataxin-3 coordinately regulate the ubiquitin ligase CHIP. *Molecular cell*, 43(4), pp.599–612.

Schwessinger, B. et al., 2011. Phosphorylation-dependent differential regulation of plant growth, cell death, and innate immunity by the regulatory receptor-like kinase BAK1. *PLoS genetics*, 7(4), p.e1002046.

Segonzac, C. et al., 2014. Negative control of BAK 1 by protein phosphatase 2 A during plant innate immunity. *The EMBO journal*, 33(18), pp.2069–2079.

Seo, D.H. et al., 2012. Roles of four Arabidopsis U-box E3 ubiquitin ligases in negative regulation of abscisic acid-mediated drought stress responses. *Plant physiology*, 160(1), pp.556–68.

Shevchenko, A. et al., 2006. In-gel digestion for mass spectrometric characterization of proteins and proteomes. *Nature protocols*, 1(6), pp.2856–2860.

Shin, H. et al., 2003. Identification of ubiquitination sites on the X-linked inhibitor of apoptosis protein. *The Biochemical journal*, 373(Pt 3), pp.965–971.

Smith, J.M. et al., 2014. Sensitivity to Flg22 is modulated by ligand-induced degradation and de novo synthesis of the endogenous flagellin-receptor FLAGELLIN-SENSING2. *Plant physiology*, 164(1), pp.440–54.

Spoel, S.H. et al., 2009. Proteasome-mediated turnover of the transcription coactivator NPR1 plays dual roles in regulating plant immunity. *Cell*, 137(5), pp.860–72.

Stacey, K.B., Breen, E. & Jefferies, C.A., 2012. Tyrosine phosphorylation of the E3 ubiquitin ligase TRIM21 positively regulates interaction with IRF3 and hence TRIM21 activity. *PLoS ONE*, 7(3), p.e34041.

Stegmann, M. et al., 2012. The ubiquitin ligase PUB22 targets a subunit of the exocyst complex required for PAMP-triggered responses in Arabidopsis. *The Plant cell*, 24(11), pp.4703–16.

Stone, S.L. et al., 2003. ARC1 is an E3 ubiquitin ligase and promotes the ubiquitination of proteins during the rejection of self-incompatible Brassica pollen. *The Plant cell*, 15(4), pp.885–98.

Stone, S.L. et al., 2006. KEEP ON GOING, a RING E3 ligase essential for Arabidopsis growth and development, is involved in abscisic acid signaling. *The Plant cell*, 18(12), pp.3415–28.

Stone, S.L., Arnoldo, M. & Goring, D.R., 1999. A Breakdown of Brassica Self-Incompatibility in ARC1 Antisense Transgenic Plants. *Science*, 286(5445), pp.1729–1731.

Strange, R.N. & Scott, P.R., 2005. Plant disease: a threat to global food security. *Annual review of phytopathology*, 43, pp.83–116.

Suarez-Rodriguez, M.C. et al., 2007. MEKK1 Is Required for flg22-Induced MPK4 Activation in Arabidopsis Plants. *Plant Physiology*, 143(2), pp.661–669.

Suarez-Rodriguez, M.C., Petersen, M. & Mundy, J., 2010. Mitogen-Activated Protein Kinase Signaling in Plants. *Annual review of plant biology*, 61, pp.621–649.

Sun, W. et al., 2006. Within-Species Flagellin Polymorphism in Xanthomonas campestris pv campestris and Its Impact on Elicitation of Arabidopsis FLAGELLIN SENSING2 – Dependent Defenses. *The Plant cell*, 18(3), pp.764–779.

Takahashi, F. et al., 2011. Calmodulin-dependent activation of MAP kinase for ROS homeostasis in Arabidopsis. *Molecular cell*, 41(6), pp.649–60.

Takeda, A.-N. et al., 2014. Ubiquitin-dependent regulation of MEKK2/3-MEK5-ERK5 signaling module by XIAP and cIAP1. *The EMBO journal*, 33(16), pp.1784–801.

Tang, J. et al., 2015. Structural basis for recognition of an endogenous peptide by the plant receptor kinase PEPR1. *Cell research*, 25(1), pp.110–20.

Tatham, M.H. et al., 2008. RNF4 is a poly-SUMO-specific E3 ubiquitin ligase required for arsenic-induced PML degradation. *Nature cell biology*, 10(5), pp.538–46.

Terbush, D.R. et al., 1996. The Exocyst is a multiprotein complex required for exocytosis in Saccharomyces cerevisiae. *The EMBO journal*, 15(23), pp.6483–6494.

Thines, B. et al., 2007. JAZ repressor proteins are targets of the SCF-COI1 complex during jasmonate signalling. *Nature*, 448(7154), pp.661–666.

Thorsten, N. et al., 1994. High Affinity Binding of a Fungal Oligopeptide Elicitor to Parsley Plasma Membranes Triggers Multiple Defense Responses. *Cell*, 78(3), pp.449–460.

Torres, M.A., Dangl, J.L. & Jones, J.D.G., 2002. Arabidopsis gp91 phox homologues AtrbohD and AtrbohF are required for accumulation of reactive oxygen intermediates in the plant defense response. *PNAS*, 99(1), pp.517–522.

Trempe, J. et al., 2013. Structure of Parkin Reveals Mechanisms for Ubiquitin Ligase Activation. *Science*, 340(6139), pp.1451–1455.

Trujillo, M. et al., 2008. Negative regulation of PAMP-triggered immunity by an E3 ubiquitin ligase triplet in Arabidopsis. *Current biology*, 18(18), pp.1396–401.

Trujillo, M. & Shirasu, K., 2010. Ubiquitination in plant immunity. *Current opinion in plant biology*, 13(4), pp.1–17.

Varfolomeev, E. et al., 2007. IAP Antagonists Induce Autoubiquitination of c-IAPs, NF-κB Activation, and TNFα-Dependent Apoptosis. *Cell*, 131(4), pp.669–681.

Vega-Sánchez, M.E. et al., 2008. SPIN1, a K homology domain protein negatively regulated and ubiquitinated by the E3 ubiquitin ligase SPL11, is involved in flowering time control in rice. *The Plant cell*, 20(6), pp.1456–69.

Vierstra, R.D., 2009. The ubiquitin-26S proteasome system at the nexus of plant biology. *Nature reviews. Molecular cell biology*, 10(6), pp.385–97.

Walker-Simmons, M., Hadwiger, L. & Ryan, C.A., 1983. Chitosans and pectic polysaccharides both induce the accumulation of the antifungal phytoalexin pisatin in pea pods and antinutrient proteinase inhibitors in tomato leaves. *Biochemical and biophysical research communications*, 110(1), pp.194–199.

Wang, C. et al., 2001. TAK1 is a ubiquitin-dependent kinase of MKK and IKK. *Nature*, 412(6844), pp.346–51.

Wang, D., Amornsiripanitch, N. & Dong, X., 2006. A Genomic Approach to Identify Regulatory Nodes in the Transcriptional Network of Systemic Acquired Resistance in Plants. *PLoS pathogens*, 2(11), pp.1042–1050.

Wang, H. et al., 2007. Stomatal development and patterning are regulated by environmentally responsive mitogen-activated protein kinases in Arabidopsis. *The Plant cell*, 19(1), pp.63–73.

Wang, Y.-S. et al., 2006. Rice XA21 binding protein 3 is a ubiquitin ligase required for full Xa21-mediated disease resistance. *The Plant cell*, 18(12), pp.3635–46.

Wen, R. et al., 2006. Arabidopsis thaliana UBC13: implication of error-free DNA damage tolerance and Lys63-linked polyubiquitylation in plants. *Plant molecular biology*, 61(1-2), pp.241–53.

Wen, R. et al., 2014. UBC13, an E2 enzyme for Lys63-linked ubiquitination, functions in root development by affecting auxin signaling and Aux/IAA protein stability. *The Plant Journal*, 80(3), pp.424–436.

Wiborg, J., O'Shea, C. & Skriver, K., 2008. Biochemical function of typical and variant Arabidopsis thaliana U-box E3 ubiquitin-protein ligases. *The Biochemical journal*, 413(3), pp.447–57.

Wright, P.E. & Dyson, H.J., 2015. Intrisically disordered proteins in cellular signaling and regulation. *Nat Rev Mol Cell Biol*, 16(1), pp.18–29.

Xu, P. et al., 2009. Quantitative Proteomics Reveals the Function of Unconventional Ubiquitin Chains in Proteasomal Degradation. *Cell*, 137(1), pp.133–145.

Xu, Z. et al., 2006. Structure and Interactions of the Helical and U-Box Domains of CHIP , the C Terminus of HSP70 Interacting Protein. *Biochemistry*, 45(15), pp.4749–4759.

Yamaguchi, Y. et al., 2010. PEPR2 is a second receptor for the Pep1 and Pep2 peptides and contributes to defense responses in Arabidopsis. *The Plant cell*, 22(2), pp.508–22.

Yamaguchi, Y., Pearce, G. & Ryan, C. a, 2006. The cell surface leucine-rich repeat receptor for AtPep1, an endogenous peptide elicitor in Arabidopsis, is functional in transgenic tobacco cells. *PNAS*, 103(26), pp.10104–9.

Yang, C.-W. et al., 2006. The E3 Ubiquitin Ligase Activity of Arabidopsis PLANT U-BOX17 and Its Functional Tobacco Homolog ACRE276 Are Required for Cell Death and Defense. *The Plant cell*, 18(4), pp.1084–1098.

Ye, H. et al., 2002. Distinct molecular mechanism for initiating TRAF6 signalling. *Nature*, 418(6896), pp.443–447.

Yee, D. & Goring, D.R., 2009. The diversity of plant U-box E3 ubiquitin ligases: from upstream activators to downstream target substrates. *Journal of experimental botany*, 60(4), pp.1109–21.

Yin, Q. et al., 2009. E2 interaction and dimerization in the crystal structure of TRAF6. *Nature structural & molecular biology*, 16(6), pp.658–66.

Yin, X.-J. et al., 2007. Ubiquitin Lysine 63 Chain – Forming Ligases Regulate Apical Dominance in

Arabidopsis. *The Plant cell*, 19(6), pp.1898–1911.

Yuan, W.-C. et al., 2014. K33-Linked Polyubiquitination of Coronin 7 by Cul3-KLHL20 Ubiquitin E3 Ligase Regulates Protein Trafficking. *Molecular cell*, 54(4), pp.586–600.

Zeng, L.-R. et al., 2004. Spotted leaf11, a negative regulator of plant cell death and defense, encodes a U-box/armadillo repeat protein endowed with E3 ubiquitin ligase activity. *The Plant cell*, 16(10), pp.2795–808.

Zhang, J. et al., 2007. A Pseudomonas syringae effector inactivates MAPKs to suppress PAMP-induced immunity in plants. *Cell host & microbe*, 1(3), pp.175–85.

Zhang, J. et al., 2010. Receptor-like cytoplasmic kinases integrate signaling from multiple plant immune receptors and are targeted by a Pseudomonas syringae effector. *Cell host & microbe*, 7(4), pp.290–301.

Zhang, M. et al., 2005. Chaperoned ubiquitylation--crystal structures of the CHIP U box E3 ubiquitin ligase and a CHIP-Ubc13-Uev1a complex. *Molecular cell*, 20(4), pp.525–38.

Zhang, Z. et al., 2012. Disruption of PAMP-induced MAP kinase cascade by a pseudomonas syringae effector activates plant immunity mediated by the NB-LRR protein SUMM2. *Cell Host and Microbe*, 11(3), pp.253–263.

Zhao, C. et al., 2014. EDR1 Physically Interacts with MKK4/MKK5 and Negatively Regulates a MAP Kinase Cascade to Modulate Plant Innate Immunity. *PLoS Genetics*, 10(5), p.e1004389.

Zhao, Y., Yu, H. & Hu, W., 2014. The regulation of MDM2 oncogene and its impact on human cancers. *ABBS*, 46(3), pp.180–189.

Zheng, Z. et al., 2006. Arabidopsis WRKY33 transcription factor is required for resistance to necrotrophic fungal pathogens. *The Plant Journal*, 48(4), pp.592–605.

Zhou, J. et al., 2000. NPR1 Differentially Interacts with Members of the TGA/OBF Family of Transcription Factors That Bind an Element of the PR-1 Gene Required for Induction by Salicylic Acid. *MPMI*, 13(2), pp.191–202.

Zhou, J. et al., 2015. The dominant negative ARM domain uncovers multiple functions of PUB13 in Arabidopsis immunity, flowering, and senescence. *Journal of experimental botany*, 66(11), pp.3353–66.

Zipfel, C. et al., 2004. Bacterial disease resistance in Arabidopsis through flagellin perception. *Nature*, 428(6984), pp.764–7.

Zipfel, C., 2009. Early molecular events in PAMP-triggered immunity. *Current opinion in plant biology*, 12(4), pp.414–20.

Zipfel, C. et al., 2006. Perception of the bacterial PAMP EF-Tu by the receptor EFR restricts Agrobacterium-mediated transformation. *Cell*, 125(4), pp.749–60.

Zipfel, C. & Felix, G., 2005. Plants and animals: a different taste for microbes? *Current opinion in plant biology*, 8(4), pp.353–360.

7. Appendix

7.1 Tables

Table I: Primers used for SDM on *PUB22* and *PUB22*$^{U-box}$ in entry vectors.

Mutation	Sequence	Enzyme	Diagnostic
F10E forward	ATATATGAAGACGAGTTCCTTTGTCCAATCTCTCT	Bpil	none
F10E reverse	ATATATGAAGACGAACTCGGAAGGAATCTCTATCT		
I25R forward	ATATATGAAGACCGAGTTTCCACCGGAATAAC	Bpil	none
I25R reverse	ATATATGAAGACGAAACTCGCACCGGATCT		
W40A forward	ATATATGAAGACGCGCTCTTTTCCGGTAAGA	Bpil	HaeII
W40A reverse	ATATATGAAGACAAGAGCGCCTTCTCGATG		
T62I forward	ATATATGAAGACATTCCAAACCACAC	Bpil	none
T62I reverse	ATATATGAAGACTTTGGAATAAGATCAGTT		
T62A forward	ATATATGGTCTCGGCGCCGAACCACACTCTTCGCC	Bsal	HaeII
T62A reverse	ATATATGGTCTCGGCGCCAGATCAGTTTCGGTTATG		
T62E forward	ATATATGGTCTCGAGCCCAACCACACTCTTC	Bsal	BanII
T62E reverse	ATATATGGTCTCGGGCTCAAGATCAGTTTCG		
T88A forward	ATATATGAAGACAGCTCCAAAACCTCCGATC	Bpil	none
T88A reverse	ATATATGAAGACTTGGAGCTGGGATCCTCTC		
T88E forward	ATATATGAAGACGAGCCCAAACCTCCGATCTG	Bpil	BanII
T88E reverse	ATATATGAAGACTTGGGCTCTGGGATCCTCTCT		
S422A forward	ATATATGAAGACGCGCCTTGTGTCCCAAGAAAT	Bpil	HaeII
S422A reverse	ATATATGAAGACCAAGGCGCTTCCCTCCAAACC		
S422E forward	ATATATGAAGACGAGCCCTGTGTCCCAAGAA	Bpil	BanII
S422E reverse	ATATATGAAGACCAGGGCTCTTCCCTCCAAA		

Table II: Primers for cloning

Description	Plasmid	Sequence
PUB22^{U-box} no stop forward	pENTR3C	GGCCATTUATGGATCAAGAGATAGAGA
PUB22^{U-box} no stop reverse	pENTR3C	GGTGATTUCTAGATGCGAAGATGAC
PUB22 Sall forward	pMal-c2X	CATGTCGACATGGATCAAGAGATAGAGA
PUB22 PstI reverse	pMal-c2X	CATCTGCAGTCAAGCAGGATACGAAT
PUB24 EcoRI forward	pMal-c2X	CATGAATTCATGAATATATATACGTACA
PUB24 PstI reverse	pMal-c2X	CATCTGCAGTTAGATCTTTGGCCCTTTG

7. Appendix

Table III: Primers for genotyping

Description	Sequence	Locus
PUB22 LP	AATGCCCGTCGTGGATATC	*At*3G52450
PUB22 RP	ATGTCCATGGGGAAGGAATAG	
PUB23 LP	CAATCTTGGTGCACCCTAAAC	*At*2G35930
PUB23 RP	TTTTCATCAGCAGGGATATGC	
PUB24 LP	GACGACGTCGTATCAAAGGAC	*At*3G11840
PUB24 RP	TCGATTGAGGATTGATCGATC	
MPK3 LP	ATTTTTGTCAACAATGGCCTG	*At*3G45640
MPK3 RP	TCTGCCTTTTCACGGAATATG	

Table IV: RT-qPCR primers

Description	Sequence
PP2A (*At*1G13320) forward	TAACGTGGCCAAAATGATGC
PP2A (*At*1G13320) reverse	GTTCTCCACAACCGCTTGGT
PUB22 forward	TGCAATTGGGAGTTGTAGCA
PUB22 reverse	GATTCCCTCCAAACCCTAGC

Table V: Fusion constructs used in this study

Construct	Point mutations	Vector type	Fusion protein	Size [kDa]
pCAMBIA/des/cLuc-PUB22$^{U\text{-}box}$	W40A, T62A, T62E, T62I, F10E, I25R	Plant expression	PUB22$^{U\text{-}box}$-cLUC	31,3
pCAMBIA/des/nLuc-PUB22$^{U\text{-}box}$	W40A, T62A, T62E, T62I, F10E, I25R	Plant expression	PUB22$^{U\text{-}box}$-nLUC	58,4
pCL112-Avr3a K80I103	-	Plant expression	nYFP-Avr3a	36
pDest15-PUB22$^{U\text{-}box}$	-	Bacterial expression	GST-PUB22$^{U\text{-}box}$	40,4
pDest17-PUB22$^{U\text{-}box}$	-	Bacterial expression	His-PUB22$^{U\text{-}box}$	15,4
pDest17-UBA1	-	Bacterial expression	His-UBA1	123,4
pDest17-UBC8	-	Bacterial expression	His-UBC8	19,7
pESPYCE-PUB22	W40A	Plant	HA-cYFP-PUB22	62,1

|				
				expression
pESPYNE-MPK11	-	Plant expression	cMyc-nYFP-MPK11	63,8
pESPYNE-MPK3	-	Plant expression	cMyc-nYFP-MPK3	64,1
pESPYNE-MPK4	-	Plant expression	cMyc-nYFP-MPK4	64,1
pESPYNE-MPK6	-	Plant expression	cMyc-nYFP-MPK6	66,1
pESPYNE-MPK8	-	Plant expression	cMyc-nYFP-MPK8	87,5
pET28-Exo70B2	-	Bacterial expression	His-Exo70B2	71,5
pGex-4T-1-MPK3	-	Bacterial expression	GST-MPK3	70,5
pGex-4T-1-MPK6	-	Bacterial expression	GST-MPK6	72,9
pGWB406::PUB22prom::GFP-PUB22	-	Plant expression	GFP-PUB22	77,3
pGWB415-PUB22	-	Plant expression	HA-PUB22	55,4
pGWB418-Exo70B2	-	Plant expression	cMyc-Exo70B2	74,2
pGWB506-Exo70B2	-	Plant expression	GFP-Exo70B2	96,2
pMal-c2X-PUB22	W40A, T62A, T62E, T88A, T88E, I25R, F10E, T62/88A, T62/88E	Bacterial expression	MBP-PUB22	92,4
pMal-c2X-PUB24	-	Bacterial expression	MBP-PUB24	96,5
pRT100-cMyc-PcMKK5	KR, DD (Lee et al. 2004)	Plant expression	cMyc-MKK5	47
pUBN-GFP-PUB22	W40A, T62A, T62E, T88A, T88E, T62/88A, T62/88E, S422A, S422E	Plant expression	GFP-PUB22	77,7

7. Appendix

Table VI: PUB22 *in vivo* phosphorylation sites. Two-week-old seedlings expressing *UBQ10prom::GFP-PUB22*[W40A] grown in ½ MS liquid medium, were treated for 30 min with 1 µM flg22. After IP with GFP-trap beads, protein samples were analysed by SDS-PAGE and stained. Excised bands were analysed by LC-MS/MS. The phosphorylation site in the column P-Site has the highest phosphorylation probability of all possible phosphorylation sites in the peptide sequence based on the interpretation of the MS/MS fragment ion pattern by the phosphoRS software. The probabilities as opposed to the other possible sites are given in the column Probability. (mass-to-charge ratio [m/z], retention time [RT], number of peptide spectrum matches [#PSMs])

Kinase	Peptide Sequence	Charge	m/z [Da]	RT [min]	Exp Value	Mascot Ion Score	#PSMs	P-Site	Probability
In vivo	TDLT(p)PNHTLR	3	416.531	27.69	3.10E-03	34	8	T62	100 %
In vivo	IPT(p)PKPPICK	3	410.881	31.38	6.80E-04	34	53	T88	100 %

Table VII: PUB22 phosphorylation sites identified from *in vitro* assays. Site specific phosphorylation of PUB22 by MPK3 and MPK4 was studied by *in vitro* kinase assay followed by HR/AM LC-MS. The phosphorylation site in the column P-Site has the highest phosphorylation probability of all possible phosphorylation sites in the peptide sequence based on the interpretation of the MS/MS fragment ion pattern by the phosphoRS software. The probabilities as opposed to the other possible sites are given in the column Probability. § T62 is the site with the second highest probability as opposed to T66 which was considered the most probable site by the software.

| Kinase	Peptide Sequence	Charge	m/z [Da]	RT [min]	Exp Value	Mascot IonScore	#PSMs	P-Site	Probability
MPK3	QVITETDLT(p)PNHTLR	3	606.630	16.78	1.50E-03	41	461	T62	100 %
MPK3	IPT(p)PKPPICK	3	410.882	14.15	2.50E-02	29	224	T88	100 %
MPK3	VWRES(p)CVPR	3	455.876	14.54	1.80E-02	30	21	S422	100 %
MPK4	QVITETDLT(p)PNHTLR	3	606.629	16.83	1.76E-01	21	37	T62	12.40 % §
MPK4	IPT(p)PKPPICK	3	410.882	14.34	3.62E-02	27	88	T88	100 %
MPK4	VWRES(p)CVPR	3	455.876	14.58	3.39E-01	18	7	S422	100 %

7.2 Figures
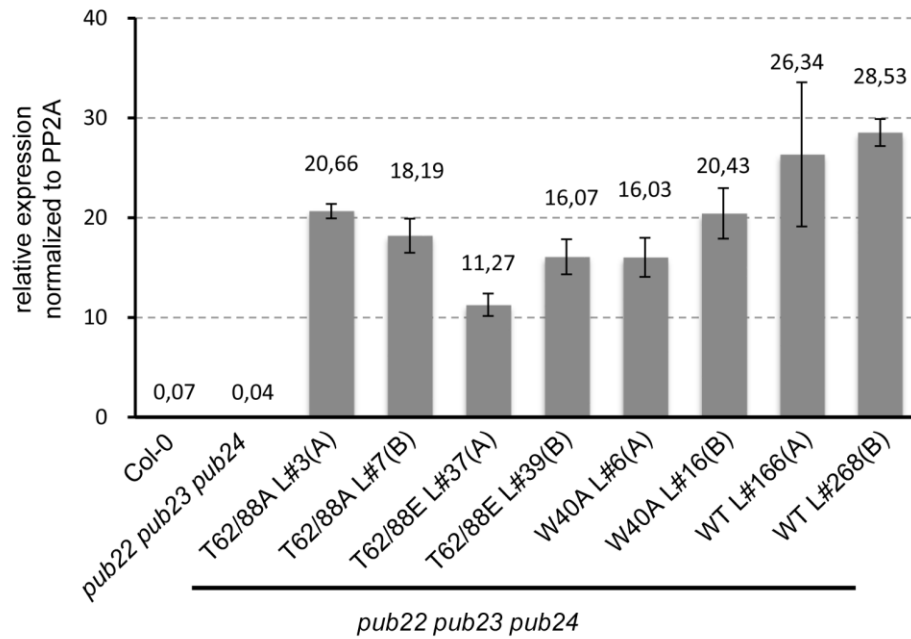
Figure 7-1 RT-qPCR analyses of PUB22 WT and mutant variants transgenic lines. RT-qPCR of selected T3 homozygous transgenic lines carrying *UBQ10prom::GFP-PUB22* WT and variants W40A, T62/88A and T62/88E. Samples were taken from adult plants and PP2A (*At*1G13320) was used as a reference gene. Data shown as mean +/- S.E.M. (n=3).
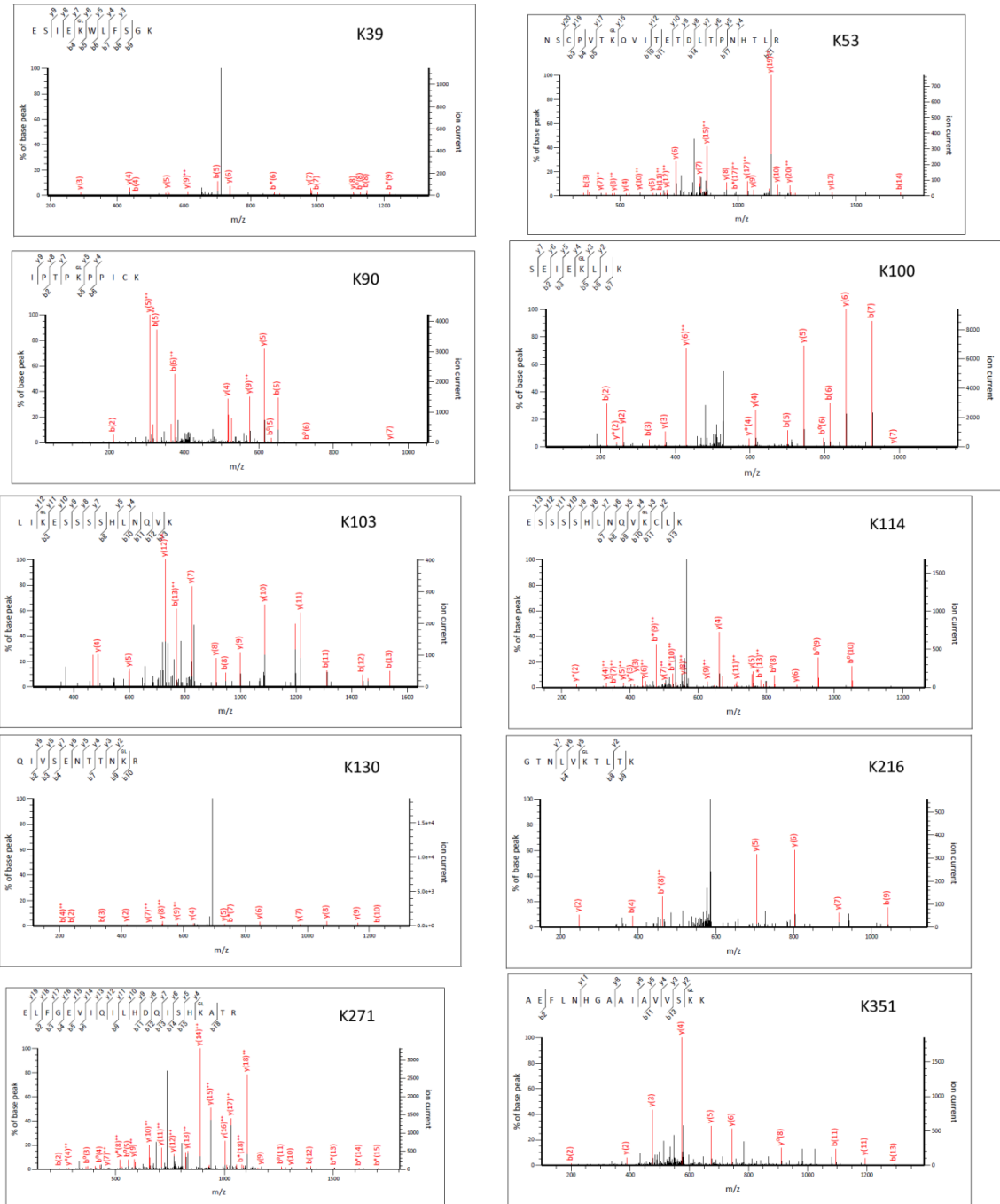
**Figure 7-2 MS spectra of peptides with a di-glycine footprint found on GST-PUB22.** Purified GST-PUB22 was used for *in vitro* autoubiquitination assay with His-UBA1 and His-UBC8 overnight at 30°C. After SDS-PAGE separation, excised bands were analysed by LC-MS/MS.
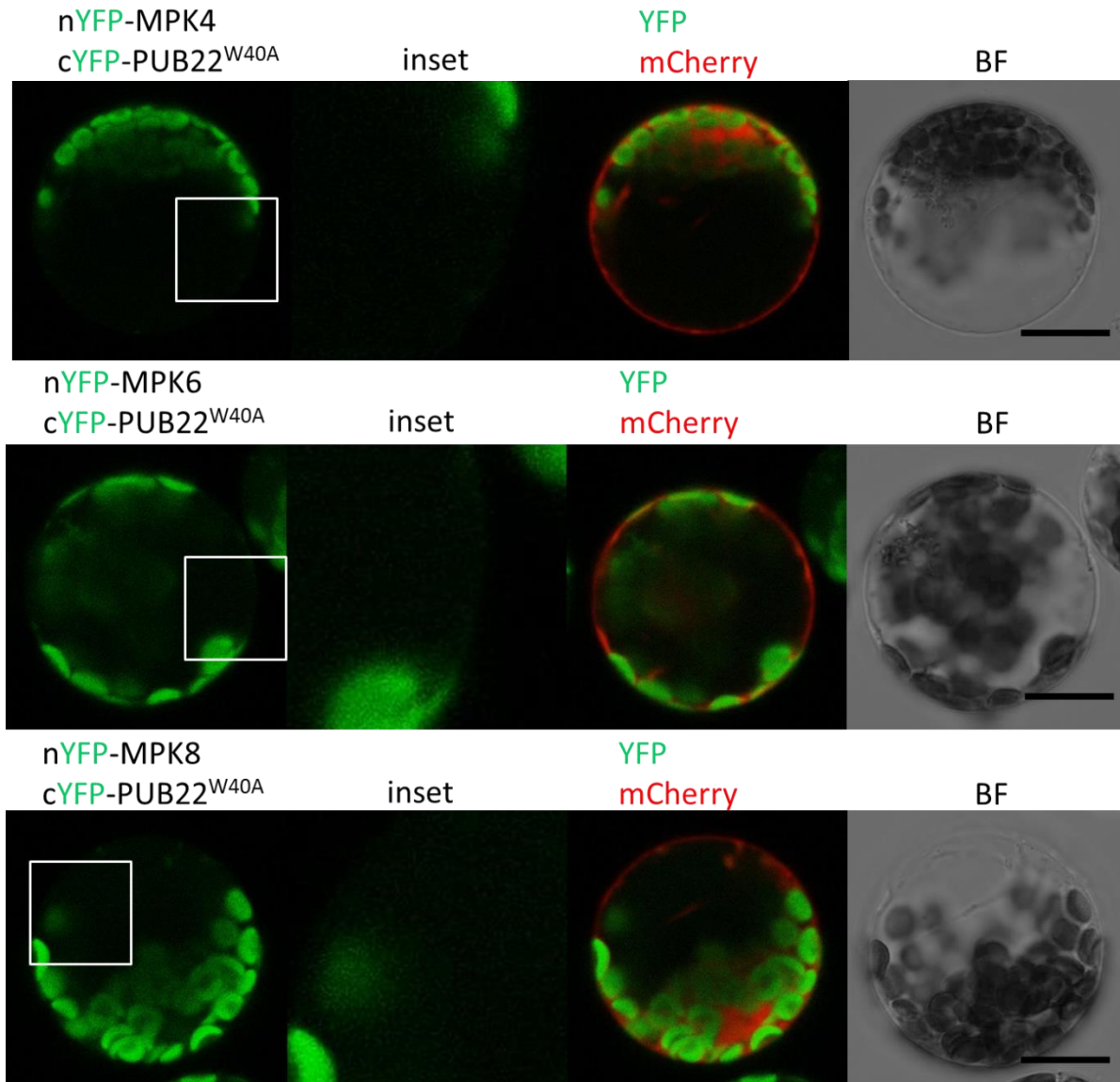
Figure 7-3 PUB22^{W40A} BiFC interaction analysis with MPK4, MPK6 or MPK8. *35Sprom::cMyc-nYFP-MPK4*, *MPK6* or *MPK8* and *35Sprom::HA-cYFP-PUB22^{W40A}* constructs were co-transformed into *Arabidopsis thaliana* mesophyll protoplasts derived from *pub22 pub23 pub24* mutant plants together with a mCherry nuclear and cytoplasmic marker. One day after transformation, YFP reconstitution and mCherry fluorescence were analysed by confocal laser scanning microscope. Scale bar = 20 µm. Similar results were obtained in 3 independent experiments.
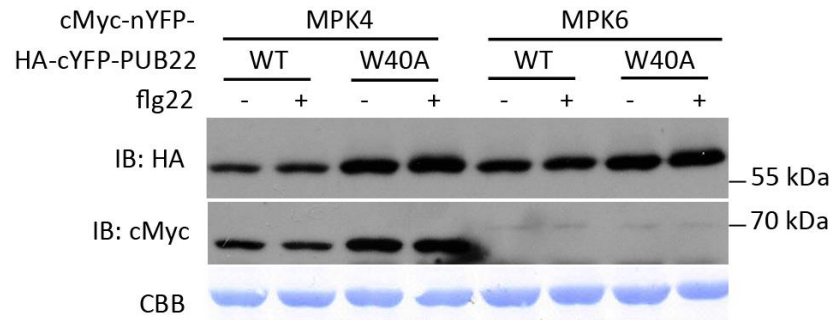
**Figure 7-4 PUB22^W40A, MPK4 and MPK6 BiFC fusion proteins expression analysis.** Total protein samples from BiFC experiments were analysed by SDS-PAGE and immunoblot using anti-HA and anti-cMyc antibodies. 1 µM flg22 was used for 30 min. Similar results were obtained in 3 independent experiments.
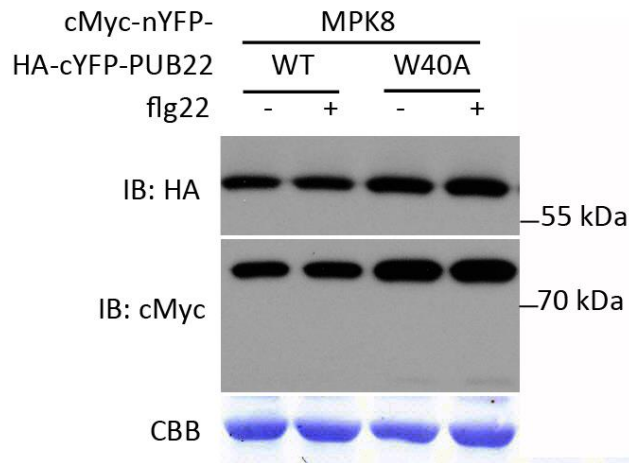

Figure 7-5 PUB22^W40A, MPK8 and MPK11 BiFC fusion proteins expression analysis. Total protein samples from BiFC experiments were analysed by SDS-PAGE and immunoblot using anti-HA and anti-cMyc antibodies. 1 µM flg22 was used for 30 min. Similar results were obtained in 3 independent experiments.
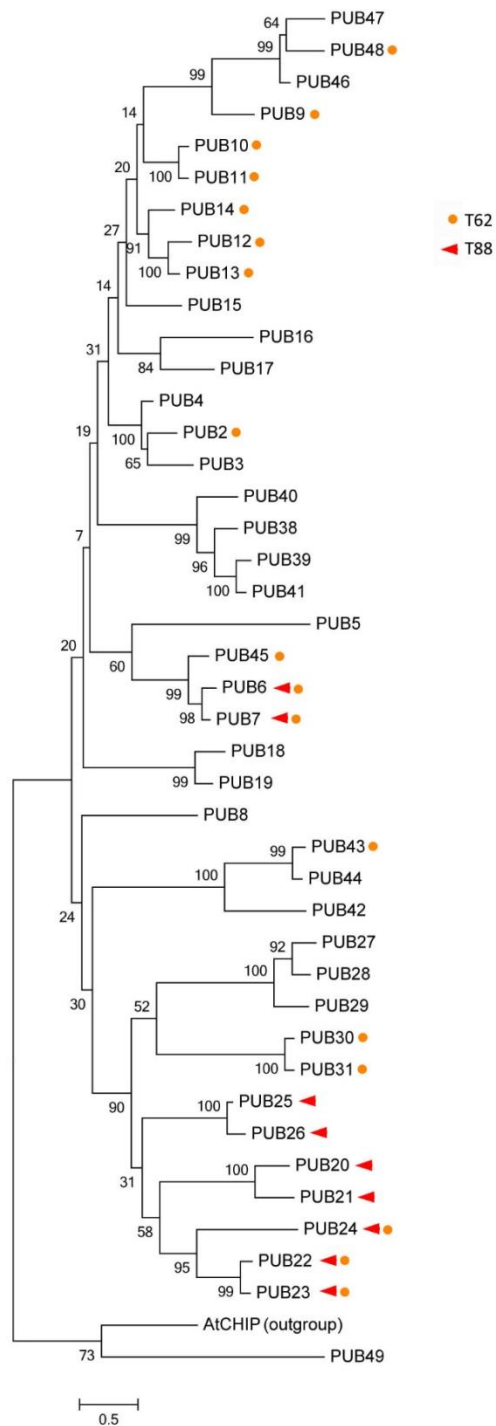
Figure 7-6 Phylogenetic relations between Arabidopsis PUB proteins class II and III. Alignment was performed using MAFFT and manually edited. Alignment was then used for phylogenetic analysis using maximum likelihood. Highlighted are PUB proteins with a conserved Thr followed by Pro at position 62 (orange circle) and 88 (red arrowhead). (Generated by Dr. Trujillo and Prof. Quint).
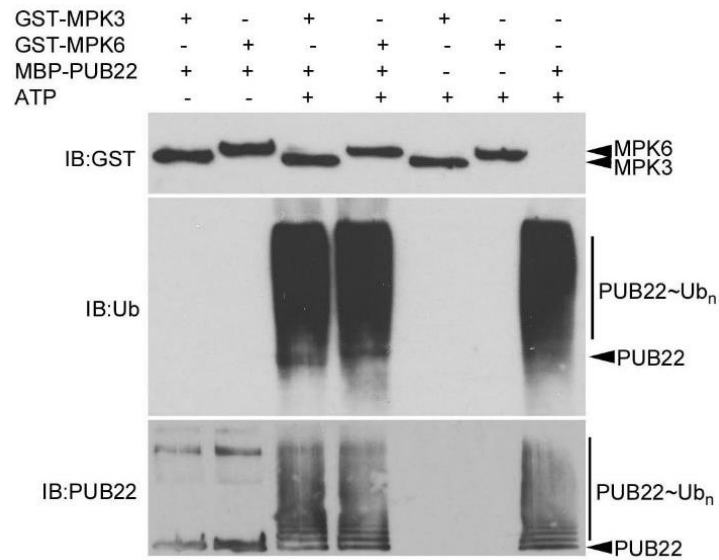
Figure 7-7 PUB22 does not ubiquitinate MPK3 or MPK6 *in vitro*. MBP-PUB22 WT, GST-MPK3 and GST-MPK6 were purified. The ligase was preincubated together with GST-MPK3 or GST-MPK6 and subsequently with His-UBA1 and His-UBC8 for the indicated time at 30°C. Proteins were analysed by SDS-PAGE and immunoblot using anti-GST, anti-ubiquitin and anti-PUB22 antibodies. Similar results were obtained in 3 independent experiments.
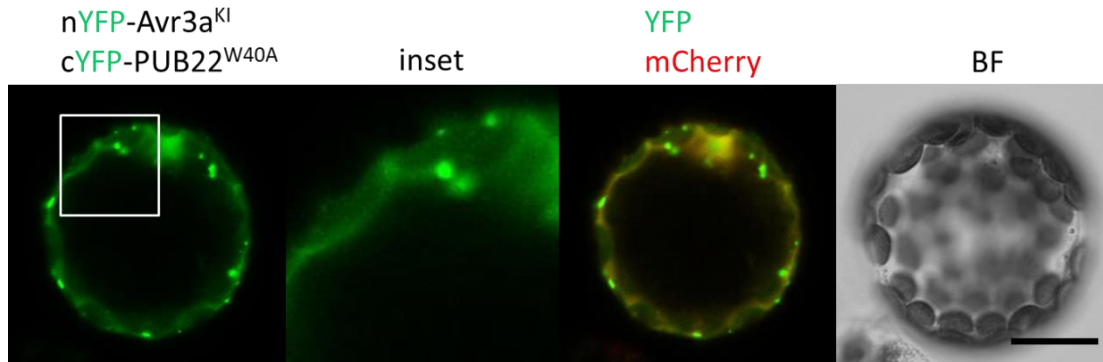
Figure 7-8 BiFC interaction analysis with PUB22^{W40A} and Avr3a^{KI}. *35Sprom::cMyc-nYFP-Avr3a^{KI}* and *35Sprom::HA-cYFP-PUB22^{W40A}* constructs were co-expressed in Arabidopsis mesophyll protoplasts derived from *pub22 pub23 pub24* mutant plants together with a mCherry nuclear and cytoplasmic marker. One day after transformation, YFP reconstitution and mCherry fluorescence were analysed by confocal laser scanning microscope. Scale bar = 20 µm. Similar results were obtained in three independent experiments.
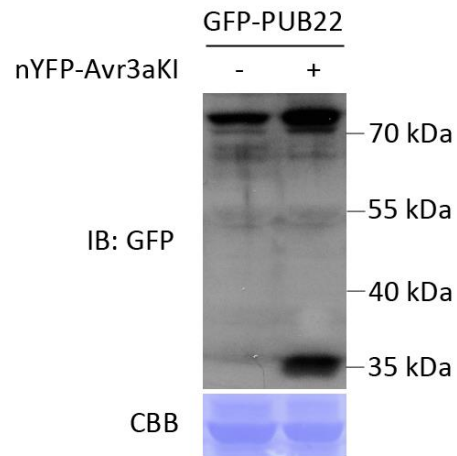
Figure 7-9 Stability analysis of PUB22 in combination with Avr3a. *UBQ10prom::GFP-PUB22* and *cMyc-nYFP-Avr3a^{KI}* constructs were transformed into Arabidopsis mesophyll protoplasts derived from *pub22 pub23 pub24* mutant plants. One day after transformation, total protein samples were analysed by SDS-PAGE and immunoblot using anti-GFP antibodies. CBB was used as control for equal loading. Similar results were obtained in three independent experiments.

Acknowledgements

Firstly, I would like to express my sincere gratitude to Marco for the constant support throughout my doctorate and master studies, for the conception of this exciting project and for his vibrant encouragement. Without your help, it would not have been possible to conduct this research. Also, I would like to thank Prof. Dierk Scheel and Dr. Justin Lee for the fruitful scientific discussions and comments. Moreover, I would like to thank the entire thesis committee for dedicating their time to evaluate my work.

My sincere thanks also go to all the people mentioned throughout my manuscript, whose work considerably contributed to the development of my project, your help was precious. An exceptional thanks goes to Lennart for sharing his protocol and expertise in protoplast transformation. I would like to express my gratitude also to my former and current fellow labmates for the nice working atmosphere and the fun time. Also, I would like to thank my neighbour colleagues from Nico's working group for sharing materials, protocols and ideas.

A very special thanks goes to my friends and especially my family, for the constant moral support in my adventurous choice of living and working far from home, for the many care packages not to forget the taste of home and for the many rides to come visit me (IT: Un ringraziamento speciale va ai miei amici e soprattutto ai miei familiari, per il costante supporto morale nella mia scelta impegnativa di vivere e lavorare lontano da casa, per tutti i pacchi spediti per non dimenticare il sapore di casa e per i tanti viaggi per venirmi a trovare). Finally, I would like to say a huge thank you to my boyfriend Frederik, for the sleepless nights discussing bad results and for ultimately always infecting me with his enthusiasm.

Personal Information

- -

Date of birth: 24/10/1986
Place of birth: Padova (ITALY)
Nationality: Italian

Education

- -

Jun 2017	**Ph.D. degree in Natural Sciences – Plant Biology** **Martin-Luther Universität Halle-Wittenberg (Germany)** Degree mark: 1.0 *Summa cum Laude* Thesis title: Phosphorylation of the E3 ubiquitin ligase PUB22 controls its ubiquitination activity to dampen the immune response Thesis supervisor: Dr. Marco Trujillo
Oct 2010	**Master-2nd cycle degree – Molecular Biology** **Università di Padova (Italy)** Name of the course of study: BIOLOGIA MOLECOLARE Degree mark: 101 (out of 110) Thesis title: Cell biological analysis of U-box type E3 ubiquitin ligases in plants Thesis supervisors: Dr. Marco Trujillo, Prof. Barbara Baldan
Sep 2008	**Bachelor-1st cycle degree – Molecular Biology** **Università di Padova (Italy)** Name of the course of study: BIOLOGIA MOLECOLARE Degree mark: 91 (out of 110) Thesis title: *Vitis vinifera* transcriptome analysis via second generation sequencing method Thesis supervisor: Prof. Giorgio Valle **Pre-university studies**
Jul 2005	**Secondary school diploma** **Liceo Scientifico "E. Fermi" (Padova - Italy)** High School with a focus in Science School-leaving examination mark:77 (out of 100)

Publications

—————————————————————————————————————

2017	Furlan, G., Nakagami, H., Eschen-Lippold, L., Majovsky, P., Kowarschik, K., Jiang, X., Hoehenwarter, W., Lee, J., and Trujillo, M., **Dampening of the immune response by changes in PUB22 ubiquitination modes triggered by MPK3** (2017) The Plant Cell, Vol.29: 726-745 https://doi.org/10.1105/tpc.16.00654
2017	Furlan, G., and Trujillo, M., **In vitro ubiquitination activity assays in plant immune responses** (2017) Springer Methods in Molecular Biology, Vol. 1578, Libo Shan and Ping He (Eds) Plant Pattern Recognition Receptors, 978-1-4939-6858-9
2012	Furlan, G., Klinkenberg, J., and Trujillo, M., **Regulation of plant immune receptors by ubiquitination** (2012) Frontiers in Plant Science, Vol.3, Article 238 10.3389/fpls.2012.00238

Halle …………………………………………

....

Giulia Furlan

.

Eidesstattliche Erklärung

Ich habe diese Arbeit selbständig und ohne fremde Hilfe verfasst, andere als die von mir angegebenen Quellen und Hilfsmittel nicht benutzt und die den benutzten Werken wörtlich oder inhaltlich entnommenen Stellen als solche kenntlich gemacht.

Außerdem versichere ich hiermit, dass ich mich bis jetzt noch nicht um einen Doktorgrad beworben habe.

Halle …………………………………

…………………………………………

Giulia Furlan